

Argonne National Laboratory

REACTOR DEVELOPMENT PROGRAM PROGRESS REPORT

May 1968



The facilities of Argonne National Laboratory are owned by the United States Government. Under the terms of a contract (W-31-109-Eng-38) between the U. S. Atomic Energy Commission, Argonne Universities Association and The University of Chicago, the University employs the staff and operates the Laboratory in accordance with policies and programs formulated, approved and reviewed by the Association.

MEMBERS OF ARGONNE UNIVERSITIES ASSOCIATION

The University of Arizona
Carnegie Institute of Technology
Case Institute of Technology
The University of Chicago
University of Cincinnati
Illinois Institute of Technology
University of Illinois
Indiana University
Iowa State University

The University of Iowa
Kansas State University
The University of Kansas
Loyola University
Marquette University
Michigan State University
The University of Michigan
University of Minnesota
University of Missouri

Northwestern University
University of Notre Dame
The Ohio State University
Purdue University
Saint Louis University
Washington University
Wayne State University
The University of Wisconsin

LEGAL NOTICE

This report was prepared as an account of Government sponsored work. Neither the United States, nor the Commission, nor any person acting on behalf of the Commission:

A. Makes any warranty or representation, expressed or implied, with respect to the accuracy, completeness, or usefulness of the information contained in this report, or that the use of any information, apparatus, method, or process disclosed in this report may not infringe privately owned rights; or

B. Assumes any liabilities with respect to the use of, or for damages resulting from the use of any information, apparatus, method, or process disclosed in this report.

As used in the above, "person acting on behalf of the Commission" includes any employee or contractor of the Commission, or employee of such contractor, to the extent that such employee or contractor of the Commission, or employee of such contractor prepares, disseminates, or provides access to, any information pursuant to his employment or contract with the Commission, or his employment with such contractor.

Printed in the United States of America
Available from

Clearinghouse for Federal Scientific and Technical Information
National Bureau of Standards, U. S. Department of Commerce
Springfield, Virginia 22151

Price: Printed Copy \$3.00; Microfiche \$0.65

ARGONNE NATIONAL LABORATORY
9700 South Cass Avenue
Argonne, Illinois 60439

REACTOR DEVELOPMENT PROGRAM
PROGRESS REPORT

May 1968

Robert B. Duffield, Laboratory Director
Stephen Lawroski, Associate Laboratory Director

<u>Division</u>	<u>Director</u>
Chemical Engineering	R. C. Vogel
Idaho	M. Novick
Metallurgy	M. V. Nevitt
Reactor Engineering	L. J. Koch
Reactor Physics	R. Avery
Remote Control	D. P. Mingesz (Acting)

Report Coordinated by
L. B. Fosdick and A. Glassner

Issued July 2, 1968

FOREWORD

The Reactor Development Program Progress Report, issued monthly, is intended to be a means of reporting those items of significant technical progress which have occurred in both the specific reactor projects and the general engineering research and development programs. The report is organized in accordance with budget activities in a way which, it is hoped, gives the clearest, most logical overall view of progress. Since the intent is to report only items of significant progress, not all activities are reported each month. In order to issue this report as soon as possible after the end of the month editorial work must necessarily be limited. Also, since this is an informal progress report, the results and data presented should be understood to be preliminary and subject to change unless otherwise stated.

The issuance of these reports is not intended to constitute publication in any sense of the word. Final results either will be submitted for publication in regular professional journals or will be published in the form of ANL topical reports.

The last six reports issued
in this series are:

November 1967	ANL-7399
December 1967	ANL-7403
January 1968	ANL-7419
February 1968	ANL-7427
March 1968	ANL-7438
April 1968	ANL-7445

REACTOR DEVELOPMENT PROGRAM

Highlights of Project Activities for May 1968

EBR-II

In a program designed to identify and remove the source of fission-product leakage, the reactor was operated for 682 MWdt in Runs 27H, 27I, 28A, 28B, and 28C. Experimental Subassembly XO28 was identified as the probable source of this leakage and was removed from the core. The other fueled experiments which had been removed previously were returned to the core in two increments. After the return of each increment, the reactor was operated to monitor any further leakage from experiments and to obtain information regarding the effect of the added ceramic-fueled subassemblies on reactor kinetics. The cumulated total of EBR-II operation is 17,386 MWdt.

Production of driver fuel continued at a normal rate in the cold line, but was limited in the FCF hot line because of a lack of storage space and the need to accommodate surveillance work.

ZPR-3

Experiments were concluded with Assembly 51, the first core of the FTR Phase-B critical program. Work began on Assembly 52, the second core of the program. Many results from Assembly 51 are reported herein.

ZPPR

Installation of the reactor assembly and associated equipment was 90% complete at the end of the month. The matrix was completed for the 10- by 10-ft assembly, and the rod drives for the first core were installed.

The criticality-monitoring system for the vault and workroom has been assembled and tested. Preparations for fuel-acceptance tests and storage of ZPPR fuel are complete.

The development of a detailed design for ZPPR Core I has been completed.

THE UNIVERSITY OF CHICAGO

THE UNIVERSITY OF CHICAGO LIBRARY

The University of Chicago Library is pleased to announce the acquisition of a new copy of the book "The History of the United States" by James M. Smith. This book is a comprehensive history of the United States, covering the period from the first settlement to the present. It is a valuable resource for students and scholars alike. The book is available in both print and digital formats. The print edition is available for purchase at a special price. The digital edition is available for free access to all library members. The book is a must-read for anyone interested in the history of the United States.

The University of Chicago Library is pleased to announce the acquisition of a new copy of the book "The History of the United States" by James M. Smith. This book is a comprehensive history of the United States, covering the period from the first settlement to the present. It is a valuable resource for students and scholars alike. The book is available in both print and digital formats. The print edition is available for purchase at a special price. The digital edition is available for free access to all library members. The book is a must-read for anyone interested in the history of the United States.

The University of Chicago Library is pleased to announce the acquisition of a new copy of the book "The History of the United States" by James M. Smith. This book is a comprehensive history of the United States, covering the period from the first settlement to the present. It is a valuable resource for students and scholars alike. The book is available in both print and digital formats. The print edition is available for purchase at a special price. The digital edition is available for free access to all library members. The book is a must-read for anyone interested in the history of the United States.

TABLE OF CONTENTS

	<u>Page</u>
I. PLUTONIUM UTILIZATION--CIVILIAN--EBWR	1
A. Research and Development	1
1. Operational Consultation and Support	1
II. LIQUID-METAL FAST BREEDER REACTORS--CIVILIAN	4
A. Fuel Development--LMFBR	4
1. Metallic	4
2. Oxide	7
3. Carbide--Fabrication and Evaluation	7
4. Fuel Cladding and Structure--Jacket Alloys	9
B. Physics Development--LMFBR	11
1. Theoretical Reactor Physics--General Fast Reactor Physics	11
2. Experimental Reactor Physics--Fast Critical Experiments--Experimental Support (Idaho)	15
3. Experimental Reactor Physics--Fast Critical Experiments--Experimental Support (Argonne)	19
4. ZPR-3 Operations and Analysis	20
5. ZPR-6 and -9 Operations and Analysis	28
6. ZPPR Operations and Analysis	28
7. ZPR Fuel and Nonfissile Materials-- Technical Assistance	31
8. ZPPR Construction	33
9. FFTF Critical Experiment Program	34
C. Component Development--LMFBR	37
1. Sodium Technology Development--Engineering Development	37
2. Reactor Mechanisms Development--Materials Evaluation	39
3. Fuel Handling, Vessels and Internals	45
D. Systems and Plant--LMFBR	45
1. 1000-MWe Plant	45
E. EBR-II	48
1. Research and Development	48
a. Reactor Experimental Support--Reactor Analysis and Testing	48

TABLE OF CONTENTS

	<u>Page</u>
b. Nuclear Analysis Methods Development	60
c. Fuel Swelling and Driver Surveillance	60
d. Mark-II Driver Fuel Element Development	62
e. Equipment--Fuel Related	64
f. Equipment--Reactor and Primary Coolant System	65
g. Secondary Sodium and Power Systems	67
h. New Subassemblies Design and Experimental Support	68
i. Instrumented Subassembly	71
j. Process Chemistry	74
k. Experimental Irradiations and Testing	77
l. FCF Process Analysis and Testing	81
m. FCF Equipment Improvements	81
n. FCF Experimental Support--Hot Fuel Examination Facility (HFEF)--Feasibility and Cost Study	82
o. Superheater and EM Pump Study and Test	82
p. Feasibility Study of Fuel Failure Detection--Chemical and Mechanical Methods	84
q. EBR-II Materials-Coolant Compatibility	85
2. Operations--Reactor Plant	87
3. Operations--Fuel Cycle Facility	90
Publications	95
III. GENERAL REACTOR TECHNOLOGY	96
A. Applied and Reactor Physics Development--Research and Development	96
1. Theoretical Reactor Physics	96
2. Nuclear Data	97
B. Reactor Fuels and Materials Development	103
1. Fuels and Cladding--Behavior of Reactor Materials	103
2. Radiation Damage of Structural Materials--Research and Development	107
3. Techniques of Fabrication and Testing--Basic Fabricability--Research and Development	109
C. Engineering Development--Research and Development	111
1. Development of Master-Slave Manipulator Systems	111
2. Instrumentation and Control	113

TABLE OF CONTENTS

	<u>Page</u>
3. Heat Transfer, Fluid Flow, and Mechanics of Materials	114
4. Liquid-metal Linear Generator	117
5. Engineering Mechanics	118
D. Chemistry and Chemical Separations	119
1. Aqueous and Volatility Processes--Research and Development--Fluoride Volatility Process	119
2. Closed Cycle Processes--Research and Development--Compact Pyrochemical Processes	125
3. General Chemistry and Chemical Engineering--Research and Development	127
Publications	132
IV. NUCLEAR SAFETY	134
A. Other Reactor Kinetics--Research and Development	134
1. Fuel Meltdown Studies with TREAT	134
2. Materials Behavior, Equation of State, and Energy Transfer	135
3. Reactor Control and Stability	136
4. Coolant Dynamics	138
B. Operations	143
1. TREAT Operations	143
C. Chemical Reaction--Research and Development	144
1. Chemical and Associated Energy Problems (Thermal)	144
D. Effluent Control--Research and Development--Gaseous Effluent Studies	146
1. Plutonium Volatility Safety	146
Publications	148
PUBLICATION--GENERAL	148

I. PLUTONIUM UTILIZATION--CIVILIAN--EBWR

A. Research and Development1. Operational Consultation and Support (N. Balai)

Last Reported: ANL-7438, pp. 1-2 (March 1968).

a. Postirradiation Vessel Surveillance. Table I.A.1 summarizes the residual atmospheres and pressures in the accelerated irradiation capsules after they were exposed to 8.4×10^{19} n/cm² (of neutron energy $E > 1$ MeV) during the 4830 hr in which the reactor operated at an average power of 44 MWt. Capsule 4 contained control specimens that were not exposed to neutrons. Although two capsules had low residual gas pressure, inspection of the five Type 304 stainless steel high-pressure irradiation capsules with dye penetrant did not reveal unsound areas in the closure welds. None of the stainless steel capsules was hardened during the 4830-hr exposure.

TABLE I.A.1. Condition of Irradiation-surveillance Capsules and Specimens

Capsule No.	Final ^a Condition of Capsule Gas		Hardness of SA-212B Specimens, Rockwell-B Scale ^b	
	Pressure (psig)	Composition (%)	Avg	Min-Max
1	42	99.9 He	91.0	85.7-92.4
2	494	99.9 He	89.9	88.8-90.8
3	509	99.9 He	92.1	90.2-94.0
4 ^c	Atm	Contained water	80.2	78.2-82.9
5	475	99.4 He, 0.4 N ₂ , 0.1 O ₂	90.6	89.5-92.1

^aInitial fill pressure was 500 psig.

^bBased on average of three readings of each of the 30 pieces from the 15 broken Charpy vee-notch specimens (except for Capsule 4, on which one reading was taken on each of 12 pieces from 6 broken Charpy specimens).

^cCapsule 4 contained "control" specimens to determine the effect of temperature; it was in the 489°F steam dome of the reactor, where it saw essentially no neutrons. The other four capsules, which were at 489°F in the peak thermal-neutron flux in the reflector, were exposed to 8.4×10^{19} n/cm² of neutrons whose energies were greater than 1 MeV. Capsules 1 and 3 were shielded by 0.5-in.-thick 2%-boron stainless steel to reduce their exposure to thermal neutrons.

Table I.A.1 also shows that the SA-212B specimens were hardened only nominally during the 4830-hr surveillance irradiation.

The previously reported effects of radiation damage in Charpy vee-notch impact specimens of SA-212B steel have been confirmed. Additional impact data have been obtained from Charpy bars that had been in the other four capsules. As shown in Fig. I.A.1, irradiation caused an ~35% reduction of notched-bar impact strength (at 300°F) as well as an ~90°F upward shift of transition temperature at the reference level of 15 ft-lb specified in ASME SA-300. Note that the scatter band for unirradiated specimens (which is based on data from ~60 samples that were used to calibrate three impact test machines) has been used instead of the data from the control specimens in Capsule 4. This was done because the transition curve for the control specimens is believed to be invalid inasmuch as Capsule 4 lost its helium charge and water was found in the capsule. The enhanced impact strength of the control specimens is believed to have been caused by either one or both of the following processes: (a) decarburization of the notch surfaces (all control specimens had a uniform dense oxide coating) and (b) a long-term anneal at 489°F.

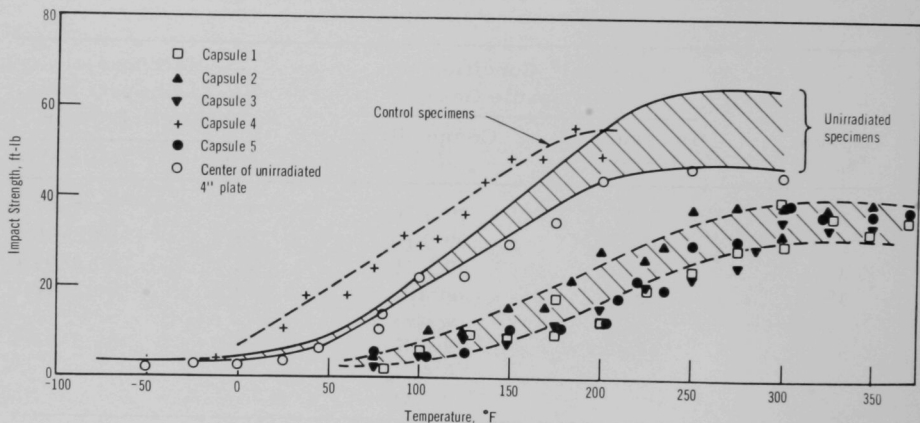


Fig. I.A.1. Strength of Irradiated (8.4×10^{19} n/cm²) SA-212B Vessel Surveillance Specimens after EBWR Operation with Plutonium Fuel. The data for the unirradiated control specimens in Capsule 4 are believed to be invalid.

This report completes the planned surveillance of the effects of radiation on the EBWR vessel steel. The accumulated exposure during the accelerated irradiation of the test specimens is estimated to be 8.4×10^{19} n/cm² ($E > 1$ MeV). Earlier evaluation* of damage effects showed no measurable reduction of impact resistance of vessel-steel specimens after they had

*Balai, N., *Impact, Magnetic, and Resonance Properties of Irradiated SA-212B Pressure Vessel Steel*, Trans. Am. Nucl. Soc. 7, No. 1, pp. 116-117 (1964).

been exposed to 1.6×10^{19} n/cm² ($E > 1$ MeV). The exposure of the vessel wall, at the core midheight and behind the 1-in.-thick 1%-boron stainless steel thermal shield, is estimated to have been 1.2×10^{18} n/cm² ($E > 1$ MeV). (The exposure estimates are based on activation data from foils and wires irradiated in the annulus between the vessel and biological shield at 20 MWt power in 1959.) Thus the surveillance program indicates that the wall of the EBWR reactor vessel was not damaged by radiation during its operational life.

b. Cracks in the Vessel Cladding. Bend tests have been completed on six 12-in.-long curved-beam samples from a clad practice plate.* In all samples, the cladding cracks propagated, in tension, through the thickness of the cladding between the resistance-welded "thumbprints." None of the cracks propagated into the SA-212B base plate, although the strain was beyond the yield point, i.e., 1% total. All beams were bent permanently.

Calculations that assume fully supported uniform beam sections show that beam strength varied within the range for a section without cladding and for a full-thickness member (including cladding). The variable load-carrying capacities of the beams at the elastic yield strength were influenced by the earlier cracks in the cladding. Table I.A.2 summarizes results of the bend tests. These beam-test data supplement earlier results described previously.*

TABLE I.A.2. Load Capacities of Composite Test Beams at 50,040 psi (Y.S. of SA-212B)

Sample No.	Beam Dimensions (in.) ^a		Load Capacity (lb)		
	Width	Thickness	Calculated	Measured	% of Calculation
1	0.522	0.387	216	187	86.7
2	0.554	0.385	228	164	75.2
3	0.495	0.388	206	165	80.1
4	0.520	0.377	204	168	82.4
5	0.520	0.384	212	167	78.8
6	0.552	0.353	190	b	-

^aIncludes cladding thickness of 0.109 in.

^bAccidentally overbent in fatigue test machine before bend test.

*Balai, N., et al., ANL-7117 (Nov 1965).

II. LIQUID-METAL FAST BREEDER REACTORS--CIVILIAN

A. Fuel Development--LMFBR

1. Metallic

a. Physical Metallurgy of Metallic Fuel Alloys (D. R. O'Boyle)

(i) Irradiation Behavior of Uranium-Plutonium-base Alloys

Not reported previously.

A program has been initiated to determine the mechanism that controls swelling in U-Pu-base fuels and also to establish the effects of temperature, pressure, burnup, and fuel composition on the swelling rate. Although bubble formation is normally associated with fuel swelling, other mechanisms may also be responsible for volume changes. In uranium and uranium-base binary alloys at burnups of less than 1 a/o, Angerman and Caskaey* and Leggett *et al.*** observed intergranular tears and crystallographically aligned tears within grains in the range of temperatures from 400 to 600°C. Above 600°C crystallographically aligned tears no longer were observed, grain-boundary tearing diminished in intensity, and small gas bubbles appeared dispersed randomly throughout the matrix.

The program will be a joint effort of ANL and Pacific Northwest Laboratory (PNL). Studies will be made before and after irradiation with binary and ternary alloys that have been injection-cast and heat treated. Uranium specimens will also be included in the study as control specimens. Alloy preparation and preirradiation studies will be made at ANL; PNL will perform the irradiations in temperature- and pressure-controlled capsules, and examine the alloys after irradiation. The results will be correlated with phase and irradiation studies of U-Pu-Zr alloys at ANL and also will be used as input data for computer studies of fuel-element performance. Data evaluation and technical publications will be a joint effort of both laboratories.

Specimens will be irradiated isothermally and at constant pressure within a range of temperatures from 400 to 800°C and a range of pressures from 50 to 5000 psi. Burnups will vary from 0.05 to several atomic percent. In initial studies high-purity alloys will be used; later, alloys with controlled additions of carbon, aluminum, silicon, and iron, with particular emphasis on the effects of silicon, will be included.

* Angerman, C. L., and Caskaey, G. R., Swelling of Uranium by Mechanical Cavitation, J. Nucl. Mater. 13(2), 182-196 (1964).

** Leggett, R. D., Bierlein, T. K., Mastel, B., and Taylor, H. A., Basic Swelling Studies, Proc. AIME Symp. on Radiation Effects, Ashville, North Carolina, September 1965, USAEC Report BNWL-SA-154.

High-purity depleted uranium, enriched uranium, "adjusted" uranium with minor alloy additions, and plutonium have been obtained for alloy preparation. Four injection-cast melts of the high-purity alloys have been made: U, U-5 w/o Pu, U-14 w/o Pu, and U-14 w/o Pu-12 w/o Zr. Each melt has been enriched with ^{235}U to a level that will give the same fission rate as U-14 w/o Pu when exposed to the same neutron flux.

Six as-cast and 18 heat-treated specimens from the uranium melt, and six as-cast and six heat-treated specimens (annealed in the body-centered-cubic, gamma-phase field for 24 hr) from each of the other three melts have been machined and shipped to PNL. These specimens are being encapsulated, and irradiation is expected to begin within a month.

Optical metallography as well as chemical, isotopic, and spectrochemical analyses of the four castings have begun at ANL.

Preparations have started for the next four melts: U-1 w/o Pu, U-2 w/o Pu, U-10 w/o Pu, and U-14 w/o Pu-6 w/o Zr. As reactor space becomes available, specimens from these melts will be sent to PNL for irradiation.

b. Fuel Element Performance (W. F. Murphy)

Last Reported: ANL-7445, pp. 1-2 (April 1968).

The three annular zones of a transverse section of element ND-30 (a nominally U-15 w/o Pu-10 w/o Zr fuel element irradiated to 4.6 a/o in Subassembly XA07 in EBR-II) have been analyzed for the fission-product neodymium in an attempt to find a nonmigrating fission product that could be used for burnup analysis. The results are compared in Table II.A.1 with those previously obtained for technetium (see ANL-7445, Fig. I.A.1, p. 1). Both neodymium and technetium apparently migrate from the middle zone, but at different rates.

TABLE II.A.1. Variation of Neodymium and Technetium in Annular Zones

Zone	Atomic Ratios ^a	
	$\frac{\text{Nd}}{\text{U} + \text{Pu}} \times 10^{-4}$	$\frac{\text{Tc}}{\text{U} + \text{Pu}} \times 10^{-3}$
Center	7.9	3.9
Middle	3.9	0.9
Outer	10.2	3.5

^aBased on original U + Pu composition.

Two elements (NC-17 and ND-24) irradiated in Subassembly XG05 to 6.9 a/o burnup were examined by neutron radiography at EBR-II. The fuel compositions were nominally U-15 w/o Pu-10 w/o Ti and U-15 w/o Pu-10 w/o Zr, respectively. The cladding of both elements was V-20 w/o Ti, the effective fuel densities were ~65%, and the maximum cladding temperatures were 540°C. Both elements appeared to be intact.

Examination of the neutron radiographs revealed similarities with the companion pair of elements that were irradiated to 5 a/o burnup (see Progress Report for April 1967, ANL-7329, p. 42). The fuel appeared to have expanded to the inside diameter of the cladding in both NC-17 and ND-24. The U-Pu-Ti fuel column in NC-17 was without axial separations and extended from the bottom plug up to and around the cruciform-type restrainer. The total elongation of the fuel was about 8.3%, of which about 3% was around the restrainer. Similar results (8.8% elongation) had been obtained with the fuel irradiated to 5 a/o burnup.

The U-Pu-Zr fuel in ND-24 had moved almost 3/8 in. off the bottom plug, and three axial separations were evident in approximately the middle third of the fuel column. The largest separation was about 3/16 in. The length of the fuel column, corrected for the separation, had decreased 3.3%. The U-Pu-Zr fuel element exposed to 5 a/o burnup had similar separations, but the fuel had elongated 3.6%.

Experimental Subassembly XO28, which contains fifteen U-15 w/o Pu-10 w/o Zr fuel elements (Group M-3), has been removed from EBR-II after accumulating a burnup of 1 a/o. The subassembly is suspected of containing a failed capsule that is leaking fission gas to the reactor coolant. The capsules in the subassembly will be examined by neutron radiography to locate the failed element.

c. Fabrication Development

Last Reported: ANL-7403, pp. 5-8 (Dec 1967).

(i) Fabrication of Irradiation Group M-4 Fuel Elements (H. F. Jelinek)

Thirty-one fuel elements have been fabricated and assembled preparatory to encapsulation and irradiation. The fuel pins (Group M-4) were requested as nominal U-15 w/o Pu-12 w/o Zr alloy pins clad in Types 304, 316, and 318 stainless steel, and in V-15 w/o Cr-5 w/o Ti and V-15 w/o Ti-7.5 w/o Cr alloys.

The fuel elements were fabricated from pins produced from four melts. The ranges of compositions among the four melts were 14.9 to 15.5 w/o Pu and 11.0 to 12.0 w/o Zr. The largest single impurity

was oxygen, which ranged from 300 to 1300 ppm. In two melts oxygen contamination was held to 300 and 600 ppm. Each melt was sampled and analyzed for isotopes, major and minor elements, and casting density. Metallographic specimens were prepared from representative castings, and historical samples were selected and stored.

The cladding hardware was assembled and examined, welding parameters were established, and specimens for burst and corrosion tests were prepared. The fuel elements, similar in design to those developed for Group M-4, were assembled, inspected, and transferred to the Fuels Performance Group for encapsulation. Fuel element inspection included bond testing, sodium level determination, leak detection, and determination of extent of surface contamination.

2. Oxide

a. Fuel Element Performance (F. L. Brown)

Last Reported: ANL-7445, pp. 2-3 (April 1968).

A reaction layer of 0.0025-in. average thickness was found at the interface of the mixed-oxide fuel and the V-20 w/o Ti alloy cladding after irradiation to a burnup of 3.5 a/o of element TVOV-1. Electron probe microanalyses of the reaction layer show approximately 8 w/o oxygen but no uranium, plutonium, or fission products. This substantiates thermodynamic calculations made elsewhere that indicate the possibility of such oxidation of the cladding. No significant quantities of oxygen were found in the unaffected regions of the cladding.

3. Carbide--Fabrication and Evaluation

a. Fuel Element Performance (J. H. Kittel)

Last Reported: ANL-7445, p. 3 (April 1968).

Irradiation of elements HMV-5, SMV-2, and NMV-11, which contain vibratorily compacted, physically mixed (discrete UC and PuC particles) fuel, was completed in Subassembly XG05 after a burnup of approximately 7 a/o at linear power ratings in the range from 24 to 26.6 kW/ft. The elements are clad with Hastelloy-X, Type 304 stainless steel, and Nb-1 w/o Zr alloy, respectively. Smear densities of the fuel range from 80 to 85% of theoretical. Neutron radiography indicated that all elements are intact with no apparent adverse structural features.

b. Compatibility between Fuel Carbide and Jacket Alloys
(T. W. Latimer)

Last Reported: ANL-7438, p. 6 (March 1968).

Tests of contact compatibility for 4000 hr at 800°C were completed with three alloys: Type 316 stainless steel, Timken alloy 16-25-6, and Hastelloy-X. After 1000 hr, the alloys had undergone effects that were considered to be small enough to justify testing for longer periods. The fuel was hyperstoichiometric ($U_{0.8}Pu_{0.2}C$) (5.25 w/o equivalent carbon) containing about 20 v/o $(U,Pu)_2C_3$.

(i) Type 316 Stainless Steel. Results of the 4000-hr test with Type 316 stainless steel showed effects very similar to those of an identical test with Type 304 stainless steel (see Progress Report for December 1967, ANL-7403, p. 10). Carbide precipitation was found within a zone in the stainless steel that averaged 140 μ from the $(U,Pu)C$ interface. The precipitation was observed both at grain boundaries and along slip lines within grains. Similar precipitation was observed in only a few isolated areas in the remainder of the stainless steel pellet.

As in the Type 304 stainless steel couple, sigma phase was almost entirely absent from the interface area of increased carbide precipitation, but was uniformly precipitated in the remainder of the pellet. This absence can be explained by the decreased content of chromium and molybdenum in the matrix as a result of the carbide precipitation.

(ii) Timken Alloy 16-25-6. The zone of fine molybdenum-rich precipitates found previously (see Progress Report for March 1967, ANL-7317, p. 55) in the 1000-hr tests was again observed after the 4000-hr test. No increase was observed in the depth of this zone as compared to the 25- μ depth found after the shorter tests.

(iii) Hastelloy-X. After the 4000-hr test, intergranular and intragranular precipitation was found in Hastelloy-X near the interface. The precipitate penetrated to an average depth of 90 μ (maximum depth = 140 μ). These precipitates were not observed after the 1000-hr tests.

No significant increases in the average depth of the $(U,Pu)Ni_3$ layer (5 μ) in the $(U,Pu)C$ or the chromium- and molybdenum-rich layer (3 μ) in the Hastelloy-X were found after the longer heat treatment. Likewise, the slightly larger reaction zones found at spots at which the cladding was in contact with $(U,Pu)_2C_3$ had not increased significantly.

4. Fuel Cladding and Structure--Jacket Alloys

a. Irradiation Studies of Fuel Jacket Alloys (R. Carlander)

Last Reported: ANL-7445, pp. 4-6 (April 1968).

Irradiation of vanadium alloys to fluences up to 3×10^{22} n/cm² resulted in an increase in yield strength at temperatures below 650°C, but did not appear to affect the tensile ductility over the temperature range from 400 to 750°C (see Progress Report for March 1968, ANL-7438, pp. 7-8). Since tensile tests of high strain rate are used, the resultant data, although encouraging, are not singularly applicable to fuel-element because the cladding in a fuel element is subjected to low strain rates and biaxial stress during irradiation. Uniaxial creep tests on irradiated materials are being made to represent steady-state reactor operating conditions better.

Uniaxial creep tests were conducted with specimens of V-20 w/o Ti that had a preirradiation grain size of 10 μ. The specimens were irradiated at 585°C in EBR-II in Sub-assemblies XA07 and XA09 to nominal fluences of 3×10^{22} and 2×10^{22} n/cm², respectively. The postirradiation tests were conducted at 650°C (in vacuum) with stresses between 17.5 and 35 kg/mm². The results are listed in Table II.A.2 and plotted in Fig. II.A.1. Unirradiated values are also shown in the figure for comparison.

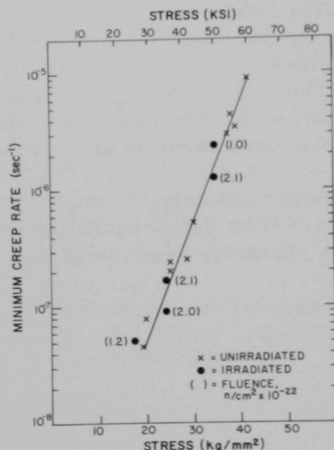
TABLE II.A.2. Minimum Creep Rate of Irradiated V-20 w/o Ti Alloy at 650°C

Fluence (n/cm ² x 10 ⁻²²)	Stress (kg/mm ²)	Minimum Creep Rate (sec ⁻¹)
1.2	17.5	5.1×10^{-8}
1.0	35.0	2.4×10^{-6}
2.0	24.5	9.0×10^{-8}
2.1	24.5	1.7×10^{-7}
2.1	35.0	1.3×10^{-6}

The postirradiation tests were conducted at 650°C (in vacuum) with stresses between 17.5 and 35 kg/mm². The results are listed in Table II.A.2 and plotted in Fig. II.A.1. Unirradiated values are also shown in the figure for comparison.

Fig. II.A.1

Minimum Creep Rate of V-20 w/o Ti Alloy as a Function of Applied Stress at 650°C



Irradiation up to a fluence of 2×10^{22} n/cm² had no effect on the minimum creep rate of V-20 w/o Ti alloy (see Fig. II.A.1). This lack of change in the minimum creep rate agrees with the small increase in tensile strength and the absence of an effect on the tensile ductility of the alloy at 650°C after irradiation to 3×10^{22} n/cm² (see ANL-7438, pp. 7-8).

During irradiation, changes in the mechanical properties of austenitic stainless steels at elevated temperatures are believed to be influenced by helium gas bubbles generated by n, α reactions and by voids produced by vacancy clustering. Thus, the indicated resistance of V-20 w/o Ti alloy to changes in mechanical properties as a result of irradiation may be due to the lack of a significant buildup of these irradiation-induced defects. In order to confirm this observation, a specimen of V-20 w/o Ti irradiated to 3×10^{22} n/cm² is being analyzed by transmission microscopy.

b. Fabrication Development of Fuel Jacket Alloys (N. J. Carson)

Last Reported: ANL-7427, p. 8 (Feb 1968).

V-15 w/o Cr-5 w/o Ti alloy was chosen for a quenching study because of its availability and the knowledge gained from previous studies. Specimens were quenched from temperatures between 800 and 1600°C. The hardness, grain size, and second-phase distribution of the quenched specimens are being compared with the characteristics of specimens slow-cooled from identical temperatures. All specimens have been prepared and photographed; however, interpretation of the photographs is just beginning.

In order to interpret accurately the behavior of this alloy, the behavior of unalloyed vanadium and of binary vanadium alloys under similar test conditions must be known. Therefore, two 15-lb billets were consolidated. The first was a V-10 w/o Cr alloy billet and the second was an unalloyed vanadium billet. A portion of the V-10 w/o Cr alloy billet will be used in the structure study, and the remainder will be used in a fabrication study. The V-10 w/o Cr alloy specimens are also needed for both creep and corrosion tests. The unalloyed vanadium will be used to determine the effect of heat-treatment on microstructure in the absence of alloying elements.

Approximately 50 running feet of V-15 w/o Cr-5 w/o Ti alloy tubing (0.290-in. OD by 0.260-in. ID) was made for use in the creep tests. The tubing is presently being inspected.

B. Physics Development--LMFBR

1. Theoretical Reactor Physics--General Fast Reactor Physics

a. Reactivity Coefficients (H. H. Hummel)

Last Reported: ANL-7391, pp. 20-21 (Oct 1967).

(i) Higher-order Perturbation Theory. Calculations of reactivity changes in second-order perturbation theory, and of many other reactor parameters in first-order perturbation theory, require previous calculation of the first-order derivatives of the neutron flux.* Similarly, calculations of reactivity changes in (M+1)-order perturbation theory and of many other reactor parameters in Mth-order perturbation theory require previous calculation of the Mth-order flux derivatives.

A general method is being developed to calculate the flux derivatives within the framework of perturbation theory. Application of the method to an ELMOE** fundamental-mode calculation of the spectrum at the center of ZPR-6 Assembly 48† has yielded the results shown in Figs. II.B.1, II.B.2, and II.B.3. The figures show, respectively, the zeroth, first, and second derivatives of the energy spectrum with respect to the sodium concentration. The spectrum is normalized to yield a unit fission source. The cross sections used in the calculations were somewhat arbitrary. Derivatives of the spectrum were found to be in excellent agreement with those from finite-difference calculations.

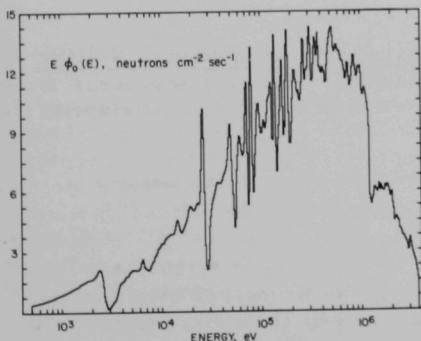


Fig. II.B.1. Neutron Flux in Assembly 48 of ZPR-6

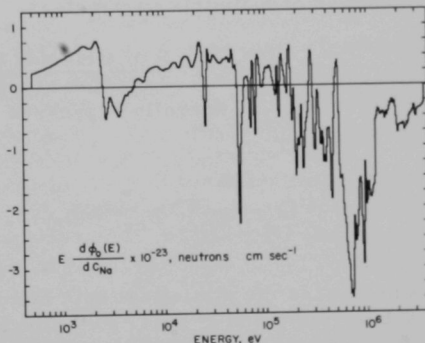


Fig. II.B.2. First Derivative with Respect to Sodium Concentration of the Neutron Flux in Assembly 48 of ZPR-6

*Usachev, L. N., *Atomnaja Energija* 15, 472 (1963); Storrer, F., *Fast Breeder Reactors*, Pergamon Press, 683 (1966); Gandini, A., *J. Nucl. Energy* 21, 755 (1967).

**Rago, A. L., and Hummel, H. H., ANL-6805 (1964).

†Broomfield, A. M., *et al.*, ANL-7320, p. 205 (1966).

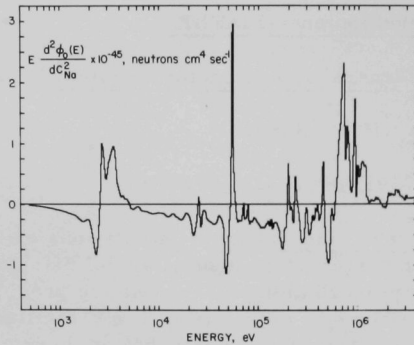


Fig. II.B.3

Second Derivative with Respect to Sodium Concentration of the Neutron Flux in Assembly 48 of ZPR-6

(ii) Statistical Behavior of Complex Poles for Two Interfering Levels

(a) Introduction. An important problem in the calculation of fission and capture cross sections and of Doppler effects of fissile materials in the energy range below a few keV is evaluation of multilevel effects. Since in most of the energy region of interest resolved resonance parameters are not available, a statistical theory must be applied to generate such parameters. As part of the studies of this topic, an illustrative example of the statistical characteristics of multilevel resonance parameters was carried out for the case of two interfering levels. Even though the assumed two-level case may be unrealistic, the distribution functions in their explicit functional form will shed some light on the statistical behavior of S-matrix parameters.

(b) R-matrix and S-matrix Representation of Nuclear Cross Sections. The reaction cross section for a particular process x and total spin j is generally expressed in terms of a collision matrix with elements $U_{cc'}$:

$$\sigma_x^j = \pi \lambda^2 g_j \sum_{c'} |\delta_{cc'} - U_{cc'}|^2,$$

where g_j is the statistical spin factor, $\delta_{cc'}$ the Kronecker delta, and the subscripts c and c' refer to the incident and exit channels, respectively. The corresponding total cross section is expressed as

$$\sigma_T^j = \pi \lambda^2 g_j 2\text{Re}(1 - U_{cc}).$$

The collision matrix usually has been described by either one of two representations. The first of these is the R-matrix model.* In R-matrix theory, the elements of the collision matrix are given by

$$U_{cc'}^{(R)} = e^{i(\phi_c + \phi_{c'})} \left[\delta_{cc'} + i \sum_{\mu, \nu} \Gamma_{\mu c}^{1/2} \Gamma_{\nu c'}^{1/2} A_{\mu\nu} \right],$$

where

$$\Gamma_{\mu c}^{1/2} = (2p_c)^{1/2} \gamma_{\mu c};$$

p_c = penetration factor of channel;

$\gamma_{\mu c}$ = reduced-width amplitude;

ϕ_c = hard-sphere potential-scattering phase shift;

ν, μ = levels;

$A_{\mu\nu}$ = the level matrix with the reciprocal of $A_{\mu\nu}$ defined as

$$A_{\mu\nu}^{-1} = (E_\mu - E) \delta_{\mu\nu} - \frac{i}{2} \sum_c (\Gamma_{\mu c})^{1/2} (\Gamma_{\nu c})^{1/2}.$$

For practical purposes, the direct application of the R-matrix formulation to reactor Doppler analysis is extremely complicated not only because it involves the difficulty of the inversion of the level matrix $A_{\mu\nu}$, but also because it makes subsequent Doppler broadening and flux-average computations rather impractical. Also, the energies E_μ of the R-matrix levels may not correspond to actual peaks in the cross section. On the other hand, the advantage of the R-matrix formulation lies in the fact that the statistical properties of resonance parameters such as eigenvalues E_μ and widths $\Gamma_{\mu c}$ have been studied extensively. Such knowledge of the statistical properties of resonance parameters is invaluable in the unresolved energy region.

In the second form of the collision matrix, referred to here as the "S-matrix" form, there is a simple sum of terms corresponding to actual peaks in the cross section. As given by Moldauer,** the form is

*Wigner, E. P., and Eisenbud, L., Phys. Rev. 72, 29 (1947).

**Moldauer, P. A., Phys. Rev. 135, p. B642 (1964).

$$U_{cc'}^{(S)} = e^{i(\phi_c + \phi_{c'})} \left(W_{cc'} - i \sum_{\mu} \frac{g_{\mu c} g_{\mu c'}}{E - p_{\mu}} \right),$$

where $W_{cc'}$ is an element of a complex matrix independent of E and p_{μ} , the μ th complex pole of $U_{cc'}$, is defined as

$$p_{\mu} = \epsilon_{\mu} - \frac{1}{2} i \Gamma_{\mu}^{(S)}.$$

Here ϵ_{μ} and $\Gamma_{\mu}^{(S)}$ are energies and widths, respectively, for the levels μ of $U^{(S)}$; $g_{\mu c}$ and $g_{\mu c'}$ are complex parameters.

It has been shown by Adler and Adler* that, when the collision matrix has the form $U_{cc'}^{(S)}$ with $W_{cc'}$ equal to $\delta_{cc'}$, Doppler-broadening calculations can be carried out readily in terms of the usual ψ and χ functions used in one-level Doppler-broadening calculations. The same can also be shown readily when $W_{cc'}$ is an arbitrary complex constant matrix. The formulation in terms of $U_{cc'}^{(S)}$ does have the disadvantage, however, in that there does not appear to exist a theory of the statistical distribution of the parameters. An approach taken by Moldauer** and used here is to infer the statistical properties of the parameters in $U_{cc'}^{(S)}$ from the properties of those in $U_{cc'}^{(R)}$ by diagonalizing $U_{cc'}^{(R)}$ into the form $U_{cc'}^{(S)}$.

(c) Illustrative Two-level Calculations. The case considered here was based on the following assumptions:

1. The number of capture channels equals infinity.
2. There exists a single predominant channel x , i.e., $\langle \Gamma \rangle \cong \langle \Gamma_x \rangle$.
3. The R-matrix parameters Γ_x and D (level spacing) are described by a Porter-Thomas† distribution and a Wigner†† distribution, respectively.

Figures II.B.4 and II.B.5 show the probability density functions for the S-matrix level spacing $D^{(S)}$ and width $\Gamma^{(S)}$ obtained analytically by means of the assumptions given above. The distribution functions for S-matrix parameters may differ significantly from the corresponding R-matrix parameters if $\langle D \rangle / \langle \Gamma \rangle$ becomes small. The characteristics of these curves can be explained mathematically. Other quantities of

* Adler, D. B., and Adler, F. T., Neutron Cross Sections in Fissile Elements, ANL-6792, p. 695 (1963).

** Ibid, previous page.

† Porter, C. E., and Thomas, R. G., Phys. Rev. 104, 482 (1956).

†† Wigner, E. P., Proceedings of the Conference on Neutron Physics by Time of Flight, ORNL-2309 (1956).

interest, such as the average values $\langle D(S) \rangle$ and the variance of these distributions, were also obtained analytically.

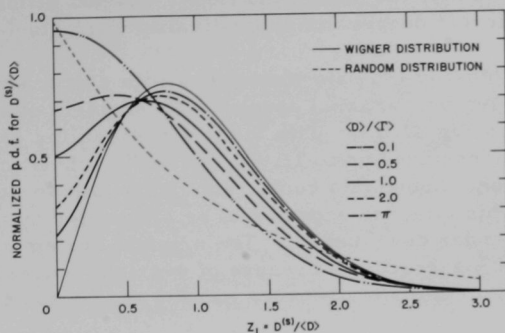


Fig. II.B.4. The Probability Density Function for the S-matrix Level Spacing

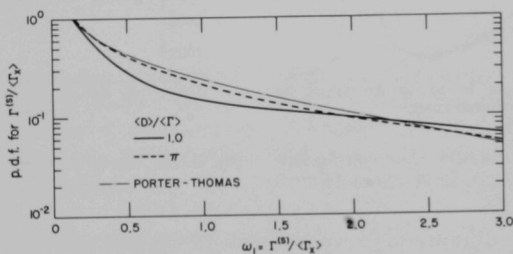


Fig. II.B.5. The Probability Density Function for the S-matrix "Total Width"

2. Experimental Reactor Physics--Fast Critical Experiments-- Experimental Support (Idaho) (W. G. Davey)

Last Reported: ANL-7445, pp. 9-10 (April 1968).

a. Neutron Spectrometry

(i) High-count-rate Electronics. In continued studies with high-count-rate electronics, a comparison was made between the new amplifier system and the equipment that has been used previously with the proton-recoil spectrometer. The objective was to retain good discrimination between gamma-ray and neutron-induced pulses at high count rates in order to permit spectrum measurements at close to critical.

A series of specific ionization spectra were taken over the energy range from 0.5 to 3 keV in Assembly 51 of ZPR-3 with both counting systems under identical conditions. Several different count rates representing different degrees of subcriticality were studied.

Most of the data were taken with a new, smaller-diameter (0.375 in.) hydrogen proportional counter. An example of such measurements is shown in Fig. II.B.6. With the new system, the gamma and proton peaks are clearly resolved up to 15,000 cps (0.2% subcritical) with essentially no distortion. Above this count rate, pulse pileup begins to distort the spectrum. This effect is expected to be eliminated by utilizing a pile-up rejector now under development. The original system shows distortion above 5000 cps (2% subcritical) because of overload pulses, and at 10,000 and 15,000 cps discrimination between gamma and proton events was lost.

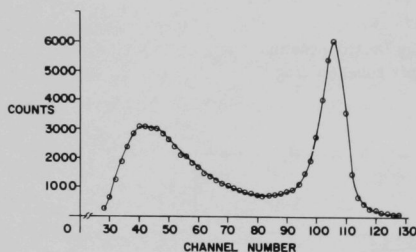


Fig. II.B.6a. Specific Ionization Spectrum for New Amplifier System at 10,000 cps

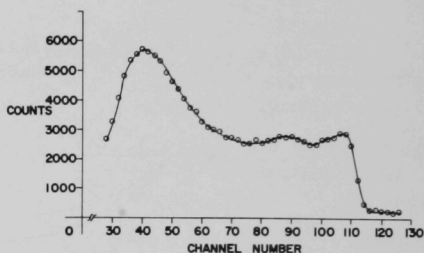


Fig. II.B.6b. Specific Ionization Spectrum for Original Amplifier System at 10,000 cps

Studies also were made in which the new electronic system was used with the larger-diameter (0.625 in.), hydrogen-filled proportional counters that were previously used for spectrum measurements in ZPR-3 Assembly 51 at 7% subcritical. Results indicated that a spectrum measurement would have been possible at 2% subcritical with the use of the pileup-rejection electronic equipment. The degree of subcriticality could have been further reduced to 0.2% with the use of the smaller counters.

b. Heterogeneity Studies. The investigation of fission-product gamma rays by use of a lithium-drifted detector continued with the study of a thorium foil irradiated in a fast spectrum in AFSR. This investigation of ^{232}Th fission-product yields was initiated to determine the differences compared to ^{235}U , ^{239}Pu , and particularly ^{238}U . Preliminary analysis showed that ^{232}Th has definitely greater relative yields of isotopes on the low-mass side of the fission-product mass distribution. Thorium is also convenient for study of fission products with low gamma-ray energies since its natural background in the low-energy region is quite low. More detailed analyses of the spectra are in progress.

An analysis has been made of a sample of EBR-II cover gas. Several components have been identified, including ^{41}Ar , ^{133}Xe , $^{133\text{m}}\text{Xe}$, ^{135}Xe , $^{85\text{m}}\text{Kr}$, ^{88}Kr , and ^{88}Rb . Several other peaks remain to be identified in the gamma-ray spectra.

A question has been raised about the conversion coefficient of the 81.01-keV ^{133}Xe gamma ray. Assuming that equilibrium of $^{133\text{m}}\text{Xe}$ and ^{133}Xe was established before the gas sample was taken, that the conversion coefficient for the 233-keV $^{133\text{m}}\text{Xe}$ isomeric transition is 6.3, and that $^{133\text{m}}\text{Xe}$ is produced to the extent of 1.4% from ^{133}I , then the calculated conversion coefficient of the 81.01-keV ^{133}Xe gamma ray is about 1.5, in good agreement with the values in the literature. A strong backscattering peak at 64 keV is observed, however, which would probably not be resolved with NaI detectors and may make the 81-keV line seem more intense than it actually is.

c. Computer Applications. The Request for Proposal for the major components of a ZPPR computer system is under review by system suppliers. Initial inquiries by the potential suppliers indicate a capability for compliance with the general specification with a broad spectrum of computers.

A preliminary version of a CDC-1604 program for producing a ZPPR fuel-inventory record tape and for keeping a current record of each fuel-piece location is operational. Improvements in versatility, including recording of the ZPR-3 plutonium fuel inventory, will be incorporated as soon as practicable. The inventory program requires information about each fuel piece (plate identification, isotopic composition, etc.) which is provided by the fuel manufacturer on IBM cards. As cards are provided, fuel-transfer records will be produced to update the master-inventory tape.

d. Integral Studies of Cross Sections. Efforts related to the data testing of ENDF/B using integral experiments and to the examination of the evaluations constituting the data file have been initiated.

The initial involvement with ENDF/B has been the review of the "Phase II" data-testing effort using the Assembly-48 benchmark analysis. Several of the companies and agencies in the fast reactor industry have submitted calculational analyses of Assembly-48 experiments using ENDF/B with varying degrees of modification. The intention was to judge the quality of particular material data on the basis of the calculational/experimental correlations. However, the modifications in the ENDF file which were made in many instances and the deviations in results between the different analyses made the useful judgment of cross-section quality quite difficult. Some errors and required re-evaluations

in the file were indicated in the analyses. A review of the analyses has provided some recommendations for improving the data-testing procedure and establishing a re-evaluation mechanism.

e. Pulsed-source Experiments. A number of developmental pulsed-source experiments have been performed in ZPR-3 Assembly 51, for the purpose of establishing suitable techniques for using this experimental method in the plutonium-fueled cores of ZPPR and ZPR-3.

Data were taken as a function of reactor subcriticality from BF_3 detectors positioned in the core, in Ni-Na Reflector I, and in Fe Reflector II. The reactor was pulsed at the core center with a Texas Nuclear 9405 neutron generator. The d,t reaction was used, with injection of 14-MeV neutrons with pulse widths of 1 μsec and repetition rates of ≈ 1400 per second.

Machine analysis of the data is in progress. Prior to curve fitting and parameter extraction, the data must be corrected for the dead time of the analyzer. Preliminary analysis of the uncorrected data indicates that at least two exponentials will be required for a proper fit. The second exponential is due to the neutrons which are returned to the core by the reflector. Similar behavior was observed in experiments with ZPR-3 Assemblies 46B and 46C, and with the SEFOR mockup.*

The raw data also show a definite delay after the pulse in attainment of a maximum slope in the die-away curve. The core data show only a negative-going exponential, whereas the reflector data indicate both a positive and negative exponent, which is characteristic of a finite pulse-propagation time from the source to the detector location.

The data were taken with the reactor varied from -213 to -1307 lh subcritical. Preliminary indications are that the ^{240}Pu spontaneous-fission neutron source does not interfere with the conduct of the pulsed-source experiments, at least up to about -200 lh subcritical.

A part of the proposed analysis of the data will be an attempt to calculate the reactivity from both the core and reflector parameters. The effects of the ^{240}Pu spontaneous-fission neutron source is as yet undetermined.

*Brunson, G.S., and Huber, R. J., A Two-region Analysis of Pulsed Neutron Die-away Measurements in Three Reflected Fast Critical Assemblies, paper submitted to Nuclear Science and Engineering.

3. Experimental Reactor Physics--Fast Critical Experiments-- Experimental Support (Argonne)

a. Neutron Spectrometry (R. Gold)

Last Reported: ANL-7419, p. 9 (Jan 1968).

Measurements of the neutron spectrum in Assembly 6 (oxide- ^{235}U fueled) of ZPR-6, have been made and some results have been reported previously (see Progress Report for February 1968, ANL-7427, p. 13). These measurements have been reanalyzed and compared with a MC^2 calculation (see Fig. II.B.7). The data (with errors attached) and the calculation were "area" normalized.

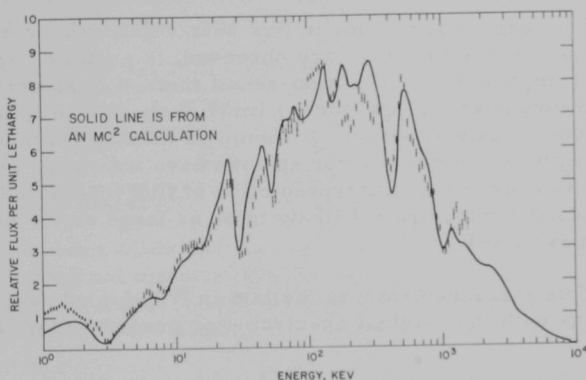


Fig. II.B.7. Comparison of the Proton-recoil Fast-neutron Spectral Measurements in ZPR-6 Assembly 6 with a MC^2 Calculation

The calibration procedures for establishing a relationship between A (gas multiplication) and V (voltage) were studied in more detail than had been done previously. Using both ^{37}A beta decay and protons from $^{14}\text{N}(n,p)^{14}\text{C}$, a broad range of multiplication versus voltage could be investigated in a single counter and without space-charge saturation. Various prescriptions for plotting A versus V were tried to see if an adequate representation over the full range could be obtained. The relationship $(\log A)/V$ plotted versus V was found to be substantially better than an older method in which $(\log A)/V$ was plotted versus $\log V$. The differences were not appreciable except below 10 keV. The improved calibration was applied to the data of Fig. II.B.7.

An adequate representation of A as a function of V is not, in itself, sufficient to insure a correct energy-scale calibration, since variations in W (electron-volt loss per ion pair) will also occur and should be

allowed for. At present, W is assumed constant (above 0.4 keV) and this simple picture probably needs improvement. Failure of this model can account for some of the discrepancy observed between the location of resonance flux-depression effects as indicated by measurement and calculation.

The resonance minima disagree by approximately 5% for the prominent resonances in iron (at 30 keV) and in sodium (at approximately 3 keV). Additional experimental work is needed.

The marked flux depression at 1 MeV has been observed in previous in-core experimental spectra, but only predicted (and not too well) in the more recent MC² results.

The large discrepancy in flux near 1 keV, where MC² predicts substantially fewer neutrons than are observed, is another interesting result of the comparison. The proton-recoil method is subject to larger systematic errors near the low-energy limit of about 1 keV, and additional work should clarify this situation. It should be mentioned, however, that the most recently measured reactor spectra have not shown any persistent trend toward an over- or an underprediction of flux (compared with calculations), and errors are not likely to be as large as the observed discrepancy near 1 keV.

This measurement was the last in ²³⁵U-fueled reactors and the last to be made with the original spectrometer used over the last two to three years.

Newer apparatus will permit better resolution (by a factor of two) and much greater reliability.

4. ZPR-3 Operations and Analysis (W. G. Davey and R. L. McVean)

Last Reported: ANL-7445, pp. 11-15 (April 1968).

a. Mockup Studies. Experiments with Assembly 51, the first core of the FTR Phase-B critical program, were concluded. Work began with Assembly 52, the second core of the program. The information below consists mainly of results from Assembly 51.

(i) Analysis of Measurements of March 1968 with Assembly 51. The measurements of the distributed worths of ²³⁸U and U₃O₈, and the worth as a function of axial position of a section of core material in the P-16 matrix position, have been given (see Progress Report for March 1968, ANL-7438, pp. 12-16). Further descriptions of the experiments and the final results are given below.

(a) Distributed Worths of ^{238}U and U_3O_8 . The distributed worths of ^{238}U and U_3O_8 were measured in the same positions in Assembly 51 in a large number of core drawers.

The reference core drawers in Assembly 51 have a 2-in.-high column of U_3O_8 . Prior to this series of measurements, the 2-in.-high column in A-type[†] drawers was replaced with two half-height (1-in.) columns. The half-height columns extended 16 in. from the reactor midplane. The remaining 1 in. of core was occupied by full-height U_3O_8 and was not changed during the substitution. The worth of U_3O_8 was measured by removing a half-height column of U_3O_7 . The worth of ^{238}U was measured by placing half-height depleted uranium in the spaces vacated by the U_3O_8 . Because of limitations of material inventory, the measurements were made in a stepwise manner, with 12 drawers and then 100 drawers, to obtain the total worth for all 112 A-type drawers.

TABLE II.B.1. Compositions of (1/8 by 1 by 2 in.) Pieces

Material	^{235}U (g)	^{238}U (g)	O (g)
U_3O_8	0.055	25.24	4.475 ^a
Depleted Uranium	0.15	74.47	0

^aResin coating (0.016 g) included as O.

The material changes were accomplished with the use of 1/8- by 1- by 2-in. pieces of U_3O_8 and depleted uranium, respectively. The compositions of the pieces are given in Table II.B.1. The steps at which

measurements were made and the experimental results are summarized in Table II.B.2. The net material change in each case was obtained by multiplying the number of pieces involved (from Table II.B.2), by the respective constituents (from Table II.B.1).

TABLE II.B.2. Summary of Distributed Worths of ^{238}U and U_3O_8

Material	Number of A-type Drawers	Number of Pieces	Worth (lh)	Remarks
U_3O_8	12	96	-5.079	Removal of U_3O_8
	100	800	+51.10	Removal of U_3O_8
	112	896	+46.02	Sum
Depleted Uranium	12	96	-20.68	Addition of ^{238}U
	100	800	-338.52	Addition of ^{238}U
	112	896	-359.20	Sum

(b) Axial Worth of Core Material in P-16 Matrix Position.

The core portion in the central matrix position (P-16) in each half was loaded with a 7-in. segment of core material, nominally composition A, and two 5-in. segments of sodium. Each segment filled the 2- by 2-in. cross section of the drawer. The axial reflectors of the matrix position remained unchanged. Reactivity measurements were taken with the core-material segments in each half occupying the following positions, as measured from the reactor midplane: 0 to 7 in., 5 to 12 in., and 10 to 17 in. The sodium was reloaded in each case to occupy the remaining volume.

[†]A-type drawers are those in even-numbered matrix columns and A*-type are those in odd-numbered matrix columns. The compositions of these drawers are given in the Progress Report for January 1968, ANL-7419, p. 11.

The composition of a 7-in. segment of core material is listed in Table II.B.3. The segments in both halves were of identical composition and were in the same position relative to the reactor midplane for each measurement. Each 5-in. segment of sodium consisted of eight pieces of sodium contained in stainless steel cans with nominal dimensions of 1/4 by 2 by 5 in. Each sodium plate contained 29.92 g of sodium and 45.74 g of stainless steel.

TABLE II.B.3. Composition of a 7-in. Core Segment

Material	Width (in.)	Total Weight (g)	²³⁹ Pu (g)	²⁴⁰ Pu + ²⁴² Pu (g)	²⁴¹ Pu (g)	²³⁵ U (g)	²³⁸ U (g)	Na (g)	C (g)	O (g)	SS (g)	Mo (g)	Al (g)
Na ₂ CO ₃	0.25	159.74						43.23	11.29	45.14	60.08		
U ₃ O ₈	0.125	206.77				0.385	175.33			31.05 ^a			
ZPPR Fuel	0.25	850.23	192.90	26.00	3.36	1.19	538.13				69.15	19.50	
Na	0.25							43.25			66.31		
SS	0.125										215.03		
Na ₂ CO ₃	0.25	159.74						43.23	11.29	45.14	60.08		
Na ₂ CO ₃	0.25	159.74						43.23	11.29	45.14	60.08		
Depleted U	0.125	520.09				1.08	519.01						
Pu Alloy	0.125	303.28	230.31	11.03	0.0997						58.24		2.70
Na	0.25							43.25			66.31		
Totals	2.0		423.21	37.03	4.357	2.655	1232.47	216.19	33.87	166.48	655.28	19.50	2.70

^a Resin coating weight (0.112 g) is included as oxygen.

The reactor during this series of measurements contained five more core drawers than the reference loading[†] to compensate for the loss of fuel in P-16. Positions K-20 and K-12 in both halves and L-21 in Half II were loaded with core drawers (Type A in K-20 and K-12; Type A* in L-21). The reactivity changes due to the displacements of the core-material segments away from the reactor midplane are given in Table II.B.4.

TABLE II.B.4. Axial Worth of Core Material, P-16 Matrix Position

Position of the Core-Material Segments (in. from the reactor midplane)	Reactivity Change (th)
0 to 7	0
5 to 12	-92.02
10 to 17	-206.78

(ii) Recent Measurements

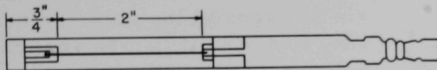
(a) Measurements of Neutron Spectrum. Measurements of proton-recoil spectra were made with high-count-rate electronics (see Sect. II.B.2.a.(i)) and a 3/8-in.-dia hydrogen counter in an attempt to derive neutron spectra close to criticality. These measurements were made with the reactor 0.2% subcritical. No count-rate distortion was observed, but the computer data buffer was unable to handle the higher count rate. Consequently, proton spectra were measured only over the energy range from 0.5 to 3.0 keV, and no complete neutron spectrum was obtained. For completeness, tests also were made with counters used for

[†] See Progress Report for January 1968, ANL-7419, p. 11.

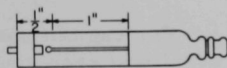
the previous measurements with the reactor 2% subcritical compared to 7% subcritical for the complete spectrum measurements already reported.

(b) Reaction Rate Traverses. Reaction rate traverses in Assembly 51 were made with three different counters. Two of these were brass, gas-filled fission counters employing ^{239}Pu and ^{238}U , and the third was a stainless steel-clad BF_3 proportional counter. These counters were traversed in two separate geometries axially and two separate geometries radially, for a total of four separate traverses for each counter. A power level of 3 W was maintained by the autorod for the BF_3 and ^{239}Pu counter measurements, and a power level of 30 W was held for the ^{238}U measurements.

$^{10}\text{B}_5$: Counter No.: RSN-2105 F-2199
Composition: $^{10}\text{BF}_3$ (20 cm)
Drawing:



^{239}Pu : Counter No.: R
Batch No.: 3-3-5007
Composition: 94.92% ^{239}Pu 0.77 mg/cm²
4.75% ^{240}Pu
0.315% ^{241}Pu Loading: 6.55 mg
0.010% ^{242}Pu
Drawing:



^{238}U : Counter No.: IC-24-4
Batch No.: 6-6-5003
Composition: Depleted Loading: 4.4 mg
80 PPM ^{235}U
Drawing:

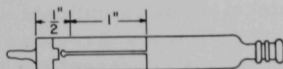


Fig. II.B.8. Counters Used in Reaction Rate Traverses

A drawing and the specification of each counter used is given in Fig. II.B.8. The counters were held by one turn of 1 mil by 3/8-in. "Scotch tape" to a stainless steel "boat," 23 in. long, which was traversed down a 5/8-in.-OD stainless steel tube. The "boat" is a 1/2-in. stainless tube cut down to leave three 1-in. flanges and a 1/2-in. strip along the bottom. This was connected by a 1/4-in. stainless steel tube to the traversing mechanism. The traversing mechanism is a mechanical drive, remotely operated from the control room, which provides a travel from 0 to 65.30 in. with a mechanical readout accuracy of 0.03 in.

In the axial position, the counters were traversed down the center of the core and through the axial blanket in the 1- and 2-P-16 drawers. The two separate geometries used were different in the orientation of the fuel plates in the 1- and 2-P-16 drawers. In the normal configuration, the fuel plates were loaded vertically as in the normal reactor loading, with the other constituents loaded around the 1-in.-square guide tube. In the rotated geometry, the fuel plates were loaded horizontally in the 1- and 2-P-16 drawers. Figure II.B.9 is a cross-sectional view of these two loading configurations.

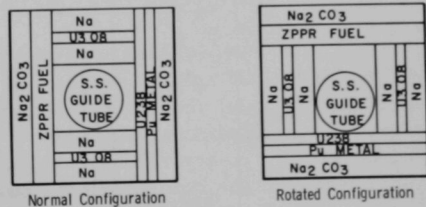


Fig. II.B.9. Axial Traverse Drawer Loadings (front view)

Radially, the counters were traversed $1\frac{1}{4}$ in. from the reactor midplane in the P-row in Half I. The plate arrangement for the A- and A*-type drawers to accommodate the traverse tube is shown in Fig. II.B.10. It should be noted that Fig. II.B.10 is illustrative only and not to scale. The two radial geometries in which the counters were traversed were:

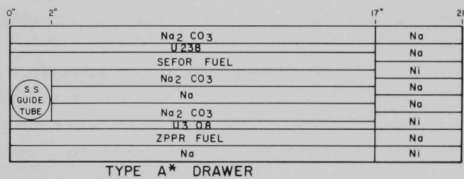
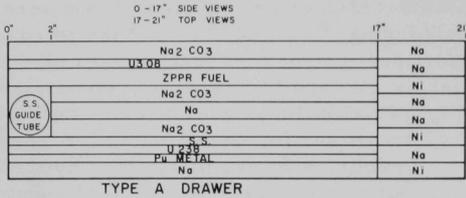


Fig. II.B.10. Radial Traverse Drawer Loadings for Assembly 51

(1) Normal--the plate arrangement in the drawers directly opposite the traverse tube, i.e., P-row Half II, was vertical.

(2) Rotated--the plate arrangement in P-row, Half II was horizontal and continuous with the loading of the P-row, Half I.

For ease of comparison, the results of each counter in the two axial geometries are plotted together and the results for each counter in the two radial geometries are plotted together; see Figs. II.B.11 through II.B.16. The radial positions of the safety rods are marked on the radial traverse graphs, as well as the core centerline and the core-reflector interface, or as to indicate where the counters entered the region of the lightly loaded drawers directly above and below the safety rods. The points on the graphs represent the position of the center of the active area of the respective counters.

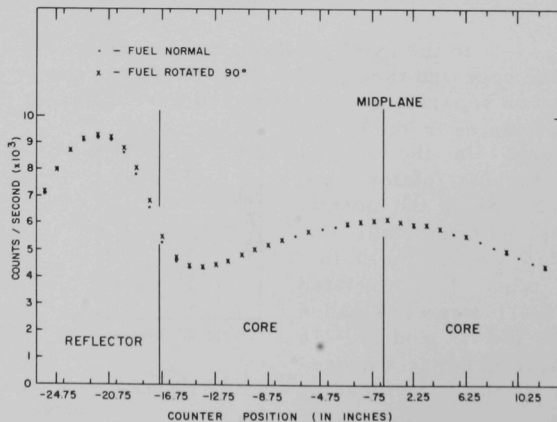


Fig. II.B.11. BF₃ Counter--Axial Traverse

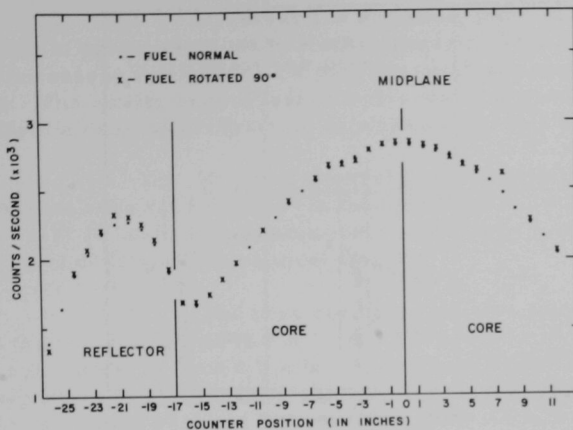
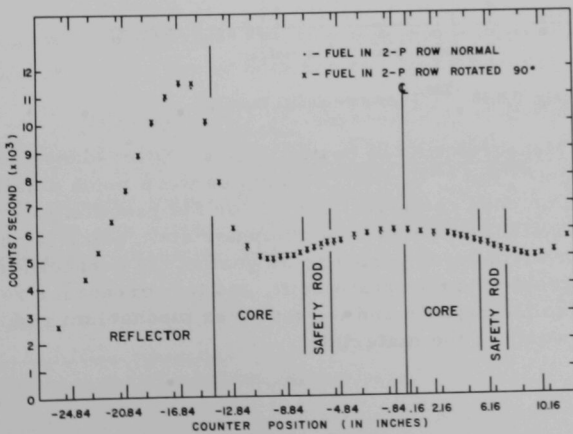
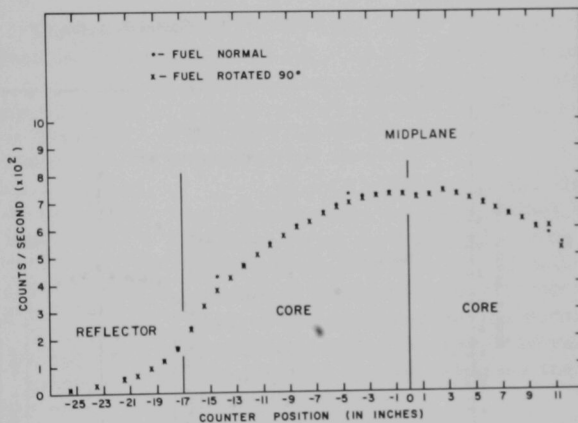
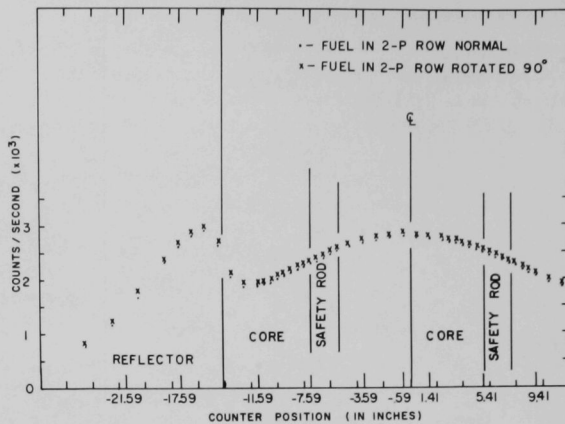
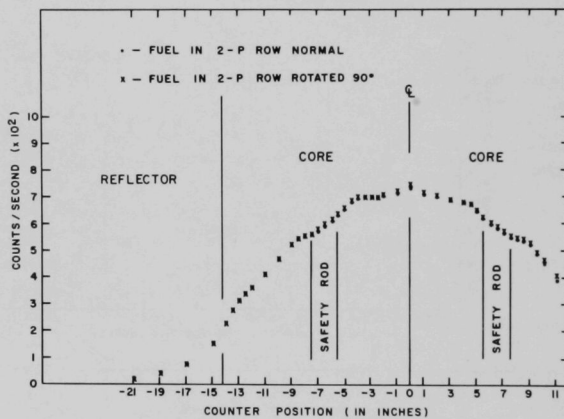


Fig. II.B.13
 ^{238}U Counter--
 Axial Traverse



Fig. II.B.15. ^{239}Pu --Radial TraverseFig. II.B.16. ^{238}U Counter--Radial Traverse

(c) Measurements of Spatial Worth. Space-dependent worth measurements of ^{239}Pu , ^{238}U , and ^{10}B samples were made axially and radially in the same core configurations as for the reaction rate traverses. The raw data will be treated by a computer code which is now in preparation to (a) convert autorod positions to worths, (b) correct for reactivity effects of reactor temperature drift, and (c) correct for reactivity effects of the sample capsule and the traverse mechanism rod, giving the space-dependent worth of the materials.

Preparations are being made to test the practical lifetime of pneumatically oscillated samples. These bench-top tests will give necessary information on possible weaknesses of this proposed technique. The ability to oscillate samples would decrease the time necessary to obtain a desired accuracy in experiments of this type.

(d) Worth of Central Core Composition. The worths of the A-type core composition* in the regions 0 to 10.03 in. and 0 to 17.03 in. of the 1-P-16 matrix position were measured by replacing the drawer composition with stainless steel frames.

The core configuration was that of the reference core* with the autorod loaded in the 1- and 2-O-23 matrix position. This loading was subcritical by 35.8 ± 0.4 lh. Removal of the 0- to 10.03-in. region resulted in a subcriticality of 321.2 ± 9.5 lh, and removal of the 0- to 17.03-in. region resulted in a subcriticality of 452 ± 26 lh.

The composition of the region after the removal of the core material is given in Table II.B.5. Remaining are the matrix tube, the core drawer, and the stainless steel

TABLE II.B.5. Composition of Central Region after Removal of A-type Core Material

Element	Atom Density ($\text{cm}^3 \times 10^{-24}$)
Fe	0.006652
Cr	0.001655
Ni	0.000724
Mn	0.000069
Si	0.000081

spacer, which amount to 0.84 g/cm^3 of stainless steel.

In this experiment the degree of subcriticality was determined by the inverse count method while using a calibrated portion of the control rod. This method is different from that for previous measurements involving the removal of plutonium, where the reported reactivity change must be corrected for the change in neutron source.

(e) Central Fission Ratios. The central fission ratios of ^{238}U to ^{235}U and ^{239}Pu to ^{235}U were measured with the use of back-to-back fission counters. These data are now being processed.

(iii) Assembly 52. Assembly 52 is the second core of the FTR Phase-B critical program. The first step in the transition from Assembly 51 to 52 has been the replacement of the iron in the outer radial reflector region with sodium and nickel. Thus the entire radial reflector will now be of a sodium and nickel composition. The resulting assembly is designated Assembly 52A.

* See Progress Report for January 1968, ANL-7419, p. 11.

5. ZPR-6 and -9 Operations and Analysis

a. Integral Studies of Large Systems (W. Y. Kato)

Last Reported: ANL-7445, pp. 15-16 (April 1968).

The ZPR-6 and -9 facilities were shut down during the first week in May in order to allow contractor personnel full access to Building 316-W for the modifications necessary prior to use of plutonium fuels in the facilities. Both facilities were completely unloaded of fuel, which was sent to a special storage area. The cells, vault, and workroom were thoroughly decontaminated. The reactor facilities were covered with plastic film and plywood in order to avoid accumulation of dirt and dust on the components. It is anticipated that the contractor will complete his modifications by about the end of October 1968.

Progress has continued on the seal welding of the shell plates on the exterior confinement shell. The structural steel subcontractor has completed his present work and has left the construction site. Crane and erection crews will return after the sand filter tanks are installed and filled with the special sand and aggregate. The structural crews will return on July 1, 1968. The remaining structural work consists of installing the shell plates of the sand filter pit and the air locks on the south side of the building. The miscellaneous iron subcontractor has installed a steel-plate partition and an associated air lock on the service floor. The interior concrete surfaces of the uranium and plutonium vaults have been ground, patched, and are ready to receive the special coatings. The plaster partition on the service floor of Building 316-W has been completed. The steel roof deck has been installed over the confinement shell and over the mechanical equipment room. The mechanical contractor has continued to prefabricate and weld the 24-in. emergency vent lines. Work has started on the installation of HEPA filter assemblies in Mechanical Equipment Room 4. Work has continued on the installation of steam and condensate lines on the service floor of Building 316-W. The old diesel generator set has been removed from Building 316-W and the new steam turbine generator set has been moved into the building. The electrical contractor has installed the light fixtures in the plutonium and uranium vaults.

6. ZPPR Operations and Analysis (W. G. Davey and P. I. Amundson)

Last Reported: ANL-7445, pp. 20-22 (April 1968).

a. Basic Studies of Large Plutonium Systems

(i) Program. The development of a detailed design for ZPPR Core I is complete. The definitive composition will be determined by the

characteristics of the fuel and diluents which are actually loaded, i.e., the "as-built" configuration.

The preanalysis is being performed on a composition which was computed from the design specifications for the materials. The specified cell design is consistent with the expected fuel and diluent plate inventory.

(ii) Experimental Equipment. The development of reactor experimental equipment continues. The status of the design and construction of these items is as follows:

(1) The mechanical system for the perturbation sample changer has been ordered. Acquisition of associated control-system components is being undertaken.

(2) Materials for selected nonfissile perturbation samples are being received. Assembly of samples into suitable holders will follow material delivery.

(3) Fabrication techniques and design requirements for fissile perturbation samples have been reviewed with personnel of ANL-MET.

(4) A bid package for the axial traverse drive system has been assembled, reviewed, and approved for construction. The package is now being reviewed by potential suppliers. Special control-system items are being reviewed and specified. Acquisition of these items will begin soon.

(5) Design of a sample-changer system for the axial traverse experiments is 80% complete, and detailed drawings are being made. The design of this system has been generalized to provide a traverse capability for both box-type reactivity samples and foil-containing packages.

(6) A mechanical system for the autorod has been assembled and tested. Drive capability has been evaluated to ensure that the response time is satisfactory for the expected mass of control blade. The control system is now being designed. Final tests await coupling of the control and mechanical systems.

(7) The criticality-monitoring system for the vault and workroom has been assembled and tested. The equipment needed for transmission of the data to the reactor console has been ordered.

(8) Preparations for fuel acceptance tests and storage of ZPPR fuel are complete. Criticality procedures have been completed, reviewed, and accepted. A supplier has made initial shipments of fuel. Acceptance tests and storage of the initial shipment of fuel will begin shortly.

b. Doppler Coefficients. The basic design of the entire Doppler system has been completed, including modifications to allow interchangeability between the ZPPR and the ZPR-6 and -9 Doppler samples. Nearly all the major commercially supplied components have been selected; most have been ordered and some received. Construction will begin upon completion of the final design check.

c. Reactor Technique Development

(i) Precision Reactivity Measurements. The uncertainty of measuring reactivity by autorod position in a reactor with a strong source is being investigated with regard to ZPPR applications. An experiment has been performed with ZPR-3 Assembly 51 to provide a comparison with theoretical predictions.

The frequency spectrum of the variations in autorod position at constant power (due to reactor noise) has been derived. Error estimates based on numerical integration of this spectrum are shown in Table II.B.6, along with the experimental values. Also shown in the table are predictions of error based on Bennett's* approximation of a constant frequency spectrum: $W(\omega) = W(0)$. The large difference in the theoretical predictions is due to the inclusion of the source term in the present study.

TABLE II.B.6. Comparison between Experimental and Theoretical Evaluations of Autorod Error (Power = 20 W)

ϵ	Integrated $W(\omega)$ (Present Study)	Experimental	$W(0)$ Approx (Bennett)
0.76×10^{-4}	4.1×10^{-3}	$(1.2 \pm 0.1) \times 10^{-2}$	4.02×10^{-4}
0.25×10^{-4}	4.2×10^{-3}	$(1.2 \pm 0.1) \times 10^{-2}$	4.02×10^{-4}
0.36×10^{-5}	6.4×10^{-3}	$(1.5 \pm 0.2) \times 10^{-2}$	4.02×10^{-4}
0.49×10^{-6}	1.47×10^{-2}	$(2.6 \pm 0.3) \times 10^{-2}$	4.04×10^{-4}
0.45×10^{-7}	4.8×10^{-2}	$(8.8 \pm 0.9) \times 10^{-2}$	4.10×10^{-4}

The formula derived by Bennett for the relationship between E, the measurement error, and σ , the standard deviation of the autorod position, is

$$E = \sigma \sqrt{8/3N}, \quad (1)$$

where N is the number of measurements. The integrated spectrum method substantiates this relationship to within 10%, although no concise expression can be derived. The conclusion reached is that Eq. (1) may be used reliably, although the more refined method must be used to obtain an estimate of the magnitude of the error and its dependence on detector efficiency.

*Bennett, E. F., and Long, R. L., Nucl. Sci. Eng. 17, No. 3 (1963).

(ii) Doppler Rod Balance Code. To reduce reactor operating time in a hot- and cold-sample Doppler experiment, a computer code has been developed to calculate Doppler rod worth as a function of position for a specified loading of balance materials. To provide a final check on the operation of the code, the ZPR-3 Assembly-51 Doppler-balance loadings and the corresponding variations of reactivity with rod motion have been recorded. The reactivity traverse data for the balance materials is not yet available although experiments have been recently completed and calculational efforts are in progress. An attempt will be made to include the effect of the buffer zone around the Doppler rod in these calculations.

(iii) Foil Techniques. Effort has been directed toward specification of a foil-counting system for ZPPR. The proposed system will be composed of three lithium-drifted germanium detectors, 10 to 30 cc in volume, each with an amplifier and a fast, 4096-channel analog-to-digital converter (ADC). The ADC's will then be multiplexed, and data storage and initial reduction will be done with a small on-line computer. The final analysis would be performed with a large computer. The system components have been specified and bids are being evaluated.

(iv) Automation of Data Acquisition

(a) Digital Position Indicators. A prototype has been completed, and tests have been initiated. Assembly of indicators for ZPPR will start after completion of the bench tests.

(b) Digital Multiplexer. Prototype development and testing is completed. Final construction will follow delivery of the components.

(c) Data-acquisition and -recording System. A vendor for the primary components has been selected. Preliminary design of the interface equipment is in progress.

(v) Training. The ZPPR Systems Training Program has been started. Lectures on various aspects of the system are given weekly. The initial lectures have dealt primarily with the characteristics of nuclear instrument and control systems, with emphasis on the safe operation of the system.

7. ZPR Fuel and Nonfissile Materials--Technical Assistance

a. Fuel Element Fabrication Development (J. E. Ayer)

Last Reported: ANL-7445, pp. 22-23 (April 1968).

(i) Danger Coefficient Elements. Thirty special danger coefficient elements were fabricated from two isotopic compositions of

plutonium: 1% ^{240}Pu and 49% ^{240}Pu . The 30 elements consisted of plates, coins, foils, disks, and an instrument traverse element.

The higher ^{240}Pu composition (49%) was alloyed with 1.25 w/o Al and cast into a single-cavity step mold to produce a casting with three thicknesses: 0.194, 0.075, and 0.046 in. The casting was broken at the steps, and the three plates were machined to specified length and width. The plates were inspected, cleaned, weighed, and assembled into Type 304L stainless steel claddings. The assembled elements were inspected, leak detected, and radiographed before being released for Reactor Physics experimentation.

The lower ^{240}Pu composition (1%) was used as an alloy of stainless steel and as Pu-1.25 w/o Al alloy. The stainless steel composition, which contained 0.7 w/o Ni, 0.7 w/o Fe, and 0.7 w/o Cr, was cast into three plate-type elements. The Pu-Al alloy was cast into plates that were rolled into 0.005-, 0.015-, and 0.030-in.-thick foils. The foils were used to make six coin-type elements, 15 elements containing coiled foils, and two disk-type elements. The remaining element was an instrument traverse element made of Pu-Al alloy. All the above elements were clad in cylindrical or prismatic containers of Type 304L stainless steel. The assembled elements were inspected, leak detected, and radiographed before release to the experimenter.

Fabrication of this series of danger coefficient elements and of those elements reported previously (see Progress Report for October 1967, ANL-7391, p. 34) complete the anticipated need for FY 1968.

(ii) Doppler Coefficient Elements. The fabrication of 32 Doppler coefficient elements required during FY 1968 for Reactor Physics experiments has been completed. A summary of the loading data for all required elements is given in Table II.B.7.

Fifteen elements loaded with PuO_2 and six loaded with $^{233}\text{UO}_2$ were reported previously (see Progress Report for December 1967, ANL-7403, Table II.B.2, p. 21). The remaining 11 are loaded with mixtures of depleted UO_2 and PuO_2 .

The Doppler elements were loaded with oxide particles by vibratory compaction. The particles for these fuel elements were prepared by blending 1-kg batches of the oxides, tableting, granulating, and firing the granules at 1600°C for 1 hr. After firing, the particles were sized by regranulating through a 50-mesh screen and collecting on an 80-mesh screen. The accepted screen fraction was loaded into Invar or Inconel claddings to smear densities between 51.0 and 57.8% of theoretical density.

TABLE II.B.7. Loading Data for Oxide Particles in Doppler Elements

Number	Contents (%)		Cladding		Type of Element	Loading			
	PuO ₂	UO ₂	ID (in.)	Material		Weight (g)	Fuel Density (g/cc)	Smear Density (%)	Packing Efficiency (%)
Inv-1	100	0	1	Invar	Sliding Seal	658	-	-	-
-2	↓	↓	1	↓	↓	1067	-	-	-
-3	↓	↓	1	↓	↓	1059	-	-	-
-4	↓	↓	1	↓	↓	965	6.15	53.6	58.1
Inc-1	↓	↓	1	Inconel	Spring Loaded	1066	6.19	54.0	57.9
-2	↓	↓	1	↓	↓	1066	6.23	54.3	58.8
-3	↓	↓	1	↓	↓	1012	6.03	52.6	56.6
-4	↓	↓	1	↓	↓	1023	6.10	53.2	57.3
-5	↓	↓	1	↓	↓	1041	6.20	54.0	57.7
-6	↓	↓	1/2	↓	↓	239	6.51	56.8	62.3
-7	↓	↓	1/2	↓	↓	243	6.55	57.1	62.6
-8	↓	↓	1/2	↓	↓	239	6.44	56.2	61.6
-9	↓	↓	1/2	↓	↓	239	6.46	56.3	61.2
-10	↓	↓	1/2	↓	↓	240	6.43	56.0	60.8
-11	↓	↓	1/2	↓	↓	240	6.52	56.8	61.5
-12	67	33	1	↓	↓	1006	5.93	52.4	56.6
-13	50	50	1	↓	↓	976	5.80	51.7	54.5
-14	50	50	1	↓	↓	1003	5.95	53.0	56.0
-15	50	50	1/2	↓	↓	221	5.91	52.7	55.4
-16	50	50	1/2	↓	↓	223	5.95	53.0	55.7
-17	50	50	1/2	↓	↓	228	6.10	54.4	56.9
Inv-5	50	50	1	Invar	Sliding Seal	970	6.23	55.5	58.6
Inc-26	33	67	1	Inconel	Spring Loaded	1065	6.32	56.8	59.1
-18	12.5	87.5	1	↓	↓	1028	6.10	55.3	57.5
-19	12.5	87.5	1	↓	↓	1079	6.37	57.8	59.9
-25	12.5	87.5	1/2	↓	↓	221	5.91	53.6	55.8
Inv-6	0	100 ²³³ UO ₂	1	Invar	Sliding Seal	914	5.78	53.7	54.7
Inc-20	↓	↓	1	Inconel	Spring Loaded	937	5.60	52.0	56.3
-21	↓	↓	1/2	↓	↓	203	5.47	50.8	55.0
-22	↓	↓	1/2	↓	↓	204	5.49	51.0	55.0
-23	↓	↓	1/2	↓	↓	215	5.78	53.7	57.2
-24	↓	↓	1/2	↓	↓	212	5.69	52.8	55.5

The vibratorily compacted elements were sealed by welding in a helium atmosphere. After welding, the elements were leak checked and surveyed for surface contamination.

8. ZPPR Construction (H. Lawroski)

Last Reported: ANL-7445, p. 36 (April 1968).

Installation of the reactor assembly and associated equipment was 90% complete at the end of May.

The matrix was completed for the 10- by 10-ft assembly. Both reactor frames were installed, and the rod-drive mounting plates were adjusted so as to be parallel to the matrix faces of the reactor. The 14 rod drives which are required for the first core were installed; these consist of the drives for eight poison blades, four fueled safety rods, and two fueled control rods. The poison blades were filled with hot-pressed boron carbide plates with a ¹⁰B enrichment of 92%, and the blades were then welded to the connection clevises. The blade assemblies have a 1/8-in. vent hole incorporated in the clevis.

The coolant plenums were installed in both halves of the reactor and touchup painting was started. The supports for mounting the source drives on the 10-ft matrix were fabricated and the source drives were then installed.

The bottom rail surfaces on the loading platform were found to be uneven and required some rework, which was completed satisfactorily. The platform was installed and checked out. Both sets of personnel shields were placed on their support rails. Electrical connections were completed and checked out.

Work continued on the seal doors. Extensive rework was required on the seal surfaces of all six seal-door frames because of warpage, misfits, and misalignments. Satisfactory alignment of five of the six seal-door hinges was completed by the end of May. The alignment of the hinges is being followed by the modification of the seal surfaces. It appears that the seal doors may be the critical item for the completion of the facility.

Fourteen-hundred fuel-storage canisters were received by ANL from the vendor. Eighteen of the first group of 189 canisters were rejected and returned to the vendor. Three of the second group of 441 were rejected. The remaining 770 are being inspected by ANL personnel.

The fuel-storage vault was approved for receiving fissile material, and inspection equipment for incoming fuel has been set up and checked out.

Equipment is being assembled for testing the filtering capability of the containment structure. Twelve atomizer nozzles and twelve impactors were received and checked out for the uranine aerosol generator used in the test. Analytical laboratory tests were started to determine the detection sensitivity of the aerosol samples. Two sight gauges for level indication in the generators were ordered. Delivery of the two field sampling units was scheduled for late May.

In general, all work appears to be proceeding well.

9. FFTF Critical Experiment Program (D. Meneghetti)

Last Reported: ANL-7445, pp. 31-32 (April 1968).

a. FFTF Critical Experiments Program, Phase B, Revised Assembly IIa Program. Modifications to the program of the next scheduled FFTF critical assembly, No. IIa, i.e., ZPR-3 Assembly No. 52, have been planned jointly by PNL and ANL. The originally scheduled Assembly No. IIa program was to be a more exhaustive series of experiments carried out in an axially split version of the ZPR-3 Assembly No. 51. Since annular cores with central test zones are being considered by PNL, the program to follow

ZPR-3 Assembly 51 is to consist of a limited number of experiments with cores representative of both of these geometries. The experiments are basically to provide data for experiment-theory correlation for ratios of test-zone flux to core power. Although additional changes may still occur, the following is a list of the revised Assembly II series. They are here referred to as ZPR-5 Assembly 52 series:

- 52a. Same as current Assembly 51 except that the nominal 30-cm-thick radial reflector is to be nickel-containing, that upper and lower depleted drawers next to the spiked safety rods are to be the normal A or A* drawers (see Sect. II.B.4.a.(ii)(b)), and that the control rods are to be repositioned so as not to fall into the gap position in subsequent assemblies of this series.
- 52b. As in 52a except with a 3 x 3 sodium column region centrally located throughout the entire assembly axially.
- 52c. As in 52b except with a 5 x 5 sodium column with the corners of core material, i.e., a 5 x 5 minus the 4 corner columns.
- 52d. As in 52a except with a 3-drawer wide sodium-gap of 11 drawers diameter and axially throughout the entire assembly.
- 52e. As in 52d except with the diameter of the 3-drawer-wide sodium gap be 17 or 19 drawers wide, i.e., up to the radial reflector.
- 52f. As in 52c except have a 7 x 7 sodium region with the 3 corner columns at each of the 7 x 7 region retained as core columns.

b. Calculated Scoping Estimates of the Critical Masses and Flux Levels for the ZPR-3 Assembly 52 Series of Cores. Estimates of the critical masses for Assemblies 52a, b, c, and f were calculated by means of a one-dimensional MACH 1 diffusion code in cylindrical geometry using the 29-energy-group cross-section Set No. 29001. The axial buckling previously used for Assembly 51 was employed. The results, normalized to the Assembly 51 experimental critical mass of 212.08 kg of $^{239+241}\text{Pu}$ and ^{235}U , are given in Table II.B.8. The critical mass of Assembly 52e was obtained by the SNARG code in the S_2 approximation, using XY-geometry with the six-energy-group cross-section Set No. 29601. It too was normalized to the experimental critical mass of Assembly 51.

TABLE II.B.8. Calculated Critical Masses and Flux Levels in Test Regions of the ZPR-3 Assembly 52 Series

ZPR-3 Assembly No.	Estimated Critical Mass (kg $^{239+241}\text{Pu}$ and ^{235}U)	Estimated Neutron Flux at Center per Unit Source in the System ($\times 10^4$)
52a	213	5.1
	211 ^a	5.1 ^a
52b	258	3.7
52c	304	3.0
52e	356 ^b	2.7
52f	356	2.4

^a33-cm-thick radial reflector. Others have been calculated with 30-cm-thick radial reflectors.

^bAssuming a circular periphery for core-drivers plus test zone.

The neutron flux at the center of each assembly per unit neutron source in the assembly also appears in Table II.B.8. For Assemblies 52a, b, c, and f it was obtained by the SNARG code in the S_2 approximation, using RZ-geometry and six neutron energy groups. For Assembly 52e, it was based upon a SNARG XY computation and normalized to one neutron produced in the assembly.

C. Component Development--LMFBR

1. Sodium Technology Development--Engineering Development

a. Sodium Quality Measurement (S. B. Skladzien)

Last Reported: ANL-7445, p. 33 (April 1968).

(i) Laboratory Techniques. Analysis of the argon blanket-gas samples taken from the sodium analytical loop, before and after the sodium hydroxide addition, has been completed. The hydroxide was added to provide a known increase in the sodium oxide concentration in the system by the reaction $2\text{Na} + 2\text{NaOH} = 2\text{Na}_2\text{O} + \text{H}_2$. The addition amounted to 1.83 g NaOH which, when completely reacted, would contribute 0.022 mole hydrogen to the system. The analyses were by gas chromatography, using a standard consisting of 250 ppm H_2 in argon. Sampling dates and the measured hydrogen concentrations were:

<u>Sample No.</u>	<u>Date</u>	<u>Hydrogen (ppm)</u>
6	12-28-67	56
NaOH added	1-2-68	
7	1-3-68	143, 165, 135, 148
8A	1-8-68	127, 127, 124
9B	1-10-68	123, 120
10	2-9-68	69, 86, 81
4-4	4-4-68	21
4-10	4-10-68	14
4-17	4-17-68	23, 20, 21

The system was held at 600°F during the entire sampling period. The decrease in hydrogen concentration that started with Sample 8A was due to the removal of blanket gas for the hydrogen analyses. Also contributing to this decrease was the use of the blanket gas to equalize the pressure in the distillation sampler with that in the vessel before opening the isolation valve between these two units. After each of these operations, makeup gas from the argon supply bottle was introduced into the blanket-gas region to restore the pressure to its normal ~0.4-0.8 psig.

Under certain gas-sampling conditions, sodium hydride could form or dissociate in the sampling line. The possibility of these events and the magnitude of the analysis error they would cause are being studied.

(ii) In-line Techniques. So that the response of the various in-line instruments could be observed, the cold-trap temperature was

reduced from 600 to 267°F to reduce the oxygen concentration in the sodium analytical loop. Vacuum-distilled dip samples taken after 18 hr or more at various levels of stable cold-trap temperatures were analyzed chemically.

The two United Nuclear Corp. (UNC) oxygen meters, Nos. 202 and 203, responded almost uniformly to each change in cold-trap temperature. Calibration lines for the meters were obtained by the method of least squares, using cell voltage versus oxygen concentration for the data points (see Table II.C.1). The slopes of the experimentally determined lines failed to agree with the calculated theoretical slopes. The equations of the lines are:

$$\begin{aligned} \text{Calculated:} \quad E &= 1,202 - 0.058 \text{ Log } C \\ \text{Meter No. 202:} \quad E &= 1,161 - 0.026 \text{ Log } C \\ \text{Meter No. 203:} \quad E &= 1,151 - 0.026 \text{ Log } C. \end{aligned}$$

TABLE II.C.1. Meter Response to Oxygen Changes

Day	Cold-trap Temperature (°C)	Oxygen Meters (V)		Oxygen Concentration ^a (ppm)
		No. 202	No. 203	
1	260	1.121	1.113	30.2
2	243	1.121	1.113	29.6
6	227	1.123	1.113	27.6
7	212	1.124	1.116	21.5
9	185	1.129	1.119	-
10	172	1.132	1.125	10.4
13	172	1.137	1.130	9.2
14	172	1.140	1.128	8.3
15	172	1.138	1.129	9.6
16	160	1.141	1.131	6.9
17	160	1.142	1.132	6.6
20	135	1.140	1.131	4.4
21	135	1.142	1.133	4.1
22	131	1.149	1.139	3.7

^aDip samples, vacuum distilled, atomic absorption analysis.

At the cold-trap temperature of 172°C, the further drift of the meters after four days could be attributed to inefficient cold trapping or slow response of the oxygen meters. This drift seemed to occur at all temperatures held more than 24 hr.

A comparison of our solubility data (cold-trap temperature versus oxygen concentration) with that of Rutkauskas* shows our values to be somewhat higher. This could mean that the system has not reached equilibrium solubility at any of the temperature levels, but our oxygen analysis after 5 days at 172°C never approached the 4.5-5-ppm concentration of Rutkauskas' data.

When the cold-trap temperature of 172°C was reached, the plugging-meter cooling rate had to be increased by decreasing flow so that a plug at the cooler temperatures could be recorded within a reasonable time (<1 hr). As a result, nonuniform plugging temperatures were observed, making calibration difficult. The plugging temperature was found to be lower generally than the cold-trap temperature; it could be made to equal cold-trap temperature if the cooling rate was low enough.

The absolute-resistance meter has performed satisfactorily during cold trapping, but system-temperature variations and lag have made it difficult to record resistance changes of 0.02 microhm (due to approximately 1-ppm oxygen concentration). Ways to improve the methods of recording and to increase accuracy are being studied.

b. Sodium Quality Control (S. B. Skladzien)

Last Reported: ANL-7445, pp. 33-34 (April 1968).

A submerged sodium oxide collector was installed in the large (4500-gal) sodium model tank. Auxiliary equipment to be installed includes an air blower and ducting, a vacuum pump, and readout instrumentation. The collector operates by the diffusion of sodium oxide into a cooled region of the collecting mesh. A low (250-300°F) temperature is maintained in this region by a thermally convecting NaK system that is insulated from the bulk sodium. Only the lower portion of the unit is inserted into the static model tank and sealed at the tank mounting flange. A test is being prepared to determine the efficiency of sodium oxide collection by this unit and the practicability of this system for application in reactor systems.

2. Reactor Mechanisms Development--Materials Evaluation

a. Sodium Effects on Wear Properties (E. S. Sowa)

Last Reported: ANL-7438, p. 27 (March 1968).

Additional tests with Clarite T-1 blocks and Carboloy shafts in sodium and argon were performed. Anomalous behaviour of the wear-measuring linear variable differential transformer disclosed that one of

*LA-3607, Quarterly Status Report No. 1 on Advanced Plutonium Fuel Program for Period July 1 through Sept. 30, 1966; Project 802--Measurement of Impurities and Development of Quality Control Techniques for High-Temperature Sodium-Coolant Systems.

the units was sticking. A calibration survey of the units showed that thermal expansion over the range 300-1200°F accounted for 0.130 in. in the readout. This compensating calibration introduces a change in operational format; runs now can be made continuously without resetting the transformer for each temperature change.

The X-Y plotter was extremely useful, allowing data to be examined at the end of each run. Erratic information could be discovered immediately and corrective measures taken.

The tests verified the initial observations about the Clarite test blocks. The wear behavior in sodium showed considerable linearity over all temperature ranges, but increased at 1200°F. The wear in argon gas was much greater than in sodium, demonstrating the capacity of the liquid metal to lubricate. The sample in argon showed greatly increased but linear wear at 1200°F for the first 1.5 hr of the run. Subsequently, the curve deviated from linearity, ultimately acquiring a negative slope. This is interpreted as buildup of transferred material on the shaft. The onset of extreme wear at 1200°F prompted an investigation of the high-temperature region with greater expansion. Consequently, another test is in progress; it started at 900°F and is advancing in 100°F steps. The data do not show the onset of rapid wear up to 1100°F; the 1200°F tests are still in progress.

b. Intermediate Range Neutron Monitor (G. F. Popper)

Last Reported: ANL-7438, pp. 28-29 (March 1968).

(i) Detectors and Cables. Two Westinghouse WX-31369 fission counters have been returned to the manufacturer for nondestructive examination and evaluation. If the present cables can be replaced with longer ones, price and delivery information will be obtained; otherwise, the detectors will be returned to Argonne. A price and delivery estimate has been received from Reuter Stokes to replace the cable on the RNS-286 fission counter. Because of the relatively high cost and long delivery, this work has been deferred.

Compensated ionization chambers and fission counters rated for 850°F maximum operating temperature with removable cables have been ordered from both Westinghouse and Reuter Stokes for test and evaluation. Compensated ionization chambers and fission counters rated for 1400°F maximum operating temperature with integral cables have also been ordered from Reuter Stokes.

The Westinghouse WX-31353-25 high-temperature cables for the WX-4036 fission counter have been received and tested at room temperature. Either the cable ends are not hermetically sealed or the high-temperature connectors take on a considerable and disturbing amount of

moisture rather quickly. The cable-insulation resistance has decreased continually over a period of time while exposed to the normal room-temperature environment. Application of 250°F heat for ~4 hr to about 12 in. of cable and the connector on the detector end brings the cable resistance back to its normal value of about 5×10^{13} ohms/ft. The capacitance of these 25-ft-long cables averaged 55 pf/ft at 1 kHz; moisture does not affect the cable capacitance significantly.

The Bostrad-22 detector extender cable has been made ready for test by attaching Westinghouse WL-23096A high-temperature connectors to it. When received, this cable had an expectedly high moisture content, as evidenced by its low insulation resistance (1.7×10^6 ohms/ft); even after 16 hr of drying at 250°F, the insulation resistance increased to only 1.7×10^8 ohms/ft. The capacitance of this 29-ft-long cable was measured and found to be 18 pf/ft at 1 kHz; again, moisture did not affect the cable capacitance significantly.

High-temperature furnace tests on both types of cables have begun. Insulation resistance, capacitance, and the effect of the cable on preamplifier noise will be evaluated.

(ii) Circuits. Room-temperature alpha and neutron integral bias curves have been obtained with the WX-4036 detector, using the high-temperature WX-31353-25 cable to connect it to the Hewlett Packard HP-5554 charge-sensitive preamplifier. A noticeable decrease in system gain and an increase in system noise resulted, as was expected. System performance, however, remains adequate for the high-temperature tests, with the noise level remaining well below the alpha threshold.

A Gulf General Atomic (GGA) PA-5 charge-sensitive preamplifier also has been used to obtain integral bias curves with the WX-4036 detector. Its performance was excellent, having a charge sensitivity of 0.6 V/pc and a noise level well below the alpha threshold. This preamplifier is designed to be used with guarded-type detectors; thus, because the WX-4036 is not a guarded detector, this preamplifier will not be used in the present series of tests.

The HP-5554 charge-sensitive preamplifiers have been received and modified for the high-temperature tests. The pulse-shaping circuits have been modified to give integrating and differentiating time constants of 0.36 μ sec, and the high-voltage-filter time constants have been changed to reduce voltage drop. A charge sensitivity of 1.2 V/pc is typical, and noise is well below the alpha threshold. A typical noise figure is 1.36×10^{-3} pc rms with a 500-pf cable on the input.

The GGA 10-decade neutron monitor underwent acceptance tests. Only minor problems had to be corrected to bring the monitor within

specifications. The system has been delivered to EBR-II. Installation will be arranged during the next reporting period.

The drawings of the wide-range neutron monitor being designed by Milletron have been given preliminary approval. However, delivery continues to slip.

c. Fission Gas Pressure Transducer (J. R. Folkrod)

Last Reported: ANL-7445, p. 34 (April 1968).

(i) Null-balance System. The transducer is in its fourth and last month of endurance and performance tests at 900°F and 0-350 psig. To date, results are very encouraging.

It has been found that if a large pressure change (i.e., 100 psi) occurs across the coupling disk of the bellows, a shift will be made in calibration. Apparently, the reference-gas pressure shifts only in one direction--downward. The pressure change is caused by an operational fault, such as an operator venting the process gas unintentionally during various operations. The downward shift has not been greater than 10 psi; over a period of time, the shift seems to disappear and the previous calibration returns. This phenomenon has occurred several times. From this experience we conclude that it is important that the operator who is using this instrument to make measurements in a reactor must never allow a large pressure change to be imposed across the coupling disk. Otherwise, the disk might be sprung and calibration lost.

d. In-core Flowmeter Development (G. F. Popper)

Last Reported: ANL-7427, pp. 33-34 (Feb 1968).

(i) Thermal and Mechanical Tests of Magnetic Materials. The B-H test apparatus has developed an unexpected problem. Although the Alnico samples originally tested correlated well with published data, when Alnico-5 test samples were examined the coercive force (H) increased as the applied field was increased beyond the saturation induction. As the H-scale on the oscilloscope was expanded to measure Alnico-5, the horizontal amplifier may have been overloaded, for the trace was driven off scale. The application of a signal limiter did not cure this condition, so it was necessary to examine other effects. The difficulty may reside in the H pickup coil that was made large enough to accommodate the largest in-pile test magnets (of ~5/8-in. OD). The present tests are being conducted with the smallest magnets of ~1/4-in. OD), so the H pickup coil is separated somewhat from the test sample, which could cause the error. A close-fitting pickup coil is being built to accommodate only the 1/4-in. OD samples, with which no major changes in the equipment will be necessary.

At maximum flux density (B) channel gain, a small unbalance voltage was detected. Although insufficient to affect the measurements of full-strength magnets, this voltage could be troublesome for measurements with the weaker, temperature-stabilized magnets and the stainless steel samples. For this reason, and to take into account variations in residual coupling between the primary and secondary circuits that may occur during the hot-cell installation, an adjustable balance circuit is being constructed.

The magnetometer furnace test apparatus is now operating satisfactorily. Sample temperature is being measured to within thermocouple accuracy. The reversible temperature effects of Alnico-5, -6, and -8 magnet samples having a length-to-diameter ratio of 8 have been determined. Stabilization procedures are being modified to eliminate slight instabilities. Stabilization is influenced by both the heating and the cooling rates.

(ii) Preliminary Prototype Magnetic Flowmeter. The FFTF preliminary prototype permanent-magnet flowmeter is being designed to be installed in the core component test loop (CCTL). The flowmeter will be independent of the fuel-assembly design so that procurement and design can proceed independent of CCTL test schedules.

(iii) Eddy-current Flowmeter. The high-temperature version of the model eddy-current flowmeter, now being fabricated, will be installed in a low-flow (≤ 10 gal/min) low-temperature ($\sim 900^\circ\text{F}$) calibration loop. The flowmeter characteristics in sodium will be studied.

e. Failed-fuel Locating Method (F. Verber)

Last Reported: ANL-7445, pp. 34-35 (April 1968).

The design drawings of the failed-fuel monitoring loop are 85% complete.

To establish the elevation of the sodium vapor trap and the gas loop, the liquid flow of the loop was simulated with water in the transparent mockup. For two test arrangements, Fig. II.C.1 shows the resulting liquid level in the vertical 1-in. tube as a function of flow rate. During the initial tests, many air bubbles were visible in the once-through circulation of water through the tubing. Although most of the bubbles appeared in the downstream 2-in. tubing, less than 1% rose to the water surface in the vertical 1-in. tube.

Subsequently, $\sim 1\text{-}2\text{-cm}^3$ charges of air, argon, and helium were injected into the water stream at a point about 13 in. below the gas-disengagement chamber; a small fraction (roughly 1%) of the resulting bubbles rose to the water surface in the vertical 1-in. tube. The flow rate during these tests was ~ 16 gal/min.

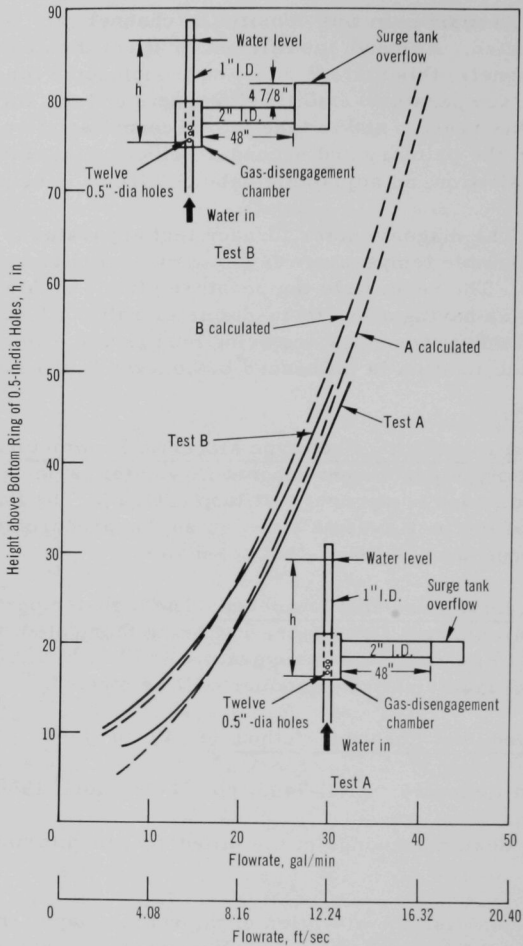


Fig. II.C.1. Water Level in 1-in. Vertical Pipe as a Function of Flow Rate

A method has been established for injecting krypton-85 gas into the sodium loop. The device will consist of a 1-in. bellows-sealed valve modified to include a flanged capsule holder in lieu of the valve seat. A Stellite point in the poppet of the valve will pierce the capsule when it is desired to release the krypton-85 into the sodium stream.

3. Fuel Handling, Vessels and Internals

a. Core Component Test Loop (CCTL) (R. A. Jaross)

Last Reported: ANL-7445, pp. 35-36 (April 1968).

After the FFTF prototype fuel tube and the test fixture were lowered into the CCTL test vessel, the vessel was sealed, pressure instrumentation was checked, and the loop was heated and filled with sodium and operated for the first time. The free-surface centrifugal sodium pump and all loop instrumentation functioned satisfactorily.

During the initial flowtest at 400°F, an abnormality in flow and pressure measurements indicated that a very large percentage of the loop sodium flow was bypassing the fuel-tube section. Further testing revealed the probable cause of the abnormality to be a lifting of the entire test vessel, the hydraulic lifting force at this point being greater than the holddown spring force. The leakage of sodium bypassed the fuel-tube test suction by returning through the test vessel directly to the section of the main pump. Corrective measures are being taken to increase the holddown spring, which necessitates removing and modifying the test fixture.

Sodium samples were taken and plugging runs were made. The initial analysis indicates a sodium oxide concentration of ~33 ppm. Initial operation of the strain gauges at this low temperature showed no malfunction or unusual occurrence.

D. Systems and Plant--LMFBR

1. 1000-MWe Plant

a. Contract Management and Technical Review (L. W. Fromm)

Last Reported: ANL-7445, pp. 36-37 (April 1968).

(i) The Babcock & Wilcox Co. Subcontract. Preparation of conceptual system design descriptions continues. ANL has commented on the first draft of the instrumentation and controls descriptions.

Seven trade-off studies have been received and five have been evaluated by ANL. The remaining trade-off studies have been completed in draft form.

The fourth technical progress report (for Sept. 1-Nov. 30, 1967) was received by ANL.

Task-III parametric studies are approximately 60% complete.

At the request of ANL, B&W has revised its work plan for Task IV. A cost estimate for the Task-IV work and the new Task-V safety work also was provided.

The architect-engineer has completed all support work, and B&W, with this input, has now completed 90% of the plant arrangement drawings.

(ii) Westinghouse Electric Corp. Subcontract. The completed Task-I report is being printed. All six of the Task-I topical reports have been received by ANL.

Task-II design work on the reactor vessel and internals has been completed, and the conceptual system design descriptions have been written and are being reviewed. Preliminary drafts of these descriptions were completed for the fuel-handling, intermediate-cooling, steam-generator, and turbine-generator systems.

Fuel-cycle costs have been calculated for four proposed fuel-management schemes. A pump subroutine that was added to the plant optimization code has been debugged.

(iii) General Electric Co. Subcontract. The evaluation of core power-flattening effects was completed; the effects of power shifts from the core to the radial blanket are being determined. The oxide-core vented-fuel parametric studies are essentially complete, and the results are being applied to the plant and system optimization studies.

The intermediate-heat-exchanger design was further refined.

Cost and descriptive information was received from the GE turbine department, and final optimization runs were initiated for the selection of the steam-cycle type and conditions.

The GE architect-engineer is preparing equipment and plant arrangement, plant conceptual specifications, and capital cost estimates.

(iv) Combustion Engineering, Inc. Subcontract. Progress on the CE 1000 MWe Follow-on Study was described to AEC-RDT personnel at a meeting.

Five of the conceptual system design descriptions developed by CE in their Task-II effort have been submitted to and reviewed by ANL.

Core thermal hydraulic and parametric studies have been completed, as has the technical material for the modular versus nonmodular core trade-off study.

The cost of expanded effort in Task-IV R&D work and in safety studies has been estimated. The safety work will be included in the report of Tasks II and III.

(v) Atomics International Subcontract. The Atomics International study is ~48% complete. The Task-I report has been issued, and work is proceeding in the following Task-III areas: nuclear-uncertainty analysis; fuel-handling analysis and design; nuclear-island and general plant arrangement; core-parameter study, including effects of fuel density on thermal behavior, nuclear behavior for a gas bubble passing through the core, and effects of variation in core parameters on fuel-cycle cost; system parameter study, and DBA and accident analysis, for which a number of accidents and the consequences of a sodium fire are being reviewed. A fault-free logic network indicating the sequence of events culminating in various accidents has been prepared.

Preparation of Task-II conceptual subsystem design descriptions and Task-III plant drawings and arrangement layouts has been delayed until FY 1969 because of FY 1968 funding limitations.

E. EBR-II1. Research and Developmenta. Reactor Experimental Support--Reactor Analysis and Testing
(R. R. Smith)

Last Reported: ANL-7445, pp. 38-59 (April 1968).

(i) Nuclear Analysis(a) Reactor Kinetics

(1) Physics Measurements for Run 28A. The recent removal of all experimental subassemblies containing ceramic fuel provided an opportunity to evaluate the effects of core composition on the power coefficient. A series of physics tests was conducted with the Run 28A (reference) configuration, which contained no ceramic fuels. Included in the test series were power-coefficient measurements, both in ascending and descending modes; reduced-flow studies at 41.5 MWt, 100% flow and 22.5 MWt, 58% flow; and rod-drop tests under the following conditions: 500 kW, 100% flow; 500 kW, 58% flow; 41.5 MW, 100% flow; 22.5 MW, 100% flow; and 22.5 MW, 58% flow. The results of these studies will be compared with corresponding results obtained for configurations in which approximately one-half and finally all of the ceramic-fueled experiments are reinserted in the core.

(2) Rod-drop Tests. Table II.E.1 summarizes estimates of the reactivity worths of the drop rod for various conditions of power and flow. An inspection of the data for 22.5 MWt, 58% flow and 41.5 MWt, 100% flow indicates an ordered increase in the estimates for rod worth in going from Rod Drop 1 to Rod Drop 2, from Rod Drop 2 to Rod Drop 3, and so on. Estimates of the standard deviation of data taken at 22.5 MWt and 100% flow, which show no such increase, lead to the conclusion that for an 80% degree of confidence the trend observed is significant. No explanation for this trend has been postulated. The results of future tests will be carefully studied to provide additional evidence of whether or not this trend is real.

TABLE II.E.1. Rod Drop (Reactivity), β

Power and Flow	Rod Drop 1	Rod Drop 2	Rod Drop 3	Rod Drop 4
500 kW	13.12	13.06	13.19	-
22.5 MWt, 100%	12.24	12.28	12.22	12.24
22.5 MWt, 58%	12.09	12.14	12.21	-
41.5 MWt, 100%	11.51	11.73	11.93	11.98

(3) Transfer Function for Mark-II Fuel Loading.

Estimates of the transfer function for the Mark-II fuel loading were made on the basis of the following assumptions: (a) a mathematical model based on the results of the rod-drop tests and transfer-function measurements conducted during Run 26, (b) a complete loss of the axial fuel-expansion component, and (c) a 91-subassembly configuration surrounded by the present stainless steel reflector. The results for the estimated reactivity-feedback function are illustrated in Fig. II.E.1. Of particular significance is the indicated existence of a slightly positive differential power coefficient at 22.5 MWt which becomes negative at some power level between 22.5 and 45 MWt. The existence of a positive differential power coefficient at 22.5 MWt for this model reflects the existence of inward bowing effects which are attributed to the thermal-mechanical effects in the stainless steel reflector.

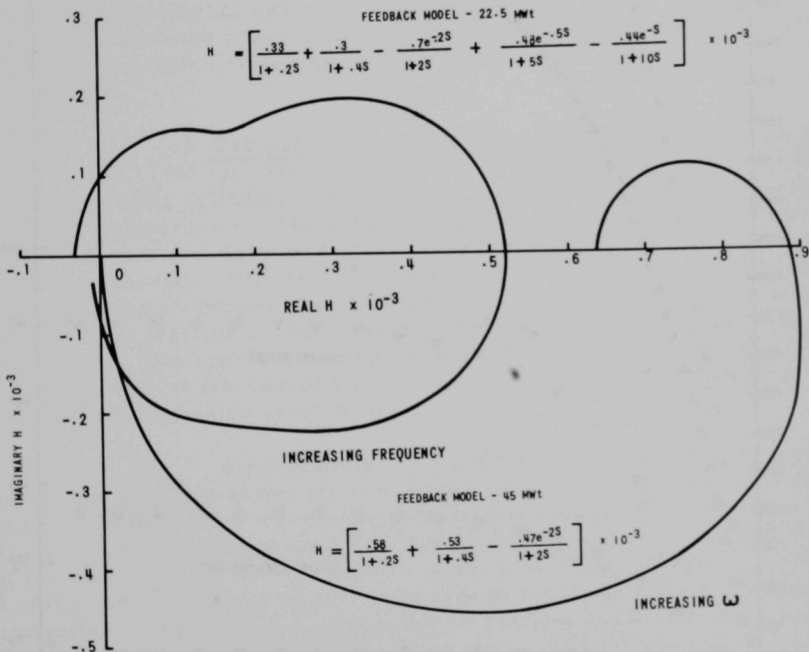


Fig. II.E.1. Transfer Function for Zero Axial Expansion

Calculations were initiated to evaluate the effect of experimental oxide and carbide subassemblies which have longer time constants than do the metallic elements on the feedback function. Figure II.E.2 is the plot of an ARGUS heat-transfer calculation for a carbide

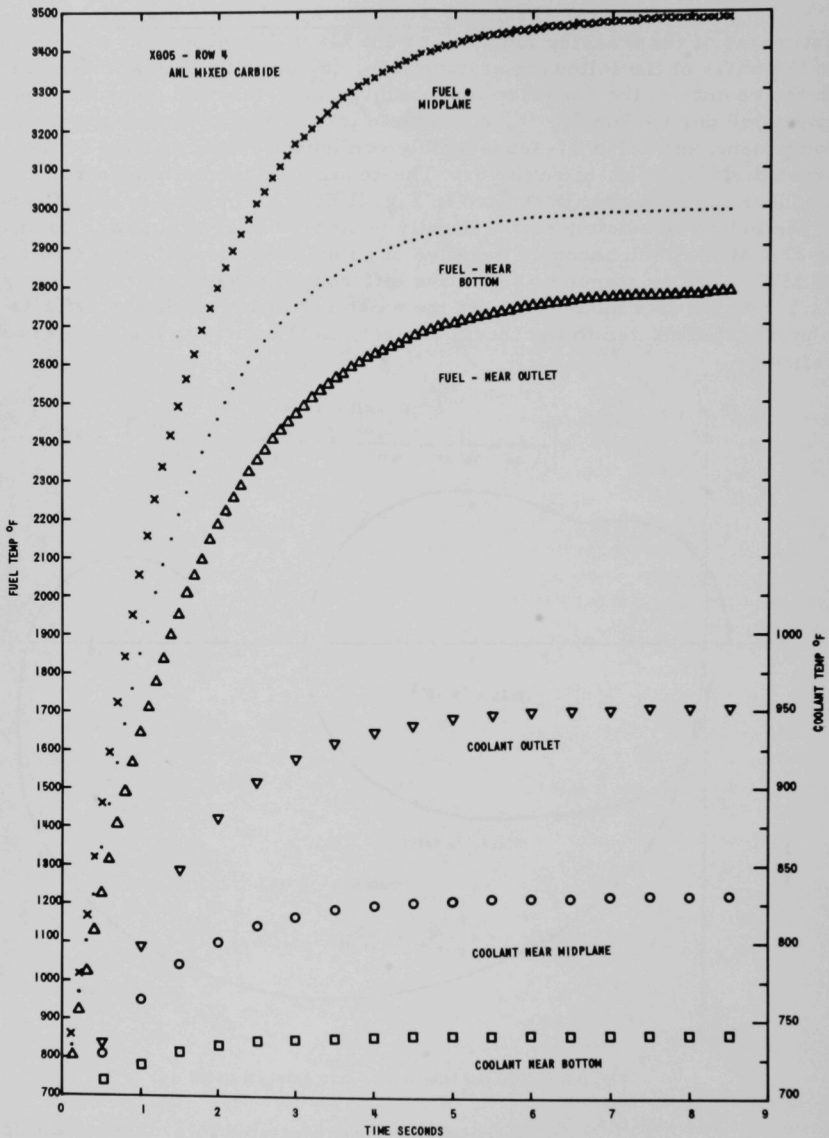


Fig. II.E.2. Transient Temperature Response for Experimental Carbide Subassembly

subassembly, showing the temperature response associated with a step input of power. The time constants are approximately 1.5 sec, whereas the time constant is 0.3 sec for metal elements.

(b) The Analog Simulation of a Reactivity Meter. The experimental reactivity meter was used continuously throughout Run 28A. Calibration of the meter was accomplished during various rod-drop experiments. The meter readings agreed within $\pm 10\%$ of the values indicated by a digital-computer evaluation of the reactivity worth of the drop rod.

Noise reduction by several orders of magnitude was accomplished by modifying the final-stage metering circuit. Efforts are being made to simplify the adjustment of gain and to introduce logic circuits to permit faster range switching. The meter has the potential of annunciating significant reactivity anomalies, but to do so, it must account for normal situations which unavoidably affect reactivity. These situations include control-rod movements, sodium temperature changes, flow changes, etc.

(c) Temperatures within Alloy Fuel Pins. Equations presented in ANL-7445, pp. 47-48, described the temperature pattern within a heat-generating cylindrical pin when the conductivity of the material is a function of temperature. The area-averaged temperature of a cross section of the pin then was determined as an index to the fuel temperature expansion. Since the expansion coefficient is markedly different, however, above the γ -phase transition temperature (550°C), a more useful procedure would be to calculate what fraction of the cross-sectional area lies above this transition temperature. The appropriate expansion coefficient can then be applied to each metallurgical fraction of the fuel for a more accurate estimate of the effective fuel-expansion coefficient.

A program for calculating the fraction of fuel above the γ -phase temperature at any pin cross section has been written. The recent temperature-dependent and swelling-dependent conductivity data from ANL-MET are included in the calculation. Preliminary results indicate that for clean fuel the hottest regions of the pins should be near the threshold of the γ -transition at 45 MWt. As burnup proceeds toward the maximum permissible value of 1.2 a/o, a substantial fraction of the fuel, perhaps 10-20%, may lie above the transition temperature. The routines developed for this calculation are being incorporated into the HECTIC program so that a more comprehensive estimate of γ -phase content throughout the whole core can be made.

(d) Mark-IIA Safety Analysis. The one-dimensional diffusion-theory reactor code M \bar{O} NA has been modified to include the following information:

- (1) absolute total flux and total flux normalized to unity at any specified mesh point;
- (2) flux energy spectra:
 - (a) the flux spectrum is computed at any specified mesh point (many mesh points may be specified);
 - (b) the region-averaged flux spectrum is computed for each region;
- (3) the following spectral indices:
 - (a) median and average neutron energy;
 - (b) median and average flux energy;
 - (c) median and average neutron fission energy;
 - (d) median and average neutron absorption energy;
 - (e) median and average neutron capture energy;
- (4) region-averaged spectral indices in (3);
- (5) isotope reaction rates or reaction rate ratios as a function of position.

As a test case, these parameters were calculated for the EBR-II wet critical core. The fission-rate distributions for ^{235}U and ^{238}U were in excellent agreement with those reported in the EBR-II Hazards Summary Report (HSR) ANL-5719 (Addendum), p. 223. Twenty-two-energy-group flux calculations were compared with 2- and 3-group calculations and with the 11-group calculations reported in the HSR Addendum, p. 144. The high-energy fluxes (>1.35 MeV) in the present calculation were larger than in the 11-group calculations by $\approx 4\%$, and the low-energy fluxes were larger by $\approx 7.5\%$. The present power-density calculations were lower by $\approx 10\%$ than those in the HSR Addendum, p. 145.

The discrepancies between present and earlier calculations are attributed to three sources of error:

- (1) The present calculations are one-dimensional, whereas the earlier calculations are two-dimensional.
- (2) An improved cross-section set was used for the present calculations (MC² Set 238).
- (3) More energy groups were used in the present calculations.

It has not been established whether the present calculations are more correct than the earlier; however, the MONA code is clearly adequate for survey calculations.

Neutron energy spectra were calculated for the 19 Mark-IIA survey cores described in Table II.E.2. A portion of the results are presented in Table II.E.3. The calculations were performed in spherical geometry, using 22 energy groups. Each core was assumed to be surrounded by a blanket of 60 v/o depleted uranium.

TABLE II.E.2. Core Loadings for EBR-II Mark-IIA Safety Analysis

Core No.	Composition of Central Core Region by Volume	Volume Fraction of Core in Central Region (%)	Composition of Outer Core Region by Volume	Volume Fraction of Core in Outer Region (%)	Comments
1	100% Mark-IIA	100	-	0	Base Case - homogeneous core
2	90% Mark-IIA 10% oxide exp.	100	-	0	homogeneous core
3	70% Mark-IIA 30% oxide exp.	100	-	0	homogeneous core
4	50% Mark-IIA 50% oxide exp.	100	-	0	homogeneous core
5	100% oxide exp.	10	100% Mark-IIA	90	
6	100% oxide exp.	30	100% Mark-IIA	70	
7	100% oxide exp.	50	100% Mark-IIA	50	
8	100% Mark-IIA	90	100% oxide exp.	10	
9	100% Mark-IIA	70	100% oxide exp.	30	
10	100% Mark-IIA	50	100% oxide exp.	50	
11	90% Mark-IIA 10% carbide exp.	100	-	0	homogeneous core
12	70% Mark-IIA 30% carbide exp.	100	-	0	homogeneous core
13	50% Mark-IIA 50% carbide exp.	100	-	0	homogeneous core
14	100% carbide exp.	10	100% Mark-IIA	90	
15	100% carbide exp.	30	100% Mark-IIA	70	
16	100% carbide exp.	50	100% Mark-IIA	50	
17	100% Mark-IIA	90	100% carbide exp.	10	
18	100% Mark-IIA	70	100% carbide exp.	30	
19	100% Mark-IIA	50	100% carbide exp.	50	

TABLE II.E.3. Calculated Spectral Indices

Core No.	Average Neutron Energy (MeV)		Median Fission Energy (MeV)		Fission Ratio 238/235	
	Core Center	Core Edge	Core Center	Core Edge	Core Center	Core Edge
*	0.463	0.334	0.455	0.294	0.0712	0.0447
1	0.437	0.317	0.428	0.278	0.0667	0.0418
2	0.427	0.311	0.421	0.274	0.0662	0.0416
3	0.408	0.299	0.408	0.265	0.0652	0.0411
4	0.389	0.287	0.394	0.258	0.0641	0.0406
5	0.367	0.316	0.400	0.276	0.0607	0.0424
6	0.339	0.309	0.366	0.266	**	0.0427
7	0.330	0.301	0.355	0.255	**	0.0430
8	0.437	0.307	0.428	0.303	0.0669	0.0410
9	0.437	0.290	0.428	0.284	0.0675	†
10	0.437	0.275	0.427	0.269	0.0684	†
11	0.430	0.312	0.426	0.277	0.0660	0.0414
12	0.414	0.304	0.421	0.275	0.0644	0.0406
13	0.397	0.295	0.416	0.274	0.0628	0.0398
14	0.389	0.313	0.435	0.275	0.0616	0.0414
15	0.371	0.305	0.421	0.280	††	0.0405
16	0.365	0.296	0.417	0.260	††	0.0396
17	0.436	0.310	0.427	0.310	0.0667	0.0412
18	0.435	0.299	0.426	0.297	0.0668	‡
19	0.431	0.290	0.423	0.289	0.0667	‡

*EBR-II wet critical core.

**These values are expected to be very close to 0.0607.

†These values are expected to be very close to 0.0410.

††These values are expected to be very close to 0.0616.

‡These values are expected to be very close to 0.0412.

These calculations indicate the following:

- does carbide fuel.
- (1) Oxide fuel soften the energy spectra more than
 - (2) Centrally loaded experiments soften the spectra at the core edge as well as the core center.
 - (3) Edge-loaded experiments do not significantly affect the spectra at the core center even when the experiment region occupies 50% of the core volume.

(e) Release of Fission-product Species to the EBR-II Cover Gas

(1) Summary. After exhaustive analysis of all data from the March and April fission-product releases, the evidence indicated failure of an experimental fuel capsule rather than of a driver element. By April 20, only two experimental metal-fuel subassemblies, XO28 and XO29, remained in the core. These were removed, and the reactor was returned to power to show that a driver element was not involved. After $4\frac{1}{2}$ days of operation with no release, the reactor was shut down and XO28, the primary suspect, was reinserted in the core. The reactor was then taken to power and, after 96 MWd of operation, the anticipated release occurred. This release was one of the strongest to date; relevant data follow. An additional very small release was observed when XO28 was subsequently lifted out of the core for transfer to the storage basket. Since the final removal of XO28 from the core, the reactor has been operated with no further evidence indicating a fission-product release. *(Discussion of the previous fission-product releases, and details of why XO28 was the primary suspect, are given in ANL-7445, pp. 49-59.)

(2) Description of Events. Following fission-product releases on April 19 and 20, 1968, experimental Subassembly XO28, the primary suspect, and XO29, the other remaining fuel experiment, were removed from the core. The reactor was then operated for 205 MWd to verify that a driver-fuel element was not the failure. Suspect XO28 was reinserted in the core in position 4D3, and the reactor was started for Run 27I, with full power achieved at 0854 on May 4.

At 0539 on May 6 with the power level still at 45 MWt, an FGM alarm* was received and the reactor was shut down, after a total of 96 MWd in Run 27I. Radiometric analyses of cover gas samples for ^{133}Xe and ^{135}Xe confirmed the release.

*Fission gas monitor -- alarm set for 20-30% increase over background level.

After the main primary coolant pumps were stopped at 0627, a second release was observed. A third release also was observed when the pumps were again started at 0930. The FGM signal during the period of the three releases increased from the normal background level of 15 cpm to 2100 cpm. The FERD* recording did not increase above background at any time during these releases.

Radiometric analyses showed that the short-lived xenon isotope ^{135}Xe increased in concentration by a factor of 140, approximately the same increase as indicated by the FGM which monitors the presence of short-lived Kr and Xe species in the cover gas. Xenon-133, which had not yet reached equilibrium, increased by a factor of 30.

Shortly after the release, airborne activity in the Reactor Building subbasement began to increase. Background level for this activity is of the order of 200 to 300 cpm, and the alarm setpoint is 10,000 cpm. An alarm was received at 0755 hours, and by 0900 the level had increased to 13,000 cpm. A reading taken at 1025 hours showed the level to be 20,000 cpm. Thereafter the activity began to decrease.

An alarm from the argon purification cell, set for 5 mR/hr, was received at 0623 hours. A general area survey of the Reactor Building at 0730 showed activity levels of 3-5 mR/hr.

(3) Discussion and Conclusions. Subassembly XO28 contains 15 capsules, loaded with a ternary metal alloy of uranium, plutonium, and zirconium, which were to be irradiated to a 10-a/o burnup, and four capsules, loaded with Mark-IA fuel, to be irradiated to a 3-a/o burnup. An exposure of 10,000 MWd was to be required to achieve the 3-a/o burnup. Upon removal following the May 6 and 7 releases, XO28 had been irradiated for a total of 1730 MWd.

Evidence that an experimental fuel capsule was the failure rather than a driver-fuel element and that Subassembly XO28 was the probable leaker was presented in detail in ANL-7445. The additional evidence observed this month supports the conclusion that XO28 contains a failed capsule. The evidence may be summarized as follows:

1. A very substantial release occurred shortly after the reactor was returned to power with XO28 reinserted in the core. At this time, XO28 was the only experimental fuel subassembly in the core.
2. The reactor has now operated a total of 734 MWd with XO28 out of the core (in April and May), and no indication of an additional fission-product release has appeared.

*Fuel element rupture detector--a monitor of delayed neutrons which would be indicative of a large sodium-bond release.

3. The ^{135}Xe activity in the cover gas increased by $1.4 \mu\text{Ci/cc}$ or a factor of 140 over the previous background, whereas the ^{133}Xe increased by $0.3 \mu\text{Ci/cc}$ or by a factor of only 30. If the failed element had been in the core during the previous run of 206 MWd (Run 27H with XO28 in the storage basket), then the long-lived ^{133}Xe activity would have been closer to its equilibrium value and the absolute activity increase would have been more nearly equal to the ^{135}Xe increase. From analysis of the xenon-activity levels, therefore, it is evident that the failed element was inserted at the start of Run 27I.

Although the failure in XO28 is thus established, there is no certainty at this time that XO28 is the only subassembly containing a defective capsule that could have caused the recent series of fission-product releases, or that there is only one defective capsule in XO28. The remaining metal-fuel experiment, XO29, and all the oxide- and carbide-fueled experiments have now been reinserted in the reactor in two increments with no sign of fission-product release during subsequent operation through May 31. Further operation will be required, however, to verify that no other failures are involved.

If the evidence continues to indicate that experimental Subassembly XO28 contains the only failed capsule or capsules, the question should then be considered whether XO28 has been the source of all the fission-product releases since November 23, 1967. On November 21, 1967, in preparation for Run 26C, two fresh driver-fuel subassemblies and several experimental fuel subassemblies, including XO28, were inserted in the EBR-II core. Analysis following the fission-gas releases of November 23 and 24, 1967, indicated that fresh fuel was the source of the fission gas. The two fresh driver-fuel subassemblies were therefore removed and the reactor returned to power on November 25. The reactor was then operated for 430 MWd with no further sign of a fission-product release and for 1066 MWd before another gas release was observed. The conclusion was reached that the defective subassembly had been removed. There are, however, three factors which indicate that XO28 could possibly be the source of all the releases since November:

1. XO28 also contained new fuel which had not been irradiated prior to November 23.
2. XO28 is the only experimental subassembly that has been in the reactor during all the releases beginning with November 23, 1967, and concluding with the May 7, 1968 release.
3. Postmortem examination of the fresh driver subassemblies considered to be defective have revealed no defective elements.

Evaluation of this question will continue. Further discussion may be found in the Progress Report for December 1967, ANL-7403, pp. 35-42, and in ANL-7445.

(f) Effect of Reduced-flow Conditions on the Power Coefficient of EBR-II. An error was made in publishing Eq. (1) on page 34 of the Progress Report for March 1968, ANL-7438. The corrected equation (with a slight change of form) should read

$$-E/Q = [(1.015 + 11100 \alpha)/R] + (2270 \alpha/R^{0.4}) + [6500 + (408/k)] \alpha.$$

(ii) Thermal Analysis

(a) Correction Factors for Subassembly-coolant Outlet Temperature. Correction factors for the thermocouple readings of subassembly-coolant outlet temperatures were deduced mathematically from the expressions which consider radial cross-flow in the upper plenum of the EBR-II core system. These corrections were applied to specific temperature measurements, and it was shown that differences of the order of 40°F may exist between actual and measured temperatures.

(b) Loss of Bond Sodium from a Fuel Element. A study has been initiated of the temperature distribution in an EBR-II fuel element as a function of time after a loss of bond sodium has occurred. Calculations were carried out with the THTB heat-transfer program on the CDC-1604 computer at the NRTS Computer Center. Two models were proposed for the calculations and both were utilized.

The first model assumed that the sodium bond was lost and all heat transfer from the fuel pin to the cladding ceased. The heat generation continued, however, and the fuel temperature increased until the entire fuel pin melted. The fuel continued to increase in temperature after melting until a time at which it flowed and contacted the cladding along the entire 360°C periphery. At this point heat transfer from the fuel to the cladding began, and at this point (time = 0) the calculation of the temperature distribution in the fuel, cladding, and coolant was started.

The heat-generation rate used in this model corresponded to the peak rate in the reactor, taking into account both the axial and radial flux distributions. Results of these calculations are presented in Table II.E.4. The time interval used in all the problems was 0.01 sec. The results of each time step were printed for the first three cases in Table II.E.4, but for the fourth case, only every fifth result was printed. Comparable results that were printed were markedly similar, however, for the 45-MWt and the 62.5-MWt power levels at the 1950°F fuel temperature (temperatures up to 0.15 sec were within about 10°F for the two cases). The power level, per se, appears to have less influence on the

peak temperatures to be reached than the temperature of the molten fuel at the time of contact. The energy stored in the molten fuel determines the peak cladding temperature.

TABLE II.E.4. Temperature versus Time for Assumed Loss of Sodium Bond

Power Level (MWt)	Time between Melting and Fuel Contact (sec)	Fuel Temperature on Contact (°F)	Peak Clad Temperature and Time It Occurred as a Function of Radial Distance from Fuel-Clad Interface								Time (sec) at Which Fuel 0.006 in. from Interface Cooled to below 1157°F	Time (sec) at Which Clad 0.001 in. from Interface Cooled to below 1157°F
			0.001 in.		0.003 in.		0.005 in.		0.075 in.			
			°F	sec	°F	sec	°F	sec	°F	sec		
45	1/20	1950	1417	0.02	1351	0.04	1300	0.05	1238	0.05	a	0.37
45	1/3	2570	1571	0.04	1493	0.04	1422	0.04	1337	0.04	0.63	0.42
45	1/2	2900	1601	0.03	1522	0.03	1461	0.07	1374	0.07	0.67	0.46
62.5 ^b	1/20	1950									0.90	0.45
62.5	1/3	2900	1660	0.02	1564	0.02	1486	0.03	1392	0.03	0.85	0.45

^aProblem was terminated 0.41 sec before reaching this point.

^bPrintout occurred only every 0.05 sec. Temperatures at 0.05, 0.10, and 0.15 sec were $\approx 10^\circ\text{F}$ higher than for corresponding 45-MWt case.

The second model consisted of a 0.144-in.-dia fuel pin located within a fuel-element jacket whose inside diameter was 0.156 in. The sodium bond was assumed lost, all heat transfer ceased, and the fuel-pin temperature rose to 1840°F (10° below melting point), at which time the fuel pin slumped against the jacket and perfect contact was made over a 30° arc of the 360° periphery. The fuel pin retained its geometry during the ensuing transient, and heat was transferred to the coolant through the fuel-cladding interface and through the varying argon-gas-filled gap on the 330° arc of the fuel not in contact with the cladding.

This model was used for one set of transient calculations. For this set, the heat-generation rate corresponded to the peak rate in the reactor at a power level of 45 MWt. The peak cladding temperature recorded was 1396°F and it occurred at 0.05 sec (calculations were performed every 0.01 sec, but the results were printed only every 0.05 sec). Almost all the heat generated in the fuel was transferred through the fuel-cladding interface. A steady-state solution was approached by the end of 0.9 sec, at which time the cladding temperature at 0.001 in. from the fuel-cladding interface was 1286°F. The solution was an unreal one, however, as 80% of the fuel was molten, but still retained its geometry and the heat transfer occurred across the solid fuel-cladding interface. In actuality, for the proposed model, the fuel which was insulated by the gas gap would have melted and flowed so as to contact the cladding, resulting in a case similar to those treated with the first model, above.

Another series of calculations with this second model was carried out for steady-state power levels at 5-MWt increments from 5 to 45 MWt. As earlier, sodium flowed past the outside of the element at 20 ft/sec and a temperature of 898°F, but a contact conductance of 50,000 Btu/hr-ft²-°F was assumed at the 30° arc between fuel and cladding.

The temperature of the fuel increased as the power level increased, and between 20 and 25 MWt a portion of the fuel reached the melting temperature. The maximum cladding temperature is less than the allowed 1157°F (625°C) even under the severe, conservative, assumed combination of heat-generation rate and coolant temperature.

b. Nuclear Analysis Methods Development (P. J. Persiani)

Last Reported: ANL-7445, pp. 60-65 (April 1968).

(i) EBR-II Bowing Model. Several improvements can be made in the static bowing model code BOW-II.* The most important involve the treatment of button-level displacements and loadings and the determination of next-guess quantities in the iteration procedure.

The fundamental difficulty in both these areas lies in the definition of the loads created by the touching of thermally deformed sub-assemblies. In particular, the forces from contact at the tops of Rows 7 and 8 in EBR-II have not been transmitted in a consistent manner to the button-level positions of the system, and the effect of this is that the present iteration scheme produces an oscillation in button-level displacements and an unrestricted imbalance of button-level forces.

A method for controlling the generated loads has been devised, but due to the complexity of the physical configuration, its effect can only be determined by the operation of the modified program. This modification is now being incorporated into the code.

c. Fuel Swelling and Driver Surveillance (F. G. Foote)

(i) Mark-IA--Investigation of Anomalous Fuel Swelling

Last Reported: ANL-7445, pp. 67-68 (April 1968).

(a) Extended Burnup of MC-S-type Fuel Pins. Subassembly C-291, known to contain only low-swelling fuel, is scheduled for additional irradiation during the last third of Reactor Run 28. The target burnup is 1.3 a/o.

Subassembly C-2027, also known to contain only low-swelling fuel, will be held in the fuel-transfer storage rack until the swelling results are available for Subassembly C-291. If these results are favorable, we will request a target burnup of 1.4 a/o for Subassembly C-2027.

*Bump, T. R., Trans. Am. Nucl. Soc. 10(2), 661-662 (Nov 1967).

(b) High-burnup Irradiations of Mark-IA Fuel. Experimental irradiation Subassemblies XO15 and XO17, now in the storage rack, will be reinserted into the core for additional burnup at the beginning of Run 28C.

(c) Effect of Trace-element Impurities upon Fuel Swelling. Irradiation of Subassemblies C-2110 and C-2112, which contain fuel with deliberate additions of trace-element impurities, will start at the beginning of Run 29. Subassemblies C-2119, C-2154, and C-2155, which contain regular recycled fuel with up to 750 ppm of silicon, also will be inserted into the core at the beginning of Run 29.

Measurements of the sodium level have been completed on fuel elements from Subassembly C-2077. Fuel-swelling values are being computed.

(d) Effect of Heat Treatment upon Swelling of U-5 w/o Fs Alloy. Burnup analyses have been received for the specimens that were irradiated in Capsule H-2 (see Progress Report for Jan 1968, ANL-7419, p. 55, Table I.E.10). The burnup values were 0.80 a/o for Specimens 1, 3, and 5; and 0.87 a/o for Specimens 2, 4, and 6.

The "as-cast" specimens from Capsules H-1 and H-2, both designated No. 1, were cooled from 1300 to 1050°C in 15 sec (mold temperature at 500°C); the specimens then were cooled to room temperature at a rate of $\approx 150^\circ\text{C}/\text{min}$.

(e) Hot Laboratory Examination of Irradiated Fuel

(1) Fuel Surveillance. Measurements of sodium level have been completed for fuel elements from the ten subassemblies removed from the core near the end of Run 27. Values of fuel swelling for the approximately 850 fuel pins are being calculated. No leaking fuel elements were detected in this group.

Four subassemblies that contain Mark-IB fuel elements are under irradiation. Subassembly C-2132 will be removed at the middle of Run 28 (after 0.6 a/o burnup) and Subassembly C-2133 at the end of Run 28 (after 0.8 a/o burnup).

Subassembly C-2124, which contains cold-line fuel, is scheduled for removal at the end of Run 28 (after 0.6 a/o burnup).

(f) Analysis of Fuel Pin Swelling. New and more accurate maximum temperatures of the fuel centerline have been received, tabulated, and transmitted to the Applied Mathematics Division. The data are being transferred to the input cards. These new calculations widen the temperature

span within a given subassembly and provide a better base from which to estimate the temperature coefficient of swelling. Swelling data from the 70% enriched fuel will also be factored into these calculations.

(ii) TREAT Experiments

Last Reported: ANL-7445, pp. 68-69 (April 1968).

(a) Fuel-motion Studies with Mark-IA Fuel Elements
(C. J. Renken)

The design of the electromagnetic transducer that will be used to measure fuel motion during a transient has been changed. As the fuel-sodium interface passes through the induction field of the transducer, the resistivities of both fuel and sodium will be changing drastically. Since resistivity data for the fuel are not available in the temperature range of interest, only a very rough estimate is possible of the combination of resistivities that will exist at any given instant during the transient.

The change in the original transducer design was made in an attempt to reduce the effect on the accuracy of the measurement of resistivity changes due to unknown combinations of fuel and sodium. In the new design, two pickup coils are interspersed with three field coils, all located coaxially. The three field coils are driven in series by the current pulse. As the interface moves through the transducer, two separate signal peaks are produced, 4.3 mm apart. This type of response, as well as the three sample points used on each of the pulsed signals from each pickup, should permit a useful measurement of the location of the fuel-sodium interface; any combination of resistivities may occur during the transient provided the sodium resistivity does not exceed 75% of the fuel resistivity.

An evaluation of the expected measurement accuracy with various assumed combinations of resistivity is in progress.

Redesign of the transducer made a considerable change necessary in the associated electronics. These changes should be completed shortly.

d. Mark-II Driver Fuel Element Development (J. H. Kittel)

(i) Element Irradiation Tests, Metallurgy, Idaho (M. A. Pugacz)

Last Reported: ANL-7445, pp. 69-70 (April 1968).

As of April 13, 1968, the experimental fuel elements in Subassembly XO29 were exposed to 1154 MWd of operation in EBR-II. The maximum calculated burnup was 0.67 a/o. At this date, the reactor was operating at full power.

Criticality procedures for movement of capsules were partially resolved. As a result, four capsules have been processed through sodium loading, welding of end closures, X-ray inspection of welds, and X-ray and pulsed electromagnetic inspections of the sodium bond. Plans are to pack and ship these capsules in the near future.

A computer program was written to calculate the creep strain in the Mark-II fuel cladding as a function of temperature. Preliminary results are listed in Table II.E.5.

TABLE II.E.5. Creep Strain in Mark-II Cladding

Type Stainless Steel	Temperature (°C)	Time Required for Creep Strain (hr)	
		0.1%	1.0%
304L	500	9,310	14,800
304L	550	7,290	9,650
304L	600	5,390	6,860
316	500	12,000	14,700
316	550	9,980	13,600
316	600	7,740	11,200

(ii) Fabrication of Mark-II Fuel Elements (A. G. Hins and F. D. McCuaig)

Fifteen prototype EBR-II, Mark-II fuel elements were manufactured and inspected for irradiation testing in CP-5. Ten 4.2-in.-long elements were instrumented for temperature measurement along the centerline of the pin, and five elements were instrumented for measurement of gas plenum pressure.

The fuel pins were made of injection-cast U-5 w/o Fs alloy (50% ^{235}U) and were 0.130 in. in diameter by 2 in. long. The holes for thermocouple wells (0.028 in. in diameter by 1 in. deep) were drilled into the upper end of the pin by the elox process. The pins were cleaned and vacuum outgassed. Tubes of Type 304 stainless steel (of 0.150-in. ID by 0.012-in. wall) were used as the cladding material.

After the fuel pins were inserted into the claddings, the elements were sodium bonded (by vacuum-pressure soak) at 500°C for 2 hr; standard end plugs were then welded to the claddings. The sodium bond was inspected by both point-probe and encircling-coil eddy-current equipment. Those elements that contained bond defects were subjected to the conventional impact-bonding cycle.

Once acceptable bonds were produced, the standard top end plugs were removed by a tubing cutter, and the adaptor end plugs, which contain thermocouples or pressure transducers, were installed. For installation of the thermocouples, the elements were heated to 150°C to melt the sodium in the thermocouple well. After rewelding, sodium levels above the fuel pin were determined by X-radiography. The thermocouple elements were tested for continuity by heating to 300°C. After visual inspection, the elements were shipped to the Fuels Performance Group for encapsulation.

e. Equipment--Fuel Related (E. Hutter)

(i) Improved Gripper and Holddown Force-limit Device

Last Reported: ANL-7438, p. 53 (March 1968).

Tests of the prototype system continued. The commercial force gauge was recalibrated with a tensile testing machine. When the gauge was used in compression, the calibration constant was found to depend on the mounting arrangement. Typical values of force measured for the same gauge reading (140° positive displacement) were 3600, 3800, 4150, and 3900 lb. The value from the factory calibration chart, 5050 lb, could not be duplicated with any of our mounting arrangements. The value 3900 lb is the calibration check for the mounting arrangement that will be used in testing the prototype system.

In tension, our calibration indicated better agreement with the factory calibration. For a reading of 140° negative displacement, our calibration value is 3850 lb as compared to the factory calibration of 4100 lb.

Much of the hysteresis that was indicated earlier still remains. It amounts to about ± 100 lb at the zero-force position. We suspect that this is caused by friction between some spring-guide rods and their clearance holes. The small clearance is not necessary, so we are increasing it.

Small fail-safe brakes will be added to the instrument-type servomechanisms that are used to retain the value of packing-gland friction (see Progress Report for January 1968, ANL-7419, p. 59) so as to minimize oscillation when power is removed and the mechanism inadvertently is moved during maintenance of adjacent equipment. While two servo units are being modified, two are being retained in the test rig. When the first two have been returned, the remaining two will be modified. To minimize occasional wire-to-wire oscillations, conductive plastic potentiometers have been ordered as possible replacements for the present wire-wound units.

Dynamic tests using a light-beam oscillograph are being started to determine the time response of the system to the force signals.

An optical meter-relay controller has been checked as a total force indicator with manually adjustable limits. Although the speed of response of this meter is relatively slow (about 0.4 sec), it will be a satisfactory backup limit during slow-speed operation. The electronic fast-trip limits will be retained.

f. Equipment--Reactor and Primary Coolant System
(B. C. Cerutti)

Last Reported: ANL-7445, p. 73 (April 1968).

(i) General Improvements

(a) Plugging Meter for Primary Purification System. The design of a new plugging meter for use in the primary purification system was completed. The plugging valve for the new system will be a modified NUPRO SS-8UW with high-temperature backup packing. The stem insert of this valve is provided with ten 40- by 40-mil grooves which function as plugging orifices. All the valves in the system will be operated remotely with flexible shafts. The plugging valve, as well as other components, are mounted in the system with "Conoseal" unions to provide for convenient maintenance or replacement.

The system utilizes a bypass valve to provide a relatively constant head at the plugging valve. This will result in a more pronounced change in the rate of flow at the saturation temperature, and the plugging temperature will therefore be determined with greater accuracy.

The new plugging-meter design includes a sodium-to-sodium heat exchanger and a sodium-to-air heat exchanger. The rate of air flow through the sodium-to-air heat exchanger may be varied from 0 to 120 cfm to provide positive temperature control for the system.

The system is provided with sequenced heating to prevent component failure due to differential thermal expansion of sodium during its melting. Other instrumentation includes leak detectors and temperature-activated cutouts for abnormal conditions. The basic system control is as reported in the Progress Report for September 1967, ANL-7382, p. 35, the only difference being in the monitoring of the system. The new plugging-loop heater and temperature readouts will be presented on a graphic panel in an area cleared by the removal of the former system.

The expected advantages of the new plugging meter are greater accuracy, simpler operation, and easier and less frequent maintenance.

(b) Boron Carbide Control Rod. Control rod No. EB-1-26059 which previously had a follower of enriched boron carbide was reworked to provide it with a 9-in.-long follower of natural boron carbide. The reworked rod, designated T-500A, was placed in control rod position No. 5 and calibrated at 500 kW. The results indicated that the reactivity worth of this rod was 178 lh. The worth of a normal control rod in this position was measured to be 138 lh.

(ii) Instrumentation

(a) Reactor Cover Gas Monitor (RCGM). On May 3, 1968, the new RCGM was temporarily installed in the depressed area in the Reactor Building floor prior to the start of Run 27I, in readiness for a possible fission-gas release from experimental Subassembly XO28. The analyzer discriminators were set for the gamma radiation of ^{133}Xe , ^{135}Xe , and ^{41}Ar with a window width of 8%.

The fission-product release of May 6, 1968 (see Sect. II.E.1.a.(i).(e)), was recorded by the RCGM as well as by the fission-gas-monitor system (FGM). Although the equipment was not precisely calibrated before the test, it operated well and demonstrated its usefulness.

(b) Primary-coolant Flow-monitoring Equipment. Following a series of problems, traceable to vacuum-tube failures in the primary-coolant flow-monitoring equipment, the vacuum-tube-type millivolt to milliamp (mV/I) converters were removed and replaced by static converters.

(c) Shield-cooling System. Improvements were made to the control system for the refrigeration compressors and the solenoid-operated valves in the shield-cooling system. Additional circuit protection and isolation were provided by fusing each of the individual solenoid valves and by installing a separate control transformer for the refrigeration compressor controls.

(iii) Sodium Sampling Pump and Filter. Procedures have been prepared for: (1) installing the sodium-sampling pump and filter in the primary-tank spare nozzle; (2) removing the sampling pump and filter, and replacing the used filter with a new one, and (3) reinstalling the sampling pump and filter in the primary-tank nozzle.

(iv) Intermediate Heat Exchanger Seal. The baffle to be installed in the annular gap between the heat exchanger and the tube bundle has been heat-treated and successfully dry-tested in the test fixture.

Additional analysis indicates that it may be more desirable to install the baffles lower on the heat exchanger than originally planned. This change in position may require modification of the baffle shape. The final revisions to the baffle design are being determined.

g. Secondary Sodium and Power Systems (B. C. Cerutti)

(i) Study--Sodium-Water Reaction, Pressure Relief, Secondary System

Last Reported: ANL-7445, pp. 74-75 (April 1968).

A basis has been developed for calculating the leak flow rate of steam from the tube side of the superheater as a result of tube rupture. Quasi-steady decompression of the steam system is assumed. Isentropic lines in the superheated vapor were fitted by a gamma-law representation; for the range of steam states of interest, the polytropic exponent is constant at the value 1.29. In the two-phase-mixture region, isentropic processes are characterized by a linear relation between specific volume and the reciprocal of pressure.

Expressions were obtained for mass flow rate per unit of break area as a function of current steam-reservoir state and current reaction-product bubble pressure. For sufficiently low back-pressures, the flow at the break is choked. Depending on the current reservoir state, choking may occur with the critical state in the superheated vapor, in the two-phase mixture, or in some cases on the saturation line.

A computer program was written to calculate the unit flow rate for arbitrary reservoir states and back-pressures in the range of interest, and curves of unit-area flow rate were obtained as a function of back-pressure for steam states at 1325 psia and 580-800°F. An upper limit to the unit flow rate, representing choked flow from a break at the inlet tubesheet, is 18.9 lb/sec-in.².

The analysis described above is a necessary link between steam-system decompression and reaction-product bubble pressure. With minor modification, the computer program can be converted to a subroutine connecting steam-system dynamics to shellside conditions.

Mass and energy balances were written for the injection of steam into a volume of sodium, temporarily assuming one-dimensional motion of a compressible sodium column in a rigid pipe. Growth of the reaction-product zone is coupled to the dynamics of the unreacted sodium. The average reaction-product state can be estimated without consideration of the overall balance of momentum; in turn, the momentum balance

determines the reaction force on the vessel. The process is analogous to a so-called Fanno model in gas combustion.

This approach will be extended to couple the reaction-product bubble state to more general (e.g., other than in a one-dimensional plane) pressure-velocity relations in the unreacted sodium, including the effect of shell dilation. This will link reaction-product zone growth to leakrate and ultimately to shell response.

h. New Subassemblies Design and Experimental Support
(E. Hutter)

(i) Radial Blanket

Last Reported: ANL-7445, p. 75 (April 1968).

Replacement of the stainless steel reflector elements in Rows 7 and 8 by nickel elements is being studied (see Progress Report for August 1967, ANL-7371, p. 37). The change would increase the reactivity available in the core, which would permit more irradiation experiments to be accommodated. Reactivity, corrosion, transport, activation, and deposition processes involved in the use of large amounts of nickel in the reactor are being evaluated.

Numerous reflector-subassembly design concepts have been evaluated (see Progress Report for February 1968, ANL-7427, p. 63), and the most favorable ones have been selected. Because nickel is an efficient reflector, it will be used for the reflector-subassembly elements. However, the nickel elements will be clad with stainless steel to avoid any problem with nickel-sodium incompatibility. Production costs for the selected designs will be less than for the uranium blanket subassemblies now in the reactor.

The most favorable reflector-subassembly bowing effect will result from distributing the proper quantity of coolant flow within the subassembly and slightly increasing clearances between the upper portions of the subassemblies. As the possibility of fuel-handling difficulties increases with increased clearances, the optimum clearance change for this nickel reflector subassembly is being studied.

(ii) Irradiation Subassemblies

Last Reported: ANL-7445, pp. 75-76 (April 1968).

(a) Mark-F. The Mark-F37 irradiation subassembly, (see Progress Report for January 1968, ANL-7419, p. 65), with 37 dummy elements consisting of 0.250-in.-dia solid rods, but without the optional orifice plate, was flow tested in the pressurized-water test loop.

The tests show that the design is acceptable for fuel-irradiation experiments within the standard limits of coolant outlet temperature.

Appropriate bushings on the lower adapter simulated the inlet-coolant-flow restriction for each reactor row. Figure II.E.3 shows the data, converted to values for 800°F sodium by means of density and viscosity corrections. The flow for each effective pressure drop with respect to row position is shown in Table II.E.6, which also shows data for a standard core subassembly that was used to calibrate the loop. The spiral-wire spacers on the elements in these subassemblies had the 6-in. pitch that is standard in all EBR-II elements. If the pitch is increased to 12 in., as has been suggested for some experiments, the pressure drops would be only slightly reduced.

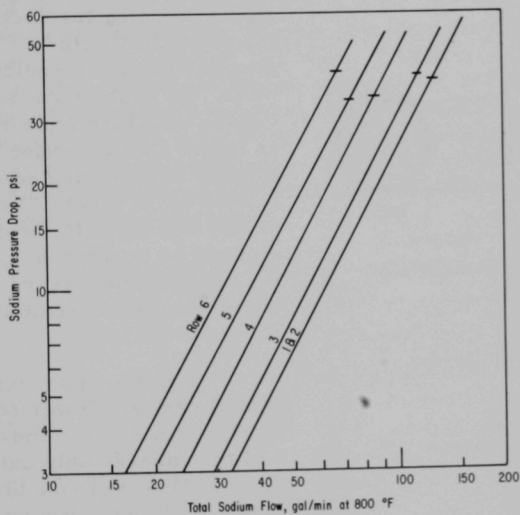


Fig. II.E.3. Flowtest of the EBR-II Mark-F37 Irradiation Subassembly for Reference 67-element Core

TABLE II.E.6. Flowtest Data for EBR-II Subassemblies

Reactor Row	Effective Pressure Drop (psi)	Flow of 800°F Sodium (gal/min)	
		Standard Core Subassembly	Mark-F37 Subassembly
1, 2	38	139	125
3	39	123	114
4	34.5	93.5	86
5	34	78	73
6	41	70	67

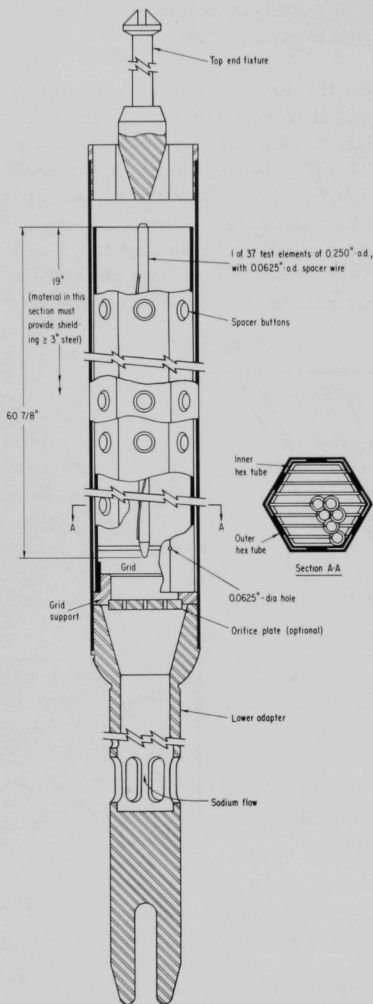


Fig. II.E.4. EBR-II Irradiation Subassembly Mark-F37 has 0.250-in. Fuel Elements in a Hexagonal Bundle Having a 1.25 Pitch-to-Diameter Ratio, which Requires 0.0625-in.-dia Spiral Spacer Wires

insulation provided by the annulus tends to reduce the effect of heat transfer from adjacent subassemblies.

With the 37 solid stainless steel dummy elements, the Mark-F37 subassembly weighs 53.2 lb in air and 47.1 lb in sodium. As for all core-type subassemblies, the Mark-F37 subassembly is designed so that the force seating it in the grid increases with flow rate; thus positive seating forces are assured for all reactor flow rates.

As shown in Fig. II.E.4, to achieve the maximum possible length ($60\frac{7}{8}$ in.) for the test fuel elements, the Mark-F37 design has no upper or lower shield or reflector sections as part of the normal structure. This is standard practice for the irradiation subassemblies. To protect the reactor cover and vessel structure from radiation damage, an upper shield section must be installed to provide shielding equivalent to at least 3 in. of steel. The design of the shield section will depend on the experiment to be conducted. Additional shielding might be necessary if many irradiation subassemblies are to be placed in the core.

The top end fixture, outer hexagonal can, and lower adapter shown in Fig. II.E.4 are standard hardware, and the subassembly outer dimensions are identical to those of other EBR-II subassemblies. New or special hardware includes the grid support (with provisions for a flow-orificing plate), the grid assembly, and an inner hexagonal tube ($61\frac{21}{32}$ in. long by 2.006 in. across the inside flats), which encloses and supports the 37 fuel elements. The main coolant flow passes through the inner hexagonal can. An annular space between the inner and outer can contains relatively stagnant sodium (there are two 0.0625-in.-dia holes that allow a slight flow through the annulus). The

i. Instrumented Subassembly System (E. Hutter)

Last Reported: ANL-7438, pp. 55-57 (March 1968).

(i) Bowing Effect with and without Spacers. Because the instrumented subassembly is held rigidly at the top by its upper extension, some loads might be produced by thermal bowing that would cause undesirable creep or reactivity phenomena. Accordingly, the BOW code* has been used to estimate the loads and deflections that will be associated with the instrumented subassembly.

Relevant results are given in Table II.E.7. Each case is identified by the nominal radial clearance between the instrumented subassembly and its thimble, at two elevations. If no spacers are installed between the hexagonal tube and the thimble, the nominal radial clearance is the largest value shown, namely, 151 mils. However, we plan two spacers, one at the top and one at the elevation of the reactor-subassembly spacer dimples (near the core horizontal centerline), which would reduce the nominal radial clearance to 15 mils at those two locations. Thus Case F represents the conditions expected after the instrumented subassembly is installed. The other cases were investigated to determine the effect of different numbers and sizes of spacers.

TABLE II.E.7. Calculated Bowing Data for Instrumented Subassemblies at 62.5-MWt Reactor Power

	Case						
	A	B	C	D	E	F	G
Nominal radial clearance between instrumented subassembly and thimble							
at top, mils	151	151	151	15	9	15	9
at elevation of spacer dimples, mils	151	15	9	151	151	15	9
Deflection of instrumented subassembly							
at elevation of dimples, mils	-18	-11	-6	-18	-18	-16	-12
Deflection of thimble							
at top, mils	+42	+36	+33	+15	+9	+15	+9
at elevation of dimples, mils	+9	+4	+3	-2	-3	-2	-4
Deflection of Row-4 subassembly							
at top, mils	+69	+63	+60	+43	+37	+43	+37
at elevation of dimples, mils	+5	+3	+2	-1	-2	-1	-3
Load exerted by Row-4 subassembly							
on top of thimble, lb	-0.4	-2	-2	-4	-5	-4	-6
on thimble dimples, lb	0	-3	-6	-5	-5	-5	-7

*Bump, T. R., Trans. Am. Nucl. Soc. 10(2), 661-662 (Nov 1967).

Deflections in Table II.E.7 indicate the radial movements (of the vertical centerlines of the components involved) away from the vertical centerline of the inlet-plenum grid-plate holes in which each component is installed. Positive deflections indicate movement away from the center of the core. If there are no spacers (see Case A), the top of the Row-4 subassembly bows outward and pushes lightly (~0.4 lb force) against the thimble, which also bows outward, but less. (Nominal clearance between Row-4 subassembly and thimble was taken to be 27 mils.) The load on the top of the thimble pushes it out farther at the dimple elevation (9 mils) than the Row-4 subassembly is pushed out at that elevation by thermal expansion of the core subassemblies (5 mils). In this case the instrumented subassembly bows 18 mils inward at the dimple elevation.

With the planned spacers (see Case F), the top of the thimble can bow and be pushed outward only 15 mils instead of the 42 mils possible in Case A. Similarly, the outward movement of the top of the Row-4 subassembly is reduced from 69 to 43 mils. This increases the load exerted on the top of the thimble to ~4 lb. The thimble is forced to move inward at the dimple elevation, by both its bowing and that of the instrumented subassembly, so that a load of about 5 lb is exerted on the thimble by the Row-4 subassembly at that elevation. Inward bowing of the instrumented subassembly is reduced slightly, to 16 mils.

Although loads and positive reactivity are both increased by adding the planned spacers, the increases are inconsequential, and there is no need to modify the spacers.

The values in Table II.E.7 are based on these maximum temperature differences across flats of the components: instrumented subassembly, 21°F; thimble, 10°F; Row-4 subassembly, 29°F. These values, which were calculated earlier for a control rod; apply to the top (downstream) end of the core and for 45-MWt reactor power (they were modified for 62.5-MWt power); in each case the inboard face is hotter than the outboard face.

It was assumed that the new reflector subassemblies (see Progress Report for February 1968, ANL-7427, p. 63), which should exert only light loads on the core, were in use. In addition, no radial movement of the top or bottom ends of the instrumented subassembly was permitted.

(ii) Data Handling. Requirements for data recording were established for the first fueled EBR-II instrumented subassembly. They apply to the first fueled experiment, so they do not involve a complete high-speed digital data-handling system.

Table II.E.8 lists the expected outputs and source resistances of the instruments in the instrumented subassembly system. All the source resistances are those expected at the subassembly junction box, except for that of the pressure transducer, which is the source resistance

at the strain-gauge transducer located on the operating floor. The source-resistance computations are based on the source resistance of each transducer, the 24-gauge lead wire from the bulkhead to the junction box, and the expected temperature profile along the length of the subassembly. The source resistances listed are conservative, i.e., the maximum expected values. The expected thermocouple outputs, where listed in millivolts, are referenced to 0°C. An output record in engineering units is desirable wherever possible.

TABLE II.E.8. Source Resistances and Expected Outputs of the Instruments in the EBR-II Instrumented Subassembly

	Source Resistance (ohm)	Expected Temperature		Thermoelements
		°C	mV	
Flowmeter [0-60 gpm (0-20 mV)]	106			
Fuel-pin thermocouples	96	≤1800-2400	≤32.9 -40.8	W-3% Re/W-25% Re
Inlet coolant thermocouple	99	250-375	10.16-15.34	Chromel/Alumel
Cladding thermocouples	107	250-500	10.16-20.65	Chromel/Alumel
Outlet thermocouples	61	250-500	10.16-20.65	Chromel/Alumel
Pressure-transducer thermocouples	68	250-500	10.16-20.65	Chromel/Alumel
Structural-material thermocouples	83	≤550-800	22.78-33.30	Chromel/Alumel
Pressure transducer [≤300 psi (16 mV)]	350 (at transducer)			

Analog strip charts and 12 two-pen recorders will continuously record the 22 signals from the instrumented subassembly plus one neutron-flux signal (for a total of 23 signals). All signals will be read in engineering units, except for flux and pressure signals. Temperatures will be displayed in °C, pressures in millivolts, and flow rates in gal/min; flux will be recorded on the same chart as flow rate. All analog recorders will have high- and low-limit alarms for each signal, and automatic and simultaneous time-marking capabilities. A chart speed of 4-12 in./hr will be used for long-term steady-state operation.

Digital records will be made for computer processing. The particular sequence of signal sampling will be established by the experimenters. Time information and signal values will be recorded digitally to establish the initial or final time when each sequence of samples was recorded. During steady-state reactor operation, each of the 22 signals from the instrumented subassembly will be limit-checked at ~90-sec intervals. If an alarm condition exists, the 23 important signals will be recorded; if the signals are not in an alarm condition, the 23 important signal values will be recorded at 30-min intervals. During startup, the instrumented-subassembly signal values, including the reactor-flux signal, will be recorded on magnetic tape at high speed. The rate of reactor power rise should be consistent with present equipment so that each of the 23 signals will be recorded at least 20 times during each doubling of reactor power. A higher sampling rate is desirable if available.

Signal conditioning is necessary to accomplish accurate recording (by preventing interaction between the types of simultaneous recording being used), to reduce noise problems caused by possible

long transmission paths, and to provide cold-junction compensation for thermocouples. Therefore, the 22 signals from the instrumented subassembly will be converted from voltage to current by standard transmitters, such as the Leeds & Northrup TC/EMF transmitter. The transmitters will contain cold-junction compensation for their respective thermocouples, and will allow the conversion of negative and positive flow readings for the flow monitor. The transmitter also will be capable of producing a high or low full-scale signal should an "open" in the transducer circuit occur.

The source resistances listed in Table II.E.8 are the calculated dc values expected at the instrumented-subassembly junction box atop the small rotating plug. Additional resistance will be encountered in the cables connecting the transmitters to the junction box. These resistances must be kept as low as possible by using short cable lengths and connection distances. The transmission of the instrumented subassembly signals from the junction box to the transmitters, and from there to the recorders, will be by twisted pairs.

(iii) Instrumented-subassembly Dismantling. A procedure has been prepared for dismantling instrumented subassemblies after they are removed from the reactor. This procedure, which forms the basis for consideration by the operating staff of the Fuel Cycle Facility, is derived from experiments with several methods of severing the instrument leads before removal of the top-end fixture.

Access to the leads requires removal of a section of the hexagonal outer tubing between the capsule tops and the top fixture. A pneumatic-hammer panel-shearing chisel made satisfactory axial cuts, but was unable to complete circumferential cuts satisfactorily. An electrically powered double-cut shear (Burke-Docken type) made cuts in both directions with ease and can also be used to sever the instrument leads; a more compact pneumatic power shear of this type, which is more easily held by manipulators, is being recommended for this operation. A conceptual design for a tube-pulling adapter for the final step of this operation is being prepared.

j. Process Chemistry (D. W. Cissel)

(i) Sodium Coolant Quality and Control

Last Reported: ANL-7445, pp. 76-77 (April 1968).

(a) Primary Sodium

(1) Radionuclides. Results of analysis for radionuclides in the primary sodium are listed in Table II.E.9. Analyses of samples taken simultaneously from the FERD loop and the primary-sodium purification system on April 25, 1968, show excellent agreement for ^{137}Cs and ^{131}I concentrations (see Table II.E.9).

TABLE II.E.9. Radionuclides in Primary Sodium

Date Sampled	Activity Corrected to	^{137}Cs [$\mu\text{Ci/g}$ ($\times 10^2$)]	^{131}I [$\mu\text{Ci/g}$ ($\times 10^3$)]	^{133}I ($\mu\text{Ci/g}$)
4/23/68	4/20/68	1.6	9.3	No analysis
4/25/68 ^a	4/20/68	1.55	9.54	No analysis
		1.62	9.78	No analysis
4/25/68 ^b	4/20/68	1.55	9.02	No analysis
		1.61	9.78	No analysis
5/2/68	5/2/68	1.55	2.08	No analysis
		1.49	2.62	No analysis
5/6/68	5/6/68	1.61	3.79	2.97×10^{-3}
		1.62	4.10	3.70×10^{-3}
5/9/68	5/9/68	1.38	3.09	No analysis

^aFrom purification-loop sampling system.

^bFrom FERD loop sampling system.

(2) Oxygen. A sample of primary sodium taken on March 5, 1968, was analyzed for oxygen by the mercury amalgamation method. Duplicate analyses yielded 20 and 24 ppm oxygen, respectively. The expected oxygen concentration based on the plugging temperature was < 5 ppm. The high values may be due to contamination of the sample during the sampling process, in transit to Illinois or during analysis.

(3) Hydrogen. A sample of primary sodium taken on March 5, 1968, was analyzed for hydrogen by the isotope dilution method. Duplicate analyses yielded 1.5 and 1.7 ppm hydrogen.

(4) Nitrogen. Analysis for CN^- was made on one sample of primary sodium. No CN^- was detected with the Orion CN^- specified electrode, for which the lower detection limit is 0.2 ppm CN^- . This value may be revised as further experience is gained with the method.

(b) Secondary Sodium

(1) Radionuclides. A sample of secondary sodium taken on April 5, 1968, was analyzed for radionuclides. ^{24}Na activity was $3.1 \times 10^{-2} \mu\text{Ci/g}$. No other isotopes were detected.

(2) Trace Metals. Two samples were analyzed for trace metal impurities. The results are listed in Table II.E.10.

TABLE II.E.10. Secondary-sodium Trace-metal Impurities

Impurity	Concentration (ppm)		Impurity	Concentration (ppm)	
	3/22/68	4/1/68		3/22/68	4/1/68
Al	3	a	Fe	2.6	3.0
Bi	0.3	a	Mg	0.8	0.4
Co	<0.7	<0.9	Mn	<0.4	<0.4
Cr	<0.6	a	Ni	<1.0	<1.0
Cu	0.5	0.5	Sn	None detected	a

^aNo analysis.

(3) Carbon. Carbon-recovery tests using cyanuric acid standards were completed. As mentioned previously,* these tests were made to check carbon recovery by the oxyacidic flux method from compounds containing carbon and nitrogen in the presence of sodium. The present series checked carbon recovery from the bond system =C=N-. Results are listed in Table II.E.11.

TABLE II.E.11. Carbon-recovery Tests for Cyanuric Acid
(88.9 μ g added)

Run No.	Carbon in Na (μ g)	Total Carbon Present (μ g)	Carbon Recovered (μ g)	Percent Recovery
1	2.8	91.7	88	96
2	3.3	92.2	88	95.6
3	3.4	92.3	95	103
Average of Runs =				98.2

Two samples of secondary sodium were analyzed for carbon. Results are listed in Table II.E.12

TABLE II.E.12. Analyses of
Secondary Sodium for Carbon

Sample Date	Carbon (ppm)
2/1/68	3.3
4/15/68	4.2

(4) Nitrogen. Analysis for CN^- was made on one sample of secondary sodium. No CN^- was detected with the Orion CN^- specific electrode, whose lower detection limit is 0.2 ppm CN^- .

(c) Primary and Secondary Argon. A summary of data from the primary and secondary continuous gas-chromatographs is shown in Table II.E.13.

*Progress Report for March 1968, ANL-7438, p. 59; Progress Report for February 1968, ANL-7427, p. 65.

TABLE II.E.13. Primary and Secondary Sodium
Cover-gas Analysis 4/16/68 through 5/15/68

	Primary			Secondary		
	High	Low	Avg	High	Low	Avg
H ₂ (ppm)	112	0	8	20	0	2
N ₂ (ppm)	24,000	2,400	6,000	1,900	1,000	1,350

Since startup of EBR-II, a gradual buildup of nitrogen in the argon of the primary cover-gas system has occurred. Periodically, the nitrogen concentration has been reduced to less than 1000 ppm by purging the system with argon during a reactor shutdown. Periodic attempts have been made to correlate this nitrogen buildup with certain phases of operation or maintenance, without success.

An investigation was recently initiated to determine the method and point of introduction of air into the system. The results indicate that introduction of air into the primary cover-gas system occurs during fuel handling, specifically during the transfer of subassemblies into or out of the primary tank.

The investigation will continue in an effort to determine more exactly which operation, system, or component is responsible for the air inleakage.

k. Experimental Irradiations and Testing (D. W. Cissel)

Last Reported: ANL-7445, pp. 78-83 (April 1968).

(i) Experimental Irradiations

(a) Status of Experiments in EBR-II. The status of experimental irradiations in EBR-II as of May 31, 1968, is shown in Table II.E.14.

In the continuing investigation to locate the source of fission-gas releases, experimental Subassembly XO28 was identified as an apparent source of fission products, and its irradiation was terminated at the end of Run 27I.

At the start of Run 28A, experimental Subassemblies XO37 and XO38, containing structural materials, were loaded into grid positions 7C3 and 7C5, respectively.

Experimental fuel-bearing Subassemblies XG02, XG03, XG04, XO10, XO19, XO20, XO31, and XO32 were reloaded into their

TABLE II.E.14. Status of EBR-II Experimental Irradiations

Subassembly (Position)	Date Charged	Capsule Content and Number of Capsules ()	Experimenter	Accumulated Exposure (MWD) 5/31/68 ^b	Estimated Goal Exposure (MWD)
XG02 ^a (7A1)	7/16/65	UO ₂ -20 w/o PuO ₂ Stainless Dummies (1) (18)	GE	14,380	16,700
XG03 ^a (7D1)	7/16/65	UO ₂ -20 w/o PuO ₂ Stainless Dummies (2) (17)	GE	14,380	22,500
XG04 ^a (7B1)	7/16/65	UO ₂ -20 w/o PuO ₂ Stainless Dummies (2) (17)	GE	14,380	42,000
XA08 ^c (4F2)	12/13/65	UC-20 w/o PuC Structural (8) (11)	ANL ANL	10,774	19,800
XO10 ^a (7F3)	3/24/66	UO ₂ -20 w/o PuO ₂ Structural (4) (11) Structural (4)	GE ANL PNL	11,311	19,600
XO12 ^c (4B2)	8/10/66	UO ₂ -20 w/o PuO ₂ (19)	NUMEC	7,150	20,100
XO15 ^c (4A2)	11/15/66	UO ₂ -20 w/o PuO ₂ (11) UO ₂ -20 w/o PuO ₂ (2) UC-20 w/o PuC (4) U-Fs (Mk-1A) (2)	NUMEC GE ANL ANL	5,495	11,000
XO16 (4D2)	1/13/67	Structural (9) Structural (10)	ANL GE	5,141	7,400
XO17 ^c (4C3)	11/15/66	UO ₂ -20 w/o PuO ₂ (11) UC-20 w/o PuC (3) U-Fs (Mk-1A) (5)	NUMEC UNC ANL	5,495	6,500
XO18 (2B1)	12/6/66	Structural (3) Structural (1) Structural (2) Structural and Heavy Metal Fission Sample (1)	GE PNL ANL ANL	5,781	21,300
XO19 ^a (6D2)	1/13/67	UO ₂ -20 w/o PuO ₂ (7) UC-20 w/o PuC (3) Structural (8) Graphite (1)	GE UNC PNL PNL	4,567	7,500
XO20 ^a (6B5)	1/13/67	UO ₂ -PuO ₂ (9) UC-20 w/o PuC (3) Structural (4) Structural (2) Graphite (1)	GE UNC PNL ANL PNL	4,567	7,500
XO21 (2D1)	2/25/67	Structural (7)	PNL	5,141	21,500
XO22 (7C4)	2/26/67	Structural (7)	PNL	5,141	5,000
XO25 (4E2)	10/10/67	Structural (19)	GE	3,493	7,400
XO26 (7D5)	10/11/67	Structural (7)	NRL	3,493	3,900
XO27 ^c (4B3)	11/21/67	UO ₂ -25 w/o PuO ₂ (18) Structural (1)	GE PNL	1,587	7,200
XO28 ^d (4D3)	11/21/67	U-15 w/o Pu-10 w/o Zr (15) U-Fs (4)	ANL ANL	1,730	9,200
XO29 ^c (4E3)	12/22/67	U-Fs (Mk-II) (37)	ANL	1,543	5,100
XO31 ^a (6C1)	11/22/67	UO ₂ -25 w/o PuO ₂ (19)	PNL	1,959	2,200
XO32 ^a (6F1)	11/22/67	UO ₂ -25 w/o PuO ₂ (19)	PNL	1,890	11,000
XO33 ^c (5E2)	12/22/67	UC-20 w/o PuC (19)	UNC	1,037	10,000
XO34 (2F1)	4/13/68	Structural (7)	ORNL	1,037	13,500
XO35 (7B4)	4/13/68	Structural (7)	ORNL	1,037	40,500
XO37 (7C3)	5/8/68	Structural (7)	INC	528	3,400
XO38 (7C5)	5/7/68	Structural (7)	INC	528	16,000
X900 (7A4)	3/20/68	Structural (18)	ANL	1,323	2,700

^aInstalled for Run 288, on.^bAccumulated exposure during May was 682 MWD for those subassemblies that were in the reactor all month.^cInstalled for Run 28C, on.^dInstalled for Run 271, then terminated.

respective grid positions at the start of Run 28B. This reloading was part of a reinsertion schedule of experimental subassemblies following removal of XO28.

The remainder of the fueled experimental subassemblies (except XO28) were returned to the reactor at the start of Run 28C.

(b) Status of Irradiation Experiment Proposals Given Approval-in-Principle (AIP). Table II.E.15 summarizes the present status of all irradiation experiments which have been given AIP but have not been inserted in the reactor.

TABLE II.E.15. Status of Experiments with AIP

Sponsor	Material to Test	No. Caps.	Suggested Reactor Row ^a	Date of AIP	Estimated Date for Delivery to Idaho Site
ANL	Oxide fuel, Group 0-3	19	3	9/22/67	12/68
	Carbide fuel, Group C-5	19	2	9/22/67	1/69
	Oxide fuel (unencap)				
	Safety Program	19	4	9/6/66	6/67 ^b
	Mark-II fuel (unencap)	455	Core	9/22/67	6/68
	Mark-II fuel (unencap) ^c	25	4	6/3/67	5/68
	Metal fuel, M-4	19	3	2/13/68	6/68
	Structural, Group S-9	19	4	9/22/67	6/68
	Magnetic materials	7	7	6/8/67	7/68
	Instrumented subassembly	1	5	5/9/68	2/69
BMI	Nitride fuels	8	7	2/13/68	7/68
GE	Oxide fuels, Group 8-B	19	7	6/7/67	2/68 ^b
	Oxide fuels (unencap), Group 3	16	4	9/6/66	6/67 ^b
	Oxide fuel, Group 7	4	4	9/2/66	2/68 ^b
	FCR structural Group L-15	4	2	1/4/68	11/67 ^b
	Oxide fuel (unencap), Group 5	16	4	1/20/67	7/68
	Oxide fuel (unencap), Group 9A	37	4	1/20/67	6/68
	Oxide fuel (unencap), Group 9B	37	6	5/9/68	9/68
	Oxide fuel (unencap), Group 9C	37	5	5/9/68	7/68
	Oxide fuel (unencap), Group 9D	37	7	5/9/68	8/68
	LASL	Oxide insulators	1	8	6/6/67
Carbide fuels		1	2	2/27/67	3/68 ^b
		6	3		6/68
NRL	Structural materials	7	7	9/6/67	10/68
ORNL	Oxide insulators	7	8	9/21/67	7/68
	Sol-gel oxide fuel	5	4	5/9/68	7/68
PNL	Oxide fuel (unencap) (low power)	37	3	9/21/67	7/68
	Oxide fuel (unencap) (normal power)	37	4	9/21/67	8/68
	Oxide fuel (unencap) (high power)	37	3	9/21/67	9/68
	Graphite materials	7	7	7/31/67	Indefinite
	Thermocouple materials	5	4	7/31/67	7/68
		2	4	7/31/67	2/68 ^b
		5	3	3/4/68	3/68 ^b
	Oxide fuel, Group X	7	7	5/9/68	5/68 ^b
	Structural, Group 7	7	7	5/9/68	6/68
	B ₄ C Poison	7	7	5/9/68	6/68
UNC	Carbide fuel (129-147)	19	7	6/6/67	7/68
	Carbide fuel (high power)	6	3	1/20/67	7/68
W	Carbide fuel (+V-alloy)	2	3	9/21/67	6/68
	Carbide fuel (+V-alloy)	9	4	9/21/67	Indefinite

^aBased upon fission rates at a reactor power of 45 MWL.

^bDate received.

^cReplacements for capsules of same type whose irradiation is nearing completion (e.g., Subassembly XO29).

(ii) Nondestructive Testing

(a) Preirradiation Inspections. Seven Mark-B-7 structural experimental capsules BNWL-16 through -22, were received from Pacific Northwest Laboratory. X-ray examination shows them to be satisfactory for installation.

(b) Neutron Radiography. Designs were completed for two new improved experimental capsule holders to be used for neutron radiography at TREAT. The holder for uranium-bearing experimental capsules was completed. The enclosed capsule holder for experiments containing plutonium is being fabricated and will be used for capsules removed from experimental Subassembly XO28.

(c) Antimony-Beryllium Neutron Source for Neutron Radiography in FCF. The trial exposures completed last month were quite satisfactory, and the $1\frac{1}{2}$ - by $1\frac{1}{2}$ -in. collimator was chosen for future use in the FCF. The beryllium source block was decontaminated and removed from the repair room at EBR-I in preparation for shipment to the FCF.

As a cross-check on heat-production calculations for the metallic-antimony gamma sources being used, a thimble for the beryllium source block was mocked up so temperature measurements could be taken. A previously irradiated antimony source registered a maximum temperature of 185°F which, when extrapolated back a month, approached 280°F; this temperature is easily within the heat dissipation capabilities of the beryllium source block.

(iii) Handling and Examination

(a) Irradiated Capsules from Experimental Subassembly XG05. GE Capsules F2C, F2H, F2O, F2R, and F2T were shipped to Idaho Nuclear Corp. at the TAN Hot Shop for transfer to a GE cask. Of these five capsules, F2O contained an obviously failed element, and the other four appeared in normal and satisfactory condition.

The remaining four fuel capsules from GE (F2D, F2G, F2V, and F2X) and one ANL-MET capsule (ND-24) are being held at the FCF for a proposed reloading in EBR-II. GE has also proposed to continue the irradiation of its five structural materials capsules from experimental Subassembly XG05. The remaining four capsules from XG05 (NC-17, SMV-2, H MV-5, and NMV-11) belong to ANL-MET and will be returned to Illinois after completion of repair of the hot cell there.

(b) Testing of Subassembly Sodium Removal Procedure

(1) Cyclical Testing of Stressed Capsules. Experimental Subassembly X900, which contains pressure-stressed tubing samples, is undergoing irradiation in position 7A4.

Three specimens removed after the fourth sodium-wash cycle were inspected metallographically. Results were very similar to those from the previous three sets of specimens for the previous cycles. No indication of stress corrosion, attack by sodium, or other changes in microstructure were found.

(2) EBR-II Subassembly Recycle Test. Three full cycles from the primary tank through a water-wash step have been completed on the recycle test of a spent driver-fuel subassembly (C-278). Five full cycles are planned, after which selected driver-pin claddings will be metallographically inspected.

1. FCF Process Analysis and Testing (M. J. Feldman)

Last Reported: ANL-7445, p. 83 (April 1968).

(i) Test and Analytical Methods

(a) Interim Examination Program. A program for interim examination of irradiation experiments is being developed for the FCF. Equipment for neutron radiography, bonding, leak testing, and profilometry is being tested out-of-cell. Flow diagrams for interim examinations are being developed. Several meetings have been held with personnel of the Hot Fuel Examination Facility (HFEF) project to coordinate the long-range interim examination program.

m. FCF Equipment Improvements (M. J. Feldman)

Last Reported: ANL-7445, p. 83 (April 1968).

(i) Auxiliary Equipment. A pneumatic tube system for transferring irradiated samples from the FCF to the Analytical Laboratory is being constructed. The underground tubing between buildings has been installed, and the terminal stations are nearing completion. This system will reduce substantially the time required to transfer samples between the two facilities.

(ii) Repair and Decontamination. Detailed designing for the equipment decontamination facility is underway. Construction of the manipulator decontamination facility has started.

n. FCF Experimental Support--Hot Fuel Examination Facility (HFEF)--Feasibility and Cost Study (N. J. Swanson)

Last Reported: ANL-7445, p. 84 (April 1968).

A trade-off study related to the siting of the HFEF revealed that several advantages could be realized if the facility were positioned at a location independent of other buildings. A site immediately north of the Fuel Cycle Facility has been identified as an acceptable location. New approaches to the conceptual layout of the facility have been possible since restraints imposed by other facilities have been removed by this siting change. A reference design from which Title I will be initiated will be completed in June 1968.

o. Superheater and EM Pump Study and Test (R. A. Jaross)

(i) Superheater Vibration Study

Last Reported: ANL-7438, pp. 67-68 (March 1968).

The potential of the EBR-II evaporator unit to produce detrimental flow-induced tube vibrations has been evaluated. State-of-the-art technology was employed to predict analytically conditions of resonance and instability. The analyses indicated that failures due to these mechanisms are not to be expected.

The evaporator is structurally identical with the superheater, except that there are no core tubes in the evaporator. However, the environmental conditions are less severe for the evaporator; the operating temperatures (677°F on the shell side; 615°F on the tube side) and temperature differentials are smaller, and the sodium flow rate is one-fourth that through the superheater (two superheater units feed into eight evaporator units).

(a) Tube Natural Frequencies. Because of the structural similarity, the eigenvalues of the frequency equation are the same as those for the superheater; the first three natural frequencies for the tubes are given in Table II.E.16 for the two possible support configurations (see Progress Report for November 1967, ANL-7399, pp. 85-86).

TABLE II.E.16. Natural Frequencies of Evaporator Tubes

n	f_n^I (Hz)	f_n^{II} (Hz)
1	16.1	21.9
2	24.9	30.4
3	35.2	41.5

Because the computed natural frequencies are compared with vortex-shedding frequencies to determine if a resonance condition

might occur, we investigated the changes in natural frequency that result from axial loading and creep relaxation.

The axial loading is induced initially by cold-springing and, under operating conditions, by differential expansion between the shell and tubes. The decimal change in fundamental natural frequency caused by this type of axial loading is given by Eq. (7), p. 78, of the Progress Report for February 1968, ANL-7427. Application to the evaporator tubes is summarized in Table II.E.17, where h is the amount the shell is upset, T_s the shell temperature, and T_t the tube temperature.

TABLE II.E.17. Percent Change in Fundamental Frequency due to Axial Loading

T_s, T_t	$h = 3/64$ in.	$h = 1/16$ in.	$h = 5/64$ in.
$T_s = T_t$	-6.9	-9.4	-12.0
677, 615	14.4	12.7	10.5
677, 646	4.4	2.2	-0.1

Long-term creep effects and operational cycling were shown to have a negligible influence on altering the natural frequencies of the superheater tubes (see ANL-7438). The same conclusions apply to the evaporator tubes.

(b) Resonant Vibrations due to Vortex Shedding. Resonant vibrations of heat-exchanger tubes induced by vortex shedding were discussed in the Progress Report for December 1967, ANL-7403, pp. 78-81. We have shown that for tubes mounted on an equilateral, triangular pitch, as in the EBR-II superheater and evaporator, the Strouhal number characterizing the vortex shedding depends on the flow-field orientation, which in turn is determined by the baffle design. For the baffle design and resultant flow-field orientation in the evaporator, the Strouhal number for vortex shedding is 0.66 (see Fig. II.E.12, p. 79, ANL-7403). The Strouhal numbers for the tubes are given in Table II.E.18 for the two possible support configurations.

TABLE II.E.18. Strouhal Numbers for Evaporator Tubes

Percent of Full-power Flow ^a	Support Configuration No. 1	Support Configuration No. 2
60	2.44	3.29
74 [45 MWt]	1.97	2.67
80	1.83	2.46
100 [62.5 MWt]	1.46	1.97

^aFull-power flow = 312,500 lb/hr; $\bar{U} = 1.32$ ft/sec.

For all flows and both support configurations (taking into account the possible changes in natural frequency caused by axial loading, as given in Table II.E.17), the Strouhal numbers for the tubes are at least twice as great as the Strouhal number for vortex shedding (0.66). Thus we conclude that vortex shedding will not induce resonant vibrations.

(c) Instabilities Caused by Parallel Flow. In the Progress Report for January 1968, ANL-7419, pp. 72-73, the possibility of exciting a fluid-elastic instability by a parallel-flow component was examined. The results of that study, which also apply to the evaporator, show that the critical flow velocities for instability caused by sodium flowing parallel to the tube axes are sufficiently high that they will not occur in a heat exchanger. Similarly, the velocities of the water flowing through the tubes are so low that no problem is anticipated from an instability caused by internal parallel-flowing fluid.

Although we can make qualitative predictions of the potential for resonant vibrations and instabilities in general, present vibration technology does not permit prediction of the long-term fatigue and wear failures that might result from small-amplitude random oscillations excited by buffeting.

p. Feasibility Study of Fuel Failure Detection--Chemical and Mechanical Methods

(i) Trace Elements Analytical Techniques (C. E. Crouthamel)

Last Reported: ANL-7445, pp. 85-86 (April 1968).

In choosing appropriate tagged elements for the identification of failed-fuel elements in EBR-II, the type and concentration of impurities already present in the sodium coolant must be known.

Two samples of EBR-II primary sodium have been received. The "as-received" samples will be analyzed by gamma spectrometry for long-lived activation products of impurities; the samples will then be reirradiated to examine short-lived activation products. The results of this survey will be used for further evaluation of the usefulness of specific elements presently being considered as tags.

(ii) Tag Confirmation Study (F. A. Cafasso)

Last Reported: ANL-7445, pp. 86-87 (April 1968).

Design, procurement, and assembly of components of a loop for evaluating the chemical stability of isotopic tags in circulating sodium is continuing. A loop sampling reservoir, a sodium-feed system, and a

cooling system for various loop components have been designed. The assembly of a drain tank and a vacuum system for the loop is nearing completion.

(iii) Mechanical Failed Fuel Locator (E. Hutter)

Last Reported: ANL-7445, p. 87 (April 1968).

The detailed drawings for the prototype failed-fuel locator are about 50% complete. Preliminary layout drawings have been prepared to explore the feasibility of using available, but restricted, laboratory space for installation of the sodium loop components.

The test loop is being designed to accommodate a future control-rod drive as well as the failed-fuel locator.

The centrifugal pump that is in laboratory storage has been judged adequate for sodium flow in the test loop and will be used instead of an electromagnetic pump.

q. EBR-II Materials-Coolant Compatibility (J. E. Draley)

Last Reported: ANL-7445, pp. 87-89 (April 1968).

(i) Examination of EBR-II Subassembly Hardware (C. F. Cheng and S. Greenberg)

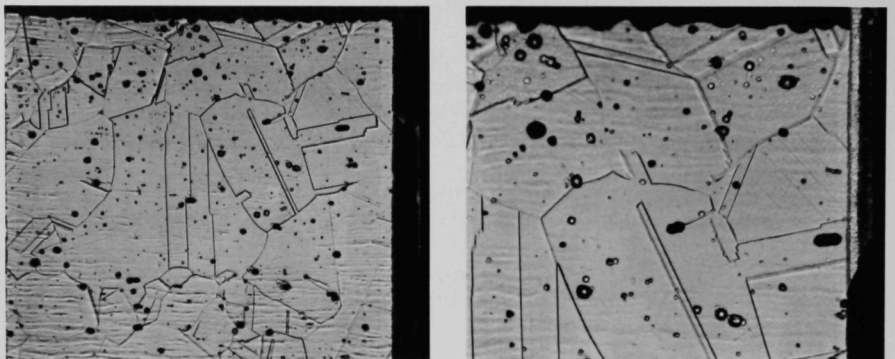
Not reported previously.

A Type 304 stainless steel shroud is being examined to determine the effects of simultaneous exposure to sodium and to fast-neutron radiation. The shroud (control rod 12) was removed from EBR-II after 15,541 MWd (Run 26C).

Microexamination of the irradiated shroud tube revealed carbide precipitation at the grain boundaries in the tube section exposed to a sodium temperature of 460°C and a fluence of 1.2×10^{22} n/cm². The section of shroud tube exposed at a sodium temperature of 432°C and a fluence of 4.6×10^{22} n/cm² had a solution-annealed structure similar to an unirradiated (as-received) tube. Carbide precipitation at the grain boundaries usually is more prominent at 460°C than at 432°C for unirradiated stainless steel.

Figure II.E.5 shows optical micrographs of a specimen (G-3) of irradiated shroud obtained from the region of low sodium temperature and high fluence (432°C and 4.6×10^{22} n/cm²). The specimen has a "step" structure, i.e., no ditches at the grain boundaries; etch structure

was obtained by ASTM oxalic acid test.* An unirradiated shroud tube also showed a similar "step" structure. However, a specimen (G-1) of irradiated shroud tube taken from the region of higher sodium temperature and lower fluence (460°C and $1.2 \times 10^{22} \text{ n/cm}^2$) exhibited a "dual" structure, i.e., some ditching at the grain boundaries in addition to steps, but no one grain completely encircled by ditches of carbide.



187.5X

(a)

10% Electrolytic Oxalic Acid Etch

(b)

375X

Fig. IIE.5. Specimen G-3--Surface of Tube Section Exposed to Sodium in EBR-II
(Temperature-- 432°C ; Fluence-- $5.6 \times 10^{22} \text{ n/cm}^2$)

Microprobe examination showed no change of surface concentration with respect to iron, chromium, and nickel contents for Specimens G-1 and G-3. This is in agreement with other Type 304 stainless steel specimens exposed to sodium (EBR-II) at 460°C and to a fluence of $7.2 \times 10^{20} \text{ n/cm}^2$.

(ii) Sodium Exposure of Type 304L Stainless Steel Fuel Cladding (R. A. Noland, W. E. Ruther, and S. Matras)

Micropolishing the seamless Type 304L stainless steel cladding of an experimental fuel element exposed to EBR-II primary sodium resulted in several grains being dislodged. Subsequent etching and chemical analyses indicated grain-boundary carburization of the alloy. The relative contributions of the sodium exposure and the sodium-removal process to this undesirable condition are being evaluated in a series of out-of-reactor experiments.

Sections of seamless and of welded tubing for fuel cladding have been prepared as follows:

- (1) as-received, degreased;
- (2) electropolished;

*ASTM test A262-64T.

- (3) as-received, sensitized in vacuum 4 hr at 650°C;
- (4) as-received, plastically deformed.

Exposure to 550°C sodium (cold trap at 175°C) is underway in a refreshed autoclave system. At the end of one week, three sets of the samples were removed from the continuing test. One set of specimens was cleaned in ethyl alcohol and then (ultrasonically) in distilled water. Two additional sets were cleaned by exposure to moist argon, followed by a dip in distilled water. One of the latter sets was held one week in moist air at 80°C and the other held one week in dry (anhydrous) air at 80°C before polishing for microscopic examination.

Comparison of the microstructures of the exposed and unexposed tubing has revealed no unexpected change. No dislodged grains were observed, and only slight differences in etching susceptibility and grain shape were noted for the exposed specimens. These changes are believed to be characteristic of a prolonged 550°C exposure (effect of temperature only). Control specimens (exposed in vacuum) will be examined when the next set of sodium-exposed specimens are removed and polished after one month of testing.

2. Operations--Reactor Plant (G. E. Deegan)

Last Reported: ANL-7445, pp. 90-91 (April 1968).

In a program designed to identify and remove the source of fission-product leakage, the reactor was operated for 682 MWdt in Runs 27H, 27I, 28A, 28B, and 28C during May. Experimental Subassembly XO28 was identified as the probable source of this leakage and was removed from the core (see Sect. II.E.1.a). The other fueled experiments which had been previously removed were returned to the core in two increments. After the return of each increment, the reactor was operated to monitor for any further leakage from experiments and to obtain information regarding the effect of the added ceramic-fueled subassemblies on reactor kinetics. The cumulated total of EBR-II operation is 17,386 MWdt.

The reactor was started up for Run 27H on April 26 with all fueled experimental subassemblies removed. The power-reactivity decrement (PRD) was measured to be 41.3 lh at 45 MWt, normalized to an 11.0-in. rod-bank position. The run was ended on May 2 after 200 MWdt of operation with no indication of a fission-product release, and experimental Subassembly XO28 was then returned to the reactor as the prime leak suspect.

During the startup for Run 27I on May 3, the PRD at 45 MWt was measured as 44.9 lh, normalized to an 11.0-in. rod-bank position. Failure of a terminal on the generator field-current shunt required the removal of

the turbine-generator from service for several hours, but operation at 45 MWt continued with steam bypassed directly to the condenser.

On May 6, after 96 MWd of operation since experimental Subassembly XO28 had been returned to the reactor, a fission gas monitor (FGM) alarm was received. The reactor was immediately shut down, and entry to the Reactor Building was restricted. The FGM indication increased by a factor of 140, and ^{133}Xe and ^{135}Xe activity levels showed large increases. Airborne radioactivity levels in the Reactor Building increased significantly and access was restricted for about 10 hr.

With this fission-product release, Run 27 was concluded and reloading for Run 28A was instituted. Fuel changes included removal of experimental Subassembly XO28 from the reactor and reinsertion of XO29. No other fueled experiments were returned to the core, and half-worth driver-fuel subassemblies were placed where experiments would be loaded later in Rows 4 and 5.

During Run 28A, a brief program of reactor physics measurements was carried out. This program consisted of rod drops from various power levels, reduced-flow tests at constant ΔT , PRD measurements, and 2-hr periods of reactor operation without manual control to observe the long-term power oscillations at various power levels and flow rates (see Sect. II.E.1.a). The PRD in ascending to 45 MWt was measured as 43.5 lh, and the descending PRD was measured as 49.5 lh (both normalized to an 11.0-in. rod-bank position). No evidence of a fission-gas leak appeared during 154 MWdt of operation in this run.

Experimental subassemblies containing ceramic fuel were placed in Rows 6 and 7 for Run 28B. An experimental high-worth control rod containing a natural boron follower was inserted into the No. 5 position; its total calibrated reactivity worth was found to be 178 lh, a gain of approximately 40 lh over a standard control rod in that position. The experimental rod was then returned to the storage basket and replaced by a standard rod. The physics experiments of Run 28A were repeated in Run 28B to determine the effect of the added ceramic-fueled subassemblies on EBR-II reactor kinetics. Two measurements of the PRD from 0 to 45 MWt were made in Run 28B. The values, normalized to an 11.0-in. rod-bank position, were 47.4 and 46.3 lh.

Run 28B was ended on May 27 after 300 MWdt of operation with no indication of a fission-product release, and the remaining ceramic-fueled experiments were loaded in Rows 4 and 5 for Run 28C. The physics program of the previous two runs was repeated in Run 28C.

Table II.E.19 summarizes the loading changes in EBR-II during May.

TABLE II.E.19. Loading Changes in EBR-II during May 1968

Date	Grid Position	Removed	Installed ^a	Comment	
5/2/68	4D3	C-2068	XO28	Installed to verify as a source of fission gas leakage	
5/2/68	6C5	A-723	B-386	Rearrangement of grid in preparation for reinstallation of experimental subassemblies removed in Run 27	
5/2/68	6E1	A-788	B-384		
5/6/68	6E1	B-384	A-788		
5/6/68	4E3	C-2071	XO29		
5/7/68	4A2	C-2060	C-2010		
5/7/68	4B2	C-2070	C-2012		
5/7/68	4C2	C-2006	C-2060		
5/7/68	4C3	C-2066	C-2006		
5/7/68	3E2	C-2008	C-2066		
5/7/68	5E2	C-2062	C-2008		
5/7/68	6F4	A-798	B-374		
5/7/68	6B1	A-773	B-385		
5/7/68	4D3	XO28	C-2068		Removed as a fission-gas leaker
5/7/68	4F1	C-2034	C-2064	New experimental subassembly (Structural)	
5/7/68	5B2	C-2057	C-2049		
5/7/68	6B2	B-362	B-372		
5/7/68	7C5	A-821	XO38		
5/7/68	4D1	C-2033	C-2129		
5/7/68	6D5	B-364	B-384		
5/8/68	5F4	C-2058	C-2130		
5/8/68	3A2	C-2026	C-2120		
5/8/68	7C3	A-814	XO37		
5/8/68	5E4	C-2040	C-2062		
5/8/68	6F5	B-367	B-390	New experimental subassembly (Structural)	
5/8/68	5B4	C-2037	C-2070		
5/8/68	6F2	B-361	B-392		
5/8/68	6E5	B-365	B-395		
5/8/68	5E3	L-457	L-498		
5/8/68	3D2	C-2056	C-2058		
5/8/68	3D1	S-604	S-613		
5/8/68	8A4	SO-1920	-		
5/14/68	7F3	A-813	XO10		Source removal
5/14/68	4B1	C-2065	C-2166		
5/14/68	7B1	A-799	XG04	Reinstallation of experimental subassemblies for nonleakage verification	
5/15/68	6B5	B-373	XO20		
5/15/68	6C1	A-787	XO31		
5/15/68	6D2	B-371	XO19		
5/15/68	7A1	A-748	XG02		
5/15/68	3B1	C-2132	C-2136		
5/15/68	4F1	C-2064	C-2165		
5/15/68	6F1	A-789	XO32		
5/15/68	7D1	A-735	XG03		
5/15/68	5F1	L-453	T-500A		
5/16/68	5F1	T-500A	L-453	Insertion and removal of control rod containing a natural boron follower	
5/27/68	4B2	C-2012	XO12	Reinstallation of experimental subassemblies for nonleakage verification	
5/27/68	4F2	C-2007	XA08		
5/27/68	4A2	C-2010	XO15		
5/27/68	5E2	C-2008	XO33		
5/27/68	4C3	C-2006	XO17		
5/27/68	4B3	C-2009	XO27		

^aA--Depleted-uranium inner-blanket subassembly.

B--Row-6-type driver fuel subassembly.

C--Driver fuel subassembly.

L--Control rod subassembly.

S--Safety rod subassembly.

T--Control rod containing a natural boron follower.

X--Experimental subassembly.

3. Operations--Fuel Cycle Facility (M. J. Feldman)

Last Reported: ANL-7445, pp. 91-97 (April 1968).

a. Hot Line Operation. Table II.E.20 summarizes the production activities for May. Included are two core-type subassemblies each containing 37 elements of 70%-enriched fuel (C-2165 and C-2166). Subassembly fabrication was limited during most of the month owing to lack of available storage space (both in the FCF Air Cell and the reactor basket) and to surveillance work conducted on nine subassemblies received from the reactor. Some or all of the elements in each of these subassemblies were made with seamless tubing, and the integrity of this material had been questioned. Results of the surveillance are given in Sect. II.E.3.d.(ii).

TABLE II.E.20. Production Summary for Hot Line

	5/1/68 through 5/31/68	Total This Year	
1. Subassemblies received:			
Core, Control, Safety	11	52	
Other	1	7	
2. Subassemblies Dismantled (for processing)	8	52	
3. Subassemblies Dismantled (for examination, etc.)	1	6	
4. Subassemblies Fabricated	3	16	
5. Subassemblies Transferred to Reactor:	9	26	
Subassemblies Stored in L&O Vault and Interbuilding Corridor	0	0	
6. Elements Decanned:			
From Irradiated Subassemblies	330	2,981	
Rejects	0	205	
Other	0	161	
Total Decanned	330	3,347	
<u>Melt Refining</u>			
	<u>Irradiated Fuel</u>	<u>Recycle Material</u>	<u>New Fuel</u>
7. Number of Runs	7	2	0
8. Average Pour Yield, % 1968 to Date (Total)	92.6 23	91.2 10	- 1
<u>Processing</u>			
	<u>5/1/68 through 5/31/68</u>	<u>Total This Year</u>	
9. Injection-casting Runs (Total Number)	6	32	
10. Elements Processed:			
Accepted	173	1,693	
Rejected	27	259	
11. Elements Welded:			
Rewelded	558 0	1,647 0	
12. Elements Leak-tested:			
Accepted	718	1,856	
Rejected	12	30	
13. Elements Bonded (including recycle)	323	2,056	
14. Elements Bond-tested:			
Accepted	275	1,581	
Rejected	48	140	
15. Elements to Surveillance Number of Subassemblies	400 6	1,238 32	
<u>Waste Shipments</u>			
16. Cans to Burial Ground	5	31	
17. Oxide and Glass Scrap to ICPP	0	18	

A control-rod subassembly containing a boron carbide follower (T-500) was removed from the reactor storage basket and sent to the FCF. It was partially disassembled to remove the ^{10}B -enriched boron carbide follower, reassembled with a natural boron follower, straightness and tensile tested, and returned to the reactor for low-power physics experiments.

Construction has started on a decontamination facility in the wind-and-weather enclosure of FCF. This facility will provide a place to decontaminate in-cell cranes, manipulators, and other large pieces of equipment prior to attempting their contact maintenance. Construction should be complete in 12 weeks.

The second skull-oxidation furnace has been installed in the argon cell and is currently undergoing remote checkout.

b. Cold Line Operation. A special run of U-10% Fs-2% Si alloy was made in the alloy preparation furnace and the resulting alloy was cast in the leaf mold. This material will be used to increase the silicon content of the Aerojet ingots to the desired level of 400 ppm. Normal production is continuing on the cold line. A summary of the month's production data is given in Table II.E.21.

TABLE II.E.21. Production Summary for Cold Line

	5/1/68 through 5/31/68	Total This Year
1. Alloy Preparation Run:		
New Fuel	0	6
Remelts	5	24
Total	10	30
2. Injection-casting Runs	10	55
3. Pins Processed:		
Accepted	532 ^a	4,207
Rejected	49	254
4. Elements Welded	719	3,252
Elements Rewelded	0	14
5. Elements Leak-tested:		
Accepted	719	3,363
Rejected	10	50
6. Elements Bond-tested:		
Accepted	567	3,289
Rejected	48	218
7. Subassemblies Fabricated	8	33
8. Subassemblies Sent to Reactor	5	10

^aIn addition, 105 linear feet of cast pins were sent to INC in May for use in criticality measurements.

c. Maintenance and Repair. It was reported last month (see ANL-7445, p. 94) that an argon-cell crane became inoperative because of failure of the drive motors for the trolley and hoist. The problem was caused by a failure in a mineral-insulated electrical line. This is the first failure of this type of conductor since hot operation in the cell began some

four years ago. The short piece of cable was replaced with asbestos-insulated wire sheathed in flexible steel conduit. The trolley has been returned to the Argon Cell and is operating satisfactorily.

Concurrently with the argon-cell crane failure, the hoist cable on the air-cell crane came off the drum in an unknown manner. The cable wrapped around the drum shaft, breaking the cable and damaging a limit switch. The crane was removed from the Air Cell, repaired, and returned to service.

d. Analyses

(i) Chemical Analyses. The numbers of fuel-product analyses on hot line, cold line, and vendor fuel samples, together with the average values and ranges, are as follows:

<u>Analyzed for</u>	<u>Number</u>	<u>Average Value</u>	<u>Range</u>
U (total and isotopic)	12		
U (total)		94.80 w/o	94.36-95.30
²³⁵ U (% of total U)	12	52.15 w/o	51.94-52.38
Mo	16	2.47 w/o	2.37-2.59
Ru	27	1.90 w/o	1.76-2.04
Rh	6	0.271 w/o	0.264-0.286
Pd	14	0.190 w/o	0.181-0.198
Zr	7	0.099 w/o	0.084-0.120
Nb	8	0.016 w/o	0.012-0.023
Si	43	350 ppm	290-570
Al	4	165 ppm	130-180
C	10	182 ppm	132-244
Cr	6	<16 ppm	
Fe	14	475 ppm	67-944
Ni	6	170 ppm	157-186
Total Analyses:	185		

Analyses for surveillance of irradiated pins from the reactor were:

<u>Analyzed for</u>	<u>Number</u>	<u>Average Value</u>	<u>Range</u>
Si	7	180 ppm	135-220
Fe	6	500 ppm	286-945

(ii) Postirradiation Analyses of EBR-II Fuel. As a part of the surveillance program, driver fuel produced in the cold line is being evaluated by postirradiation examinations to qualify this fuel source for routine usage in EBR-II. Five additional cold-line subassemblies were added to

this program. These five subassemblies (L-498, B-3002, B-390, B-392, and B-395) were added to six others mentioned last month (C-2120, C-2121, C-2124, C-2129, C-2130, and B-388). These 11 subassemblies are either in the core undergoing irradiation or will begin their irradiations in the near future.

As mentioned last month, postirradiation examination results have become available for Subassembly C-2036, one of a pair of subassemblies included in the Driver Fuel Anomalous Swelling Program. (The other subassembly, C-2027, is now in the reactor storage basket.) These subassemblies are intended for exploration of irradiation performance of the U-5% Fs driver fuel at burnups greater than 1.2 a/o. Final results indicate that fuel in C-2036 (casting batches 4148 and 4153, the same batches of fuel contained in companion Subassembly C-2027) swelled an average of 5% as a result of irradiation to a calculated maximum subassembly burnup of 1.2 a/o. Irradiation swelling for individual elements ranged from 3.7 to 6.67%. Analytical burnup measurements for this subassembly are not yet available. From these data, the conclusion is that companion Subassembly C-2027, which accumulated 1.15 a/o in grid position 4E1 of the core, and is now being held in the reactor storage basket, can be irradiated to an additional burnup increment beyond 1.2 a/o. This proposal will be initiated when postirradiation examination results for Subassembly C-291 (approved for irradiation to 1.3 a/o) become available. Irradiation of C-291 is currently planned for the beginning of Run 29.

Postirradiation examinations have been completed on 9 of 10 driver-fuel subassemblies mentioned last month which may have seamless tubing in their elements. Sodium-level bond-testing operations failed to indicate any features which could be related to sodium-bond losses from jacket cracking, etc. Visual inspections (especially those made following thermal treatment of the elements during rebonding) also failed to reveal abnormal features in the elements. These examinations were completed on a total of 774 elements from Subassemblies B-352, B-354, B-355, B-356, B-357, B-358, B-359, B-360, and C-2003. The tenth subassembly, L-447, is now in the reactor storage basket awaiting transfer to the FCF. Metallographic analyses of some elements from the above-listed subassemblies are in progress.

As described last month, the irradiation swelling of some fuel elements from Subassembly B-355 listed above was considerably higher than expected, based on calculated burnup data. Analytical burnup results for this subassembly have recently become available and indicate a discrepancy between the subassembly burnup values determined by calculation and those determined by chemical measurement (two independent chemical methods were used). The chemically measured values were slightly higher than the calculated values. Fuel-swelling values which were unexpectedly high when based on the calculated burnup for this subassembly appear to be

much as expected if the measured burnup values are utilized. An effort is underway to resolve the calculated versus measured burnup discrepancy.

Postirradiation surveillance examinations have been conducted on Subassembly C-2138 in which 70%-enriched fuel was irradiated. This subassembly contained 19 U-Fs elements of 70% ^{235}U enrichment and 72 U-Fs elements of the normal 52% enrichment. The 70% elements were located in the central 19 positions of the subassembly. Irradiation of the subassembly was conducted during Run 27 in grid position 4B1. Irradiation swelling results for the fuel are presented in Table II.E.22.

TABLE II.E.22. Summary of Irradiation Swelling Data for Subassembly C-2138, 70% Enriched Fuel
Reactor Grid Position: 4B1

Injection-casting Batch Number	^{235}U Enrichment (w/o)	Silicon Content (ppm)	Average of Element Maximum Burnups (a/o)	Calculated Fuel Centerline Temperature ($^{\circ}\text{F}$)		Number of Elements Examined	Fuel Swelling $\frac{\Delta V}{V}$ (%)		
				Minimum	Maximum		Minimum	Average	Maximum
0700	69.78	260	0.315	1117	1159	19	1.4	1.8	2.1
4251	52.19	230	0.236	965	1006	3	0.8	0.8	0.9
4252	52.22	430	0.234	962	1027	7	0.8	1.1	1.5
4254	52.36	600	0.239	948	1067	61	0.4	1.1	2.1

The results indicate that irradiation swelling of the 70%-enriched elements is similar to that shown by normal 52%-enriched elements (at least in the calculated burnup range of 0.23 to 0.31 a/o). The magnitude of swelling at this burnup level is reasonably consistent with that expected from past examinations of large numbers of normal driver elements. The calculated centerline temperatures of the 70% elements during irradiation were approximately 1117 to 1159 $^{\circ}\text{F}$, whereas those of the 52% elements ranged from 948 to 1067 $^{\circ}\text{F}$. Metallographic and chemical analyses of elements from this subassembly are in progress.

Two additional subassemblies, C-2165 and C-2166, have been fabricated in the FCF and transferred to EBR-II. Each of the subassemblies contains 37 elements of 70% ^{235}U enrichment clustered in the center of the element array. Irradiation of these subassemblies to burnups of 0.5 and 0.7 a/o, respectively, will be initiated during Run 28. Surveillance results will be evaluated for one subassembly following irradiation to 0.5 a/o before the second will be irradiated to 0.7 a/o.

PUBLICATIONS

LIQUID-METAL FAST BREEDER REACTORS--CIVILIAN

The Manufacture of Reactivity-coefficient Elements for Zero-power Reactor Experiments

N. J. Carson, A. G. Hins, H. F. Jelinek, J. E. Ayer, and A. B. Shuck
ANL-7365 (February 1968)

Extended Capability for Fast Neutron Hodoscope Used at TREAT
A. DeVolpi, R. J. Pecina, C. H. Freese, E. W. Rolnicki, D. J. Travis,
and G. R. Larsen

IEEE Trans. NS-15(1), pp. 77-86 (February 1968)

Multi-Specimen Hot Pressing UO₂

J. T. Dusek, G. D. White, and C. T. DeFreitas

Materials Technology--An Inter-American Approach, Proc. Conf.
San Antonio, May 20-24, 1968. ASME, New York, 1968, pp. 133-135

The Calibration and Stability of a 1200°F Permanent Magnet In-core Sodium Flowmeter

M. C. Glass and G. F. Popper

IEEE Trans. NS-15(1), pp. 37-40 (February 1968)

International Symposium on Plutonium Fuels Technology, Proc. 1967 Nuc.
Met. Symp., Scottsdale, Arizona, October 4-6, 1967

K. E. Horton, R. E. Macherey, and R. J. Allio, Eds.

AIME, New York, 1968, Vol. 13

The Performance of a Counting-Mean-Square Voltage Channel in the EBR-II

G. F. Popper and J. M. Harrer

IEEE Trans. NS-15(1), pp. 22-27 (February 1968)

High Temperature Instrument Developments at Argonne National Laboratory
of Interest to the NERVA Program

G. F. Popper and A. E. Knox

Report No. RN-S-0391 to AEC-NASA Space Nuclear Propulsion
Office--Contract Year 1967--Instrumentation Development Review
Meeting Minutes--NERVA Program--Contract SNP-1, July 1967,
pp. 117-133

Transformation Kinetics of U/10 wt % Pu/19 wt % Fz Alloy and Compositions
of Its Important Primary Phases

Howard Savage

J. Nucl. Mater. 25(3), 241-248 (1968)

Summary of an Analysis of the Eddy-Current Flowmeter

D. E. Wiegand

IEEE Trans. NS-15(1), pp. 28-36 (February 1968)

III. GENERAL REACTOR TECHNOLOGY

A. Applied and Reactor Physics Development--Research and Development

1. Theoretical Reactor Physics

a. Cross Section Data Evaluation (C. N. Kelber)

Last Reported: ANL-7445, pp. 99-100 (April 1968).

(i) Evaluation of Helium-4 and -3. A compilation of helium cross-section data is being prepared in the ENDF/B format for processing through ETØE and use in the MC² code. These cross sections are desired for calculations involving gas-cooled reactors. Natural helium consists of 99.99987% ⁴He and 0.00013% ³He. In the range of interest for reactor calculations, elastic scattering is the only reaction possible for neutrons incident on ⁴He. A Fortran program was written to calculate the elastic-scattering cross section and the associated Legendre-expansion coefficients from s-, p-, and d-wave phase shifts. Several tables of these phase shifts as a function of energy are available in the literature, and an evaluation of the results of using various sets will be made.

The abundance of ³He in natural helium is so small that only the (n,p) cross section, which is very large at low energies, need be considered in the evaluation. A recent evaluation* of the ³He (n,p) cross section is being incorporated into the present compilation.

(ii) ENDF/B Processing. A revised version of ETØE has been received from APDA. This version was compiled, and a test problem was run successfully on the CDC-3600.

(iii) ²³⁹Pu Evaluation. The codes CODILLI and CURVEPLOT have now have now been checked and are functioning satisfactorily, at least insofar as reaction cross sections are concerned. The discrepancy between the two codes reported previously (see ANL-7445, p. 100) was due to an error in converting to local use one of the subroutines of CODILLI.

The 1965 Saclay fission data for ²³⁹Pu have been analyzed in the energy range from 46 to 91 eV. In general, there is agreement between our results and Farrell's analysis of the Petrel data, although differences appear to exist insofar as positions and width of the levels are concerned. A more detailed account of the results is in preparation.

* Als-Nielsen, J., Neutron Cross Sections for ³He in the Energy Range 0-10 MeV, CCDN-NW/6, ENEA Neutron Data Compilation Center Newsletter No. 6 (Sept 1967).

2. Nuclear Data

a. Burnup Analysis and Fission Yields for Fast Reactors (R. P. Larsen)

(i) Development of Analytical Procedures for Fission-product Burnup Monitors

Last Reported: ANL-7438, pp. 87-88 (March 1968).

(a) X-ray Spectrometric Determination of Rare Earth Fission Products. A method for the measurement of burnup in fast reactor fuels by an X-ray spectrometric method is under development. The application of this method to burnup determination can be carried out in two ways: (1) an individual rare earth can be assayed or (2) each of the four major rare earths (lanthanum, cerium, praseodymium and neodymium) can be assayed and the results summed.

Previous work has been directed toward the assay of individual rare earths. In a calibration study (see ANL-7438, p. 88) a precision of 1 to 2% was obtained for individual rare earths when the total amount of rare earths present was 30 to 90 μg .

A further evaluation of the data from that study shows that summing the four individual rare earths provides a more sensitive method of analysis with no decrease in precision. The data (see Table III.A.1) show that in the range from 15 to 90 μg of combined rare earths, a precision of 1 to 2% is obtained. It is anticipated that the lower limit could be extended to 5 μg by increasing the counting time in the X-ray spectrometer from 1 to 3 hr.

TABLE III.A.1. Reliability of the X-ray Spectrometric Analysis for Combined Rare Earths

Amount Present (μg)	Amount Found (μg)	Difference (%)
14.6	14.4	-1.5
	14.7	+0.7
29.2	28.8	-1.3
	29.6	+2.5
43.9	43.4	-1.2
	44.6	+1.6
58.4	58.8	-0.5
	59.2	+1.3
72.9	72.0	-1.3
	73.5	+0.8
87.9	86.6	-1.1
	88.5	+1.0

(b) Photometric Titration of Total Rare Earths. A method of determining burnup by photometric titration of total rare earths has been discussed previously (see Progress Report for January 1968, ANL-7419, p. 96). In the titration procedure, an excess of EDTA is added to the rare earths, and the excess is determined by incremental additions of standard lanthanum, with absorbance measurements being made after each addition. Previous studies have been conducted with $\sim 500 \mu\text{g}$ of rare earths.

To test the reliability of the method in determining smaller amounts of rare earths, the titration was performed with $80\text{-}\mu\text{g}$ samples. The results obtained for four standards had a relative standard deviation of $\pm 1.7\%$.

A modification of the above procedure has also been tested. In the modified procedure, the excess EDTA is titrated to a distinct visual color change with standard lanthanum; the amount of excess lanthanum present at this point is determined by a single absorbance measurement made under rigidly controlled conditions. The results of four determinations of samples containing $\sim 80 \mu\text{g}$ of rare earths had a relative standard deviation of $\pm 0.5\%$.

The modified procedure, with its simplicity of operation, offers the following advantages: smaller amounts of rare earths can be determined with no decrease in precision, the analysis can be performed more rapidly, and the method can be adapted more easily to remote operation.

b. Cross Section Measurements (A. B. Smith)

Last Reported: ANL-7438, pp. 88-91 (March 1968).

(i) Fast Neutron Cross Sections

(a) Neutron Scattering Cross Sections

(1) Hafnium. The recent results combined with those from past work has permitted the elastic-scattering cross section of hafnium from 0.3 to 1.5 MeV to be well-defined. The strongly inelastically excited $2+$ state at ~ 100 keV is also well determined. Inelastic scattering resulting in the excitation of higher lying states in not as clear, because the scattered-neutron spectra are very complex; as many as 12 inelastic groups are evident in a scattered-neutron interval of 1000 keV. This complexity is in part due to the multiplicity of isotopes in the natural element. It may be judged necessary to make further measurements at the higher energies to define properly this complex cross section. Meanwhile, the established elastic and inelastic scattering processes are being interpreted in terms of a deformed-coupled-channel-optical model and statistical theory.

(2) Gadolinium. Measurements taken concurrently with those for hafnium (above) are being processed. The complexity of the measured distributions exceeds even that for hafnium; as a result, data treatment is progressing very slowly.

(3) Samarium. The results are the third portion of the triad Hf-Gd-Sm, and the last in the analysis procedures. They are somewhat behind the gadolinium work and subject to the same difficulties.

(4) Vanadium. The experimental work is essentially completed. As a result of discussions with workers in the field questions arose regarding the existence of structure in the inelastic cross sections. A final experimental check of the structure has been done. The data processing is slow due to the development of new processing programs.

Such programs are now becoming increasingly necessary as the automated time-of-flight facility is capable of generating massive quantities of information in relatively brief times. It is not unusual to process hundreds of experimental angular distributions. These procedures consume many hours on the large central computing facility with similar time in preprocessing with smaller digital equipment. With such a work load, it was mandatory that the processing procedures be revised sharply toward greater efficiency. This has been largely accomplished, and the vanadium results are the first for which the new procedures will be used.

In the final analysis of the vanadium results, particular attention has been given to the possible existence of intermediate structure. Correlation calculations that have been carried out indicate that the observed total cross section of vanadium is described by two characteristic resonance widths. One, of about 10 keV, is characteristic of the compound nucleus. The other, with width Γ of ~ 120 keV, is characteristic of an intermediate resonance phenomena. These are indicated in Fig. III.A.1.

(5) Titanium. The inelastic neutron scattering cross sections of titanium have been determined from threshold to incident neutron energies of 1.5 MeV. The results vary widely, probably due to the effect of partially resolved resonance structure. This will be verified by a careful determination of the total cross section with high resolution over the same energy range of incident neutrons.

(6) High-resolution Fast Neutron Cross Sections of Iron. The interactions between iron and neutrons with energies between 0.3 and 1.5 MeV were studied by time-of-flight methods. In particular, the total and inelastic scattering cross sections were determined with good energy resolution. A considerable amount of structure was observed. The results were investigated in terms of different theoretical approaches.

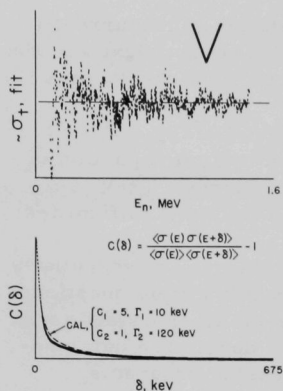


Fig. III.A.1

The Upper Portion of the Figure Shows the Measured Total Neutron Cross Section of Vanadium. The direct reaction effects have been removed by fitting the measured values with a cubic energy dependence and subtracting the smooth trend. The result shown is the remaining resonance behavior. The lower portion of the figure indicates the auto-correlation result obtained from the upper figure. The dashed line very closely describes the curve obtained from the experiment using the sum of two characteristic widths: $\Gamma \sim 10$ keV and $\Gamma \sim 120$ keV.

The above work was a joint endeavor between the Argonne National Laboratory and the Pelindaba Laboratory, Republic of South Africa.

(7) Fast Neutron Scattering from Germanium. A rough draft of the work with germanium is completed, and major portions of the associated figures have been finished. The data have been transferred to Sigma Center, Brookhaven National Laboratory.

(b) Capture and Activation Cross Sections

(1) Isomeric Cross-section Ratio for Rhodium. Data for the 42-sec-43-min activation cross-section ratio are being taken. The ultimate goals are as follows:

i) the measurements of the optical-model shape of the ratio (30 keV, 120-1450 keV);

ii) investigation of fine (= intermediate) structure of the cross-section ratio, especially in the ranges 130-250 keV and 400-500 keV, where fluctuations in σ_f have been reported. Three precise determinations of cross section were used for spectral measurements.

(2) ^{236}U , ^{238}U , and ^{232}Th Capture Measurements. The evaluation of data from the recently irradiated samples is not yet completed. The ^{236}U measurements are still troubled by the high background. The ^{238}U measurements will give some results, but not with the expected accuracy, because of the bad resolution of the Ge(Li) detector. The deficiency has been remedied.

(3) Re-evaluation of ^{238}U , Spherical-shell Transmission Experiments. A re-evaluation of the spherical-shell transmission experiment by Belanova *et al.*,* using a Monte Carlo Program has been completed. The value for the ^{238}U capture cross section reported by Belanova *et al.* will increase by about 20%. The influence of statistical fluctuations in the resonance parameters as well as the re-evaluated cross section value will be reported, in a short publication.

(c) Total Neutron Cross Sections

(1) Hafnium. In the course of measurements of partial cross sections and comparisons with ENDF-B content, considerable doubt arose as to the validity of the published total neutron cross section of hafnium. The sum of the partial cross sections appeared to be higher by half a barn or more than the total value. This discrepancy has been examined by investigating the total-cross-section measurements completed in the interval 650-356 keV; indications are that the previously reported total cross sections are indeed too small by 1/2-1 barn. The work will be continued to higher energies.

(2) ^7Li . The total cross sections of ^7Li were carefully examined, using two very high-purity samples prepared by the Los Alamos Laboratory. The sample thicknesses were chosen to optimize the measurements in the region of the 260-keV resonance. The shape, magnitude, and energy scale of the measured results compared favorably with the previous results obtained with less pure samples and with the general character of the results found in the literature. However, there was no explicit evidence of the fine structure reported by some other workers previously. The fine resonances previously observed may have been due to impurities in the samples used.

The above experimental results are now being interpreted in terms of multilevel resonance formalism.

(3) Energy Calibrations of Time-of-flight Total Cross Sections for Vanadium and Iron. Careful monoenergetic measurements of the resonance structure in the total cross sections of vanadium and iron were made at selected energies in the interval 1-1.5 MeV. The intent was to provide fiducial energy-calibration points for verification of the better resolution previously obtained using the time-of-flight technique. The latter method has the advantage of superior resolution, but does have some inherent uncertainty in the absolute determination of energy. Discrepancies of 5-8 keV between time-of-flight and monoenergetic results were noted, and appropriate corrections made to the former.

*Belanova, T. S., *et al.*, J. Nucl. Energy 20, 411 (1966).

(d) Source Reactions

(1) ^7Be -branching Ratio. The set-up for this experiment is now complete. After checking the counting equipment, measurements will start at the accelerator.

(ii) Fission Process Data

(a) ^{235}U and ^{239}Pu Fission Cross Sections. Additional data taken for ^{235}U have not yet been evaluated. Cross-section data will now only be reported when the measurements are finally completed. Spherical shells for a spherical fission counter usable for measurements applying the associated activity method (^{51}V (p,n)) are to be delivered within a month.

(iii) Instrumentation and Digital Techniques

(a) Apparatus for Total Neutron Cross Section. An automated system has found extensive use at neutron energies below 650 keV. It has now been modified to use a liquid scintillation detection system employing pulse-shape selection for gamma-ray rejection. The new detector permits an electronic biasing suitable for extending the program for total cross sections to energies well beyond 1 MeV. Initial tests were made by determining the total cross section of carbon from 750-1500 keV. The results indicated that the system was functioning in an entirely proper manner, and also provided information useful in evaluating the important standard cross section for carbon.

The techniques for total-cross-section measurement now in use at this laboratory can be summarized as follows:

1. Neutron energies below 650 keV: BF_3 detectors and monoenergetic sources; resolution, 2 keV;
2. 400-1500 keV: pseudo-white source time-of-flight techniques; velocity resolutions of ~ 0.1 nsec/m;
3. 650-1500 keV: liquid scintillation system and monoenergetic sources; resolution, 2 keV. These methods give complementary and good resolution coverage throughout the range of programmatic interest.

(b) (n,n' γ) Ring Geometry Apparatus. The necessary ring-shaped detector has been received and checked. The performance was found superior to that specified. The remaining portions of the apparatus are under construction and will be completed soon. The method will permit measurement of the inelastic excitation cross sections very near and at the reaction threshold and thereby complement the more conventional time-of-flight neutron measurements. The method is unique in inverting

the usual ring geometry, thereby avoiding errors due to polarization effects and making possible the use of relatively small and simple sample configuration.

(c) Flat-response Neutron Detector. The efficiency curve of a flat-response neutron detector used in a ^{235}U fission-cross-section experiment was measured by means of the associated activity method using ^7Li - ^7Be , ^{51}V - ^{51}Cr , and ^{65}Cu - ^{65}Zn . First results show lower efficiencies than those calculated for higher energies, which would mean a further reduction in the cross-section values at higher energies. The measured efficiencies could explain a previously observed discrepancy between gold cross sections measured relative to $^{10}\text{B}(n,\alpha)$ and $\text{Li}(n,\alpha)$ and values obtained with the flat-response neutron detector. However, the values are not yet accurate enough to draw final conclusions. On the other hand, the above difficulties in measuring efficiency with high accuracy (due to γ background) suggests a change in the detector principle to reduce γ sensitivity.

(d) Large Liquid Scintillator Tank. The drawings for the main tank are now completed and due for checking. About three months will be needed to build this unit. A sample of the liquid scintillator was mixed and checked. A final check will be performed when the multipliers ordered for the tank become available.

(e) Laboratory Operation. The nuclear accelerator was manned and operated a total of 431 hr during May. No major failures were experienced. Some attention was given to new vacuum systems incorporating vacuum evaporation techniques. The initial operation was not particularly successful but preliminary results indicate that a proper function will be realized with some minor adjustments.

B. Reactor Fuels and Materials Development

1. Fuels and Cladding--Behavior of Reactor Materials

a. Swelling and Gas Release in Metal Fuels (P. G. Shewmon)

(i) Calculational Studies of Fuel Element Behavior (V. Z. Jankus)

Not reported previously.

A computer program, designated BEMOD, has been written to model the behavior and to estimate the lifetime of a metallic fuel element during irradiation. A metallic fuel element was chosen because of the large amount of available data and the importance of these elements in EBR-II. The computer code is relatively fast and is related to the earlier "SWELL" code. The BEMOD code has just become operational, and is being used to

compare the predicted behavior of fuel element with the actual behavior to determine the adequacy of the code with respect to the description of the behavior of the cladding, the fuel, and the fuel element.

An empirical "equation of state" has been assumed to represent the compressible fuel. In this equation the volume of a section of fuel rod is assumed to be a function of burnup, ambient pressure, and average temperature. This assumption is based upon several parameters determined from swelling experiments made under pressure. Initially, when the fuel is not yet in contact with the cladding, the pressure acting upon the cladding is the same as the plenum pressure. The plenum pressure depends upon the plenum volume, the temperature, and the amount of both inert and fission gas present. The ambient pressure is determined numerically by fitting the volumes of fuel, plenum, and bond sodium into the expanding cladding. When a segment of expanding fuel comes into contact with cladding, the assumption is made (conservatively) that the fuel expands only radially, and the contact pressure is calculated from the fuel compressibility and cladding strength by assuming that the displacement of cladding is caused by thermal expansion, creep, and elastic deformation. The cladding is treated as a thin shell, and the creep is calculated by using an empirical creep rate. The calculation is continued until the cladding creep strain caused by fuel swelling reaches a prescribed value.

The irradiation growth of the fuel consists of an inexorable expansion and a breakaway swelling. The inexorable expansion is assumed to be independent of pressure and essentially proportional to the burnup. The coefficient of proportionality is assumed to be the "solid-state" swelling. Once a volume expansion of 20% is achieved, the empirically observed volume-dependent gas release starts and the solid-state swelling term is decreased proportionately. The breakaway swelling begins when a threshold burnup is reached and is assumed to be proportional to an exponent of the excess burnup. However, the fuel is assumed to be highly compressible and is expressed by an equation of the form $G_2/[1+(P/P_g)]$, where P is the ambient pressure. The parameters G_2 and P_g are obtained by fitting experimentally obtained data of restrained swelling.

(ii) Studies of Fuel Swelling and Gas Release (S. R. Pati)

Not reported previously.

(a) In-test Swelling Studies. A quartz differential dilatometer has been constructed to study out-of-pile fuel swelling. In the dilatometer the linear expansion of the specimen is sensed by a linear variable differential transformer. The signal from the transformer is amplified and recorded. The instrument will have a sensitivity of at least 1×10^{-6} in. and will accommodate specimens from 0.2 to 1 in. in length and

0.2 in. in diameter. The instrument incorporates the desirable features of automatic operation with flexible heating and cooling control, as well as continuous recording of expansion data.

Initially, the equipment will be used to study the kinetics of growth of helium bubbles in copper as a function of temperature. Preliminary experiments have been made with specimens of a copper-boron alloy irradiated in CP-5 to a yield of ≈ 20 ppm of helium. The linear expansions of the specimens have been measured by using an available dilatometer similar to the one being built. The investigations indicate the feasibility of this method for the study of swelling kinetics. In addition, the instrument will have low thermal inertia to allow for a rapid increase in the temperature of the specimen. Subsequently, the kinetics of growth of the bubbles will be followed to the new equilibrium size. This would yield information on the rate-controlling process of the growth of the bubbles.

(b) Studies of Fission-gas Release. Equipment has been designed that will measure the release rates of fission gas from solids. The specimen is heated in a resistance furnace enclosed in a high-vacuum (at least 10^{-8} Torr) chamber. The release rates of gases of interest are determined by measuring respective partial pressures by a residual-gas analyzer (mass spectrometer). The range of masses that can be detected is from 2 to 300. The sensitivity of detection for different gases in terms of partial pressure range will be of the order of 10^{-13} Torr. Provision was made to vary the conductance of the system in order to measure rates of gas evolution that range from very slow to rapid.

A series of experiments is being planned to study the effect of the pressure and the motion of grain boundaries on gas release and to study the release kinetics as a function of temperature.

b. Behavior of Gaseous Fission Products in Fuel Carbides
(L. C. Michels)

Last Reported: ANL-7427, pp. 97-98 (Feb 1968).

Apparatus has been constructed for use in a two-step thinning technique* to produce carbide specimens for transmission electron microscopy. The technique is readily adaptable to remote handling of irradiated materials. To test the apparatus, copper specimens have been successfully thinned and examined by transmission electron microscopy.

The starting specimen is a wafer approximately 0.120 in. in diameter and 0.020 in. thick. The first step consists of electrolytically

*DuBose, C. K. H., and Stiegler, J. O., Semiautomatic Preparation of Specimens for Transmission Electron Microscopy, ORNL-4066 (Feb 1967).

jet-machining the wafer to reduce the thickness of the central area to approximately 0.002 to 0.003 in. The second step is a slower electrolytic polishing of the wafer until perforation occurs in the prethinned central area. Perforation is detected by using a photodetector device that automatically breaks the polishing-current circuit when perforation occurs.

Efforts are now underway to produce thin wafers of uranium carbide. A technique is also being developed to handle small particles of UC for use in conjunction with the two-step thinning procedure. The technique will be applied later to irradiated particles of (U,Pu)C.

c. Structures and Properties of Advanced Fuel Materials
(O. L. Kruger)

Last Reported: ANL-7445, p. 103 (April 1968).

(i) Thermodynamic Properties of PuO₂. The out-of-reactor heat-transport properties of solid solutions of (U,Pu)O₂ are being investigated over the temperature range from 25 to 2000°C. Thermal conductivities of these materials are calculated from the heat capacity obtained from calorimeter experiments and the thermal diffusivity measured independently. The measurements will establish the base-line data needed for future in-reactor evaluations.

The thermal diffusivity of PuO₂ was determined from 400 to 1500°C by use of the heat-pulse technique. The disk specimens, prepared from high-purity powder, were sintered to 92.5% of theoretical density. The specimens were 0.750 in. in diameter and 0.240 in. thick. The thickness was reduced to 0.060 in. for the diffusivity measurements. The specimens were coated with a thin layer of tungsten to prevent transparency at high temperatures.

The thermal diffusivity of PuO₂ as a function of temperature is shown in Fig. III.B.1. The diffusivity decreases as the temperature increases from 0.0148 cm²/sec at 400°C to 0.00503 cm²/sec at 1500°C. The decrease appears to be linear from about 900 to 1500°C. There was no systematic change in diffusivity on heating from that obtained on cooling, and the deviation between measurements was relatively low.

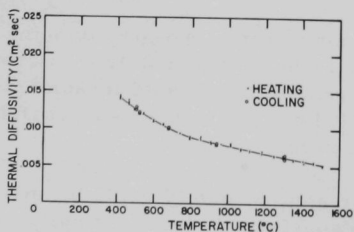


Fig. III.B.1. Thermal Diffusivity of PuO₂ as a Function of Temperature

The diffusivity and heat capacity data of PuO₂ (see ANL-7445, p. 103) were combined to obtain the thermal conductivity by the relation $K = \alpha \rho C_p$, where K is the thermal conductivity, α the thermal diffusivity, ρ the density, and C_p the heat capacity. The thermal

conductivity of PuO_2 as a function of temperature is shown in Fig. III.B.2. The conductivity of UO_2^* is also plotted for comparison. Both curves are for material of theoretical density. At low temperatures, stoichiometric PuO_2 has a slightly greater thermal conductivity, but the two curves are almost coincident above 800°C .

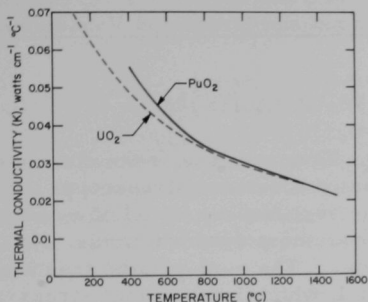


Fig. III.B.2. Thermal Conductivity of PuO_2

At low temperatures, stoichiometric PuO_2 has a slightly greater thermal conductivity, but the two curves are almost coincident above 800°C . Solid solutions of stoichiometric $(\text{U,Pu})\text{O}_2$ would be expected to have about the same thermal conductivity as that observed for UO_2 and PuO_2 . The changes in heat-transport properties of the oxides with composition and stoichiometry will be determined in future studies. The diffusivity measurements on stoichiometric oxides will also be extended to 2000°C .

2. Radiation Damage of Structural Materials--Research and Development

a. In-reactor Creep Studies on Cladding Alloys (J. A. Tesk)

Not reported previously.

A prototype creep machine** was tested and subsequently refined. The device applies a load to a specimen by pressurizing a stainless steel bellows connected to a yoke. Extension of the specimen is measured by means of a radiation-resistant transducer, which is capable of use for extended periods of time at temperatures up to 600°C .

The creep machine fits into a containment capsule that is filled with helium. In order to control the load on the specimen, pressure inside and outside of the bellows must be controlled. A system has been developed that controls the helium pressure outside the bellows to within ± 0.01 psi. A static system has also been assembled that will supply a constant pressure to the inside of the bellows. As soon as pressure transducers, metering valves, and solenoid valves arrive, the system will be converted to a dynamic system with expected pressure control of 0.1 psi over the total possible pressure range from 0 to 400 psi. The necessary safety devices have been incorporated to protect the system against overpressure. Approval of reactor operations has been obtained for the total assembly.

The transducers used for creep measurements are being calibrated at various temperatures. The expected temperature fluctuations may cause scatter in the strain data of approximately $\pm 200 \mu\text{in.}$, but the system probably can be improved to reduce the total scatter to approximately $100 \mu\text{in.}$ The sensitivity can be maintained over a total specimen

*Godfrey, T. G., Fulkerson, W., Kollie, T. G., Moore, J. P. and McElroy, D., J. Am. Ceram. Soc. **48**(6), 297 (1965).

**Designed by A. D. Rossin.

extension of approximately 1 in. by bucking the transducer output with a known voltage and recording the difference.

b. Voids in EBR-II Control-rod Shroud and Irradiated Vanadium Alloys (S. D. Harkness)

Last Reported: ANL-7445, pp. 70-72 (April 1968).

(i) EBR-II Control-rod Shroud. Five sections of the control-rod shroud have been examined by transmission electron microscopy. The observed microstructure in all but one of the sections consisted of a complicated dislocation substructure, Frank loops, and polyhedral voids. No voids were observed to lie on grain boundaries. The void-volume fractions agreed with data taken from cladding material, which implies that stress may not be important in the phenomenon.

The sample that was taken from the top of the shroud showed no voids or dislocation loops. The fluence in the region is calculated to be less than 10^{21} n/cm².

The average void size ($\langle D \rangle$), number density (N_V), and volume fraction (V_F) calculated for each section are listed in Table III.B.1. An immersion density sample was taken adjacent to Sample 4, as reported previously (see ANL-7445, last row of Table I.E.19, p. 71). The technique yielded an increase in volume of 1.04%. The excellent correlation between the results of immersion density and of transmission electron microscopy indicates all changes in the volume of the clad can be attributed to void formation.

TABLE III.B.1. Void Observations in EBR-II Control-rod Shroud

Sample	Estimated Fluence (n/cm ² x 10 ⁻²²)	Estimated Temp (°C)	$\langle D \rangle$ (Å)	N_V (No./cm ³ x 10 ¹⁵)	V_F (%)
1	2.4	375	110	1.9	0.13
2	4.5	410	100	4.2	0.21
3	4.1	450	120	3.7	0.34
4	3.1	470	198	2.6	1.06
5	<0.1	480	-	0	0

The sharp increase of void-volume fraction observed in Samples 2, 3, and 4 illustrates the temperature sensitivity of void formation. The three samples received approximately the same fluence, but lie in a region of rapidly increasing temperature.

(ii) Vanadium Alloys. A program has been initiated to determine the changes in microstructure due to fast-flux irradiations. Of particular interest is whether voids form in this body-centered cubic material in the same manner as in austenitic stainless steels.

Initial studies are being carried out on a V-20 w/o Ti alloy that was irradiated to a fluence of 3×10^{22} n/cm² at approximately 550°C. Although some difficulty has been encountered in thinning specimens for transmission electron microscopy, no voids have been observed to date. Due to the quality of the foils, the only certainty is that no voids larger than 60 Å exist in the material. Type 304 stainless steel irradiated under the same conditions exhibits voids that have an average diameter of approximately 150 Å.

3. Techniques of Fabrication and Testing--Basic Fabricability--Research and Development

a. Development of Nondestructive Testing Techniques (H. Berger)

Last Reported: ANL-7445, pp. 108-110 (April 1968).

(i) Neutron Techniques. Enriched foils of ¹⁶⁴Dy have been tested for use with the activation transfer method of neutron radiography. Dysprosium is the best foil converter used to date. Only 28.2% of the isotope ¹⁶⁴Dy in natural dysprosium captures the incident neutrons and then decays with a useful half-life of 2.32 hr.

In a flux density of 10^5 n/cm²-sec, a ¹⁶⁴Dy-enriched foil (83.2 a/o ¹⁶⁴Dy), 0.001-in. thick, requires an exposure of 20 min for good film density when an image transfer is made to Kodak Type AA film, which is equivalent to a 0.005-in. thickness of natural dysprosium. A 0.0035-in.-thick ¹⁶⁴Dy-enriched foil is about 100% more efficient than a 0.005-in. thickness of natural dysprosium.

(ii) Passive Ultrasonic Techniques. Metal pastes and brazing alloys are being evaluated in an attempt to join lithium niobate piezoelectric elements and Type 304 stainless steel capsules. Feasibility studies are being conducted with barium titanate elements because of the high cost of lithium niobate crystals. Engelhard platinum paste (Number 6082) and du Pont silver paste (Number 7095) have been fired to barium titanate. Efforts to braze the silver-copper eutectic alloy to a silver-electroded, barium titanate element were unsuccessful. Other brazing alloys will be investigated.

(iii) Development of an Electrodynamic Transducer. Current work on the electrodynamic transducer has emphasized coil design. Several types of pancake coils were made and evaluated. The best system response

was achieved with a bank-wound coil of 34 gauge copper wire. The coil was wound on a Lucite holder to the same diameter as the test piece and covered with a 3-mil-thick tape for protective purposes.

The electrodynamic transducer with a bank-wound coil was compared, under identical pulse-echo techniques, with a piezoelectric transducer (PZT-4). The ratio amplitudes of the received signal was 3000:1. Although the sensitivity of the electrodynamic transducer is low relative to the PZT-4, sensitivity was, nevertheless, sufficient to be useful in a 12-in.-long aluminum test piece. Increases in sensitivity can be achieved by increasing either the magnetic field or the current to the coil. Since the magnet is operating at full capacity (20,000 gauss), increases in power input to the coil, which does not have the severe voltage limitations of a piezoelectric crystal, will be made with an upgraded power source.

(iv) Holography. Background information is presently being obtained on the field of holography as a technique for nondestructive testing. Selection of equipment for laser-holography is progressing.

b. Basic Fabricability of Nonfissile Metals and Alloys
(N. J. Carson)

Last Reported: ANL-7427, pp. 107-108 (Feb 1968).

(i) Fabrication Development of Group VI Metals and Alloys.

Work on the development of a technique for drawing molybdenum tubing of low-carbon content at room temperature has continued. Recrystallized tube blanks were reduced to various cross-sectional areas at 200 to 250°C. The blanks were heat treated at 625°C, cut into shorter lengths, and each length drawn at a different temperature. The results obtained are given in Table III.B.2. Warm reduction apparently decreases the minimum temperature at which the low-carbon molybdenum tubes may be drawn. The lowest drawing temperature achieved was 50°C after a warm reduction of 82%.

TABLE III.B.2. Drawing of Molybdenum Tubing

Reduction in Area before Drawing (%)	Drawing Temperature (°C)	
	Successfully Drawn	No Draw
35	175	125
50	150	100
63	90	40
82	50	20

No evidence of recrystallization was observed in the samples heat-treated at 625°C. On the theory that a higher heat-treating temperature will produce a softer alloy and, thus, a lower working temperature, several samples were heat treated at 950°C prior to drawing. This heat-treatment, which was known to promote at least partial recrystallization, raised the drawing temperature. Thus, the optimum heat-treating temperature may be between 625 and 950°C.

C. Engineering Development--Research and Development

1. Development of Master-Slave Manipulator Systems (R. C. Goertz)

Last Reported: ANL-7445, pp. 110-112 (April 1968).

a. Development of Manipulator Systems

(i) Electric Master-Slave Manipulator, Mark E4A. One servo drive unit of the Mark-E4A slave arm has now been exposed to an incident dose of 10^9 R. Electromechanical functioning of the servomotors is the same as before irradiation. Also, the mechanical friction of the bearings and gears is unchanged. The friction of the brake has increased to more than 1.5 times its value before irradiation. New brake designs are being considered that will have a more nearly constant braking effect even with some changes in the coefficient of sliding friction at the brake surfaces. Mechanical negative feedback and detent systems are being considered.

Pulleys for irradiation testing have been made out of asbestos-filled phenolic, glass-filled phenolic, and polyimide (Vespel). It is expected that these materials will take 10^9 R without too much degradation of mechanical properties. The materials that do hold up all right will be tested for wear and friction characteristics.

One of the gears in the original servo drive units is made of linen phenolic. Mechanically this material works fine, but it is only good for about 10^7 R. All steel gears are being used in the servo drive unit now undergoing irradiation. Because of the low inertia requirements, the larger of these gears must be quite thin. This pushes the tooth loading up so high that the gears have to be hardened and ground. This is expensive, and we are concerned about the long-term lubrication with the high tooth loading. Consequently, we are making some gears out of polyimide (Vespel) and will test these mechanically before and after irradiation.

b. Study of Remote Handling for LMFBR Facilities. Informal meetings were held with LMFBR Program Office staff in the Plant Design, Components, Core Design, Fuels and Materials, and Fuel Recycle Sections primarily to discuss currently envisioned remote-handling problems and possible solutions. It is evident that many handling problems exist in the areas of: refueling, driver fuel and experimental subassembly instrumentation, maintenance and repair of equipment, inspection, fuel surveillance, equipment modifications, and recovery from equipment failure. These problems are compounded by the need for high plant-availability factors and by the economics involved.

The reasons for, and the usefulness of, a cell over a reactor were explored. Opinions varied considerably. Some people believed that

the advantages of a cell did not justify the cost, others that cells should definitely be incorporated in the 300-MWe and early 1000-MWe plants and that they should possibly be incorporated in later plants as well. The cells would provide convenient hot "workshops" if unforeseen troubles were encountered. They would also provide particulate containment if vented fuel were used or if unvented fuel ruptured. If efficient manipulator systems were provided in these cells, many routine operations also could be remotely performed. It may, for example, be practical to perform fuel surveillance and to remove the fuel and blanket elements from the fuel assembly in these cells prior to shipment for reprocessing.

Two basic approaches toward solving remote-handling problems were discussed. One approach makes little use of manipulator-system technology. Special-purpose equipment is designed to perform remotely many tasks, and the replacement of this equipment is carried out with cranes or crude manipulators. Repair and maintenance work is almost exclusively carried out by direct means (through suits or gloves) after the radiation level in the cell is reduced or the equipment is removed to a low-level environment. Decontamination of the equipment is often necessary before suited or gloved access is safe.

In our discussions over the past few months, we found that this approach (to varying degrees) was supported by most. It has, however, serious drawbacks associated with it which directly affect plant availability and cost.

- (1) It requires considerable design time both to provide equipment to carry out the specific tasks and to make the equipment replaceable with rudimentary handling equipment.
- (2) In many cases, it is assumed that direct access to failed equipment can readily be made safe. This may or may not be a good assumption, but once manned access is made a design requirement, the versatility of the cell or cell complex is greatly reduced. Many operations could not be efficiently performed in such a cell because of the later cleanup necessary.
- (3) Any modifications or unforeseen problems could seriously reduce the plant availability.
- (4) For even minor repairs, the entire piece of equipment must often be removed, disassembled, decontaminated, and then rebuilt--an expensive, time-consuming process.
- (5) Since any repair or modification work is slow, spares of all vital equipment should be maintained.

The other approach towards remote handling makes full use of applicable manipulator-system technology. Special-purpose machines are used only for those tasks which can be done in this manner more efficiently, reliably, and at less cost. All other tasks would be carried out with electric master-slave manipulator systems. Considerable repair and maintenance work on equipment in place could be performed with the manipulator systems. Equipment to be repaired remotely could be designed almost as if it were to be repaired directly. Decontamination of components to permit gloved repair would be minimal. Manned access is unnecessary, and the additional design and operational freedom permitted by eliminating the need for manned access is obvious. Most importantly, unforeseen problems can also be handled much more efficiently and with much less downtime.

Our opinion is that the second approach noted should be given much more consideration in subsequent studies of facility concepts. We believe the cost of developing and implementing advanced manipulator systems would be more than offset by the monetary savings which would accrue. Less special-purpose equipment would be needed, the design of this equipment could be simpler, and equipment repair and maintenance would be cheaper and faster. In addition, advanced systems, because of their versatility, would go a long way toward improving and insuring plant factors.

Our opinions are not widely shared, however. Unfamiliarity with what is now possible, and with what could be possible with advanced manipulator systems, is probably a major reason for this difference. Also, even when the increased capabilities of advanced systems are recognized, it is difficult to estimate convincingly the economic advantage in providing them.

2. Instrumentation and Control

a. Boiling Detector (T. T. Anderson)

Last Reported: ANL-7419, pp. 115-116 (Jan 1968).

(i) Prototype High-temperature Acoustic Sensor. Development of bonding methods for the high-temperature acoustic sensor is continuing. The general technique that shows the most promise involves firing a three-layer metallic suspension onto the piezoelectric crystal, then brazing metallic components to the fired film. Combinations of newly received suspensions and brazes are being evaluated; there are indications that at least one of these combinations will achieve a better bond than did the braze to evaporated-gold films that was reported previously (see Progress Report for November 1967, ANL-7399, pp. 127-128).

(ii) Geometrical Resonance Tests. Design of the acoustic detection system depends partially on the acoustical signal-to-noise discrimination of boiling in the presence of other acoustic sources. To characterize

boiling under these conditions, geometrical effects of liquid-filled vessels are being examined. As reported in ANL-7419, the frequency spectrum of

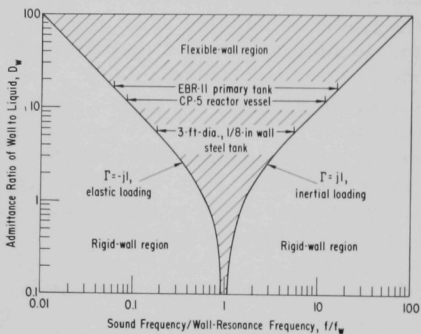


Fig. III.C.1. Frequency Range of the Free-surface Effect as a Function of Tank Geometry. Γ is the reflection coefficient for the pressure wave at the wall.

As shown in the figure, the primary tank in EBR-II is expected to behave as a free surface for a 250:1 range of frequencies. In this range, the sound pressure at the wall would be nearly zero.

For initial tests on existing reactors, acoustical monitoring can be conducted with transducers mounted outside the liquid-filled vessel on components that extend into the core region. Thus a component functions as an acoustic waveguide, transmitting sound pressure from the core region as a traveling vibration. A test program has been initiated to make this type of measurement on the EBR-II. Electronic equipment is being procured to monitor acoustic backgrounds from subaudio frequencies through 1 MHz. In support of the EBR-II tests, an acoustic probe has been constructed for use in the Juggernaut reactor. The probe, a 3/8-in.-dia, 50-in.-long rod that passes through two regions of a specially constructed three-region shield plug, will be used to determine design parameters of acoustic waveguides. With the lower end of the rod immersed in the reactor coolant, motion of control rods can be detected acoustically.

3. Heat Transfer, Fluid Flow, and Mechanics of Materials

a. High Temperature Boiling Sodium Experiment (J. V. Tokar)

Last Reported: ANL-7445, p. 112 (April 1968).

(i) Niobium-1% Zirconium Loop. All repairs and modifications of the loop facility have been completed.

sound pressure from boiling was found to contain resonances caused by standing waves in the 3-ft-dia test vessel. These frequencies, determined by boundary conditions at the vessel wall, were shown to correspond more closely to a freely moving boundary than to a rigid wall. As shown in Fig. III.C.1, this effect also applies to low-pressure reactor tanks, such as the CP-5 reactor vessel or the EBR-II primary tank. The wall-resonance frequency f_w , defined for pure radial motion, is $f_w = c_w/2\pi r$, where c_w is the sound velocity in the wall and r is the tank radius. The admittance ratio of wall to liquid is $D_w = (\rho_L c_L / \rho_w c_w)(r/t)$, where ρ is the density and t is the tank-wall

In the development of a new pump-duct design, a prototype has been constructed and tested in a small NaK loop. The tests indicate a large improvement in performance over the old design (300 versus 44 psi Δp at 5 gpm). However, the prototype is not suitable for operation above 800°F; a pump that will operate up to 1600°F is being developed.

b. Heat Transfer to Liquid Metal Heat Exchangers (R. P. Stein)

Last Reported: ANL-7438, pp. 99-102 (March 1968).

(i) Nonsymmetrical-duct Heat Exchangers. The investigation of the effect of eccentric placement of the central tube in sodium-to-sodium double-pipe heat exchangers has been interrupted by work of higher priority. Detailed analytical studies explaining the experimental data already obtained have been outlined, but their performance has been delayed.

(ii) Liquid-metal-heated Steam Generator. Construction of the experimental loop has been delayed appreciably, but work continues on expansion of the preliminary review report. Also, information has been requested from groups and individuals who have designed steam generators. The information requested includes: (a) operating conditions assumed in the design, such as flows, temperatures, and pressures, (b) methods to predict heat-transfer area used in the design, and (c) operating temperatures measured in tests of the steam generators.

Difficulties with the computational procedure to predict steam-generator heat transfer without the "engineering assumption" of a length-independent liquid-metal-side heat-transfer coefficient (see ANL-7438, p. 102) have not been resolved satisfactorily.

c. Fog Flow Heat Transfer and Fluid Flow (R. P. Stein)

Last Reported: ANL-7438, pp. 105-106 (March 1968).

The fog-flow experimental apparatus is nearly assembled. The first test section, to be used to measure mean and turbulent air velocities and static pressure, is being fabricated. A major objective of initial experiments will be to determine whether we can achieve a fully developed turbulent pipe flow within the length of duct available in the facility.

Experiments with a simplified 3-in.-dia model of the main apparatus are being conducted to test, refine, and become familiar with the various measuring devices to be used, which include a hot-wire anemometer, an isokinetic sampling probe, and a fiber-optics probe.

During initial tests of the hot-wire anemometer (Flow Corp. Model 900-1 constant-temperature anemometer), three of the 0.00035-in.-dia tungsten sensors were damaged by an initial transient surge of electrical

current through the wire when the instrument was turned on; steps will be taken to prevent a recurrence. Before the last filament burned out, the hot wire was exposed to a pure air stream and to a water-droplet-laden air stream. The instrument seemed to operate as expected, i.e., a well-defined voltage pulse across the anemometer bridge circuit was apparent when a droplet hit the wire.

The isokinetic sampling probe will measure the mass flow of droplets passing the face of the probe at "isokinetic" conditions by determining the volume of liquid sampled by the probe per unit time. The vessel initially used to collect the sampled liquid was too large to give a measurable reading in a reasonable time, so a modified 50-ml laboratory burette will be used.

The fiber-optics probe was designed to measure droplet concentration by the attenuation of a beam of white light through a fixed sensing-volume element. A photoresistor is the light sensor. Two problems have arisen in operating this probe. The first appears to be caused by the directional properties of the fiber-optics light bundles, which emit and collect light in a 70° cone, as shown in Fig. III.C.2. With no droplets within the sensing volume, the 0.110-in.-dia sensor-fiber bundle detected light from source area A only. But when droplets were present, the sensor fibers collected, in addition, light scattered from droplets within the two triangular regions around the sensing volume. Thus the droplets caused the sensor to see more light rather than less.

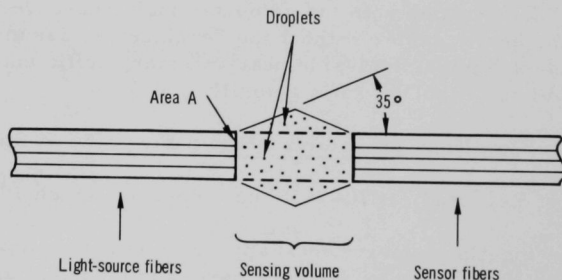


Fig. III.C.2. Fiber-optics Probe Configuration

A second problem is that liquid collects on the faces of the fiber bundles and prevents meaningful measurements. After the faces of the probe were filled with epoxy and polished smooth to within 3 mils, no film was formed; but a spurious signal remained, so a few droplet beads must have deposited on the probe faces.

To alleviate these two problems, consideration is being given to a new probe configuration and to increasing measurement sensitivity by dyeing the liquid.

4. Liquid-metal Linear Generator

a. Condensing Injector Studies (M. A. Grolmes)

Last Reported: ANL-7357, pp. 118-119 (July 1967).

As a major component in some liquid-metal magnetohydrodynamic (MHD) power cycles, the condensing injector would be required to generate large stagnation pressures. Efficient conversion of the vapor to the liquid state with minimum loss of kinetic and potential energy would be required. Realistic appraisal of the condensing injector was needed to determine the potential of this device for large-pressure augmentation in such applications. Therefore, a condensing injector with a large area-contraction ratio was developed and tested with supersonic inlet vapor velocity. Entrance, profile, and discharge vapor and liquid velocities, pressure densities, and mass ratios were measured to evaluate performance.

The steam-water condensing injector studied had inlet vapor velocities approaching Mach 1.7 and a convergent condensing section. Axial pressure profiles and maximum discharge pressures were obtained for various vapor and liquid inlet conditions. The observed maximum stable discharge pressures for these experiments were generally lower than predicted by a constant-pressure condensing model, particularly in the case of low liquid-to-vapor flow rate ratios where constant-pressure condensing was no longer achieved and the liquid-jet disintegration proceeded more rapidly. Losses other than those caused by vapor-liquid mixing and expansion in the minimum-area section were related to the liquid-jet disintegration. Also, criteria for minimum liquid-vapor flow rate ratios consistent with constant-pressure condensing were verified. Other details of the flow processes and analytical studies have been reported (see ANL-7357, p. 118) and described in detail.*

When the results of this investigation were related to previous condensing-injector studies and to previous studies of liquid-metal MHD power cycles, the evidence indicated that the range of liquid-to-vapor flow rate ratios and condensing-section area contraction that might actually be realized would be somewhat less optimistic than previously believed. Thus we conclude that realistic limitations in area contraction, and especially in required flow rate ratios, would render the condensing injector less attractive than previously believed in liquid-metal MHD power cycles operating within the conditions of previous cycle studies.** Reduced vapor-liquid velocity ratios

*Grolmes, M. A., Steam-Water Condensing Injector Performance Analysis with Supersonic Inlet Vapor and Convergent Condensing Section, Ph.D. Thesis, University of Notre Dame (also to be published as ANL-7443).

**Brown, G. A., and Levy, E. K., Liquid Metal Magnetohydrodynamic Power Generation with Condensing Ejector Cycles, Paper No. SM-74/171, Proceedings International Symposium on Magnetohydrodynamic Electrical Power Generation, Salzburg, Austria, July 4, 1966.

in the condensing section of the injector could improve injector performance, but might raise practical difficulties in overall cycle performance.

5. Engineering Mechanics

a. Anisotropic Thermoelasticity Studies (R. A. Valentin)

Last Reported: ANL-7427, pp. 115-116 (Feb 1968).

The study of inertia effects in transient thermoelastic problems has been extended to include variations in surface heat-transfer characteristics. Specifically, the dynamic transient half-space problem previously used to investigate heat-generation-induced elastic waves has been modified to include a surface conductivity specified by a Biot number relating the boundary conductance and the relaxation length of the assumed exponential spatial decay of the heat-generation rate. A parametric study of this problem is being completed to illustrate the interaction of the inertia parameter, Biot number, and rate of change of internal heat-generation rate in producing elastic waves.

Closely related to the above problem are questions concerning dynamic effects associated with rapid changes in heat generation in thin rods. Although the subject has been studied in relation to various reactivity-feedback mechanisms, the stress field produced in thin rods during rapid transients has not been considered carefully. A sample problem of this type has been analyzed and the results are being evaluated numerically.

b. Core Structural Dynamic Studies (M. W. Wambsgans)

Last Reported: ANL-7438, pp. 106-107 (March 1968).

Work continued on the application and testing of transducers developed to measure the displacement of a simulated fuel rod within a bundle and the fluid-pressure fluctuations on the surface of the rod.

An internal displacement-measuring rod was flowtested. The instrumented rod was mounted in a tubular test specimen, which in turn was mounted in a clamped-clamped configuration in the test section of a flow loop. An external displacement sensor was mounted in the wall of the test section opposite the internal sensor as a reference to evaluate the performance of the internal transducer. Displacement-time histories, as sensed by the two transducers, were recorded on magnetic tape for various flow rates. The data were processed to give spectral-density representations of the responses. Plots of the spectral density were then compared to evaluate the utility of the internal displacement-transducer concept.

Below approximately 30 Hz, the correlation was good. However, because the fundamental natural frequency of the instrumented rod (38 Hz) was close to that of the tubular test specimen (45 Hz), energy extracted by the lightly damped instrumented rod in the frequency band near its natural frequency masked the output because of the motion of the test specimen in that frequency band. A further difficulty, which compounded this effect, was caused by a leak that permitted the space between the instrumented rod and test specimen to fill gradually with water during the test. The result was a slight decrease in the natural frequencies; but more detrimental to the functioning of the instrumented rod was the strong coupling caused between the test specimen and the instrumented rod.

We conclude from the flowtests that the technique is promising and can be effective if the natural frequencies of the instrumented rod and the test specimen are separated sufficiently, with the frequency of the instrumented rod being the greater. To accomplish this, a new displacement-measuring rod is being constructed using a 0.096-in.-dia steel rod on which a plastic capsule holding the sensing coil will be mounted. The rod will be put under an axial tensile load so we can increase and vary the rod's natural frequency.

A test rod has been instrumented with seven miniature pressure transducers mounted longitudinally and circumferentially. The transducers have been calibrated and their frequency response over the range of frequencies of interest appears to be sufficiently flat that added compensation will not be required. Flowtests are planned after tests of another probe that has been instrumented to measure differential pressure.

D. Chemistry and Chemical Separations

1. Aqueous and Volatility Processes--Research and Development--Fluoride Volatility Process

a. Fluorination Chemistry and Procedures (M. J. Steindler)

Last Reported: ANL-7438, pp. 107-108 (March 1968).

A statistically designed series of five experiments simulating the fluoride volatility processing of fast breeder reactor fuels is in progress using the 2-in.-dia fluid-bed reactor. Each experiment consists of 4-hr oxidation with 20 v/o oxygen, removal of uranium by 3-hr fluorination with 10-15 v/o fluorine, and removal of plutonium by fluorination with recycled 90 v/o fluorine. The objective is to determine the effects of two levels of each of three process variables on plutonium and uranium retention in the final bed. Two weight ratios of fuel to alumina (0.3 and 0.6), two temperatures in the uranium fluorination step (350 and 450°C), and two recycle-fluorination times (10 and 20 hr) were used. In each run, the feed consists

of ~650 g solid solution UO_2 -20 w/o PuO_2 to which is added ~69 g of non-radioactive oxides of the elements formed by fission in a fast breeder reactor core. The inert bed material consists of 1100 g of 48-100 mesh alumina.

Runs FF-A1 and FF-A2, which have been completed, had the same fuel to alumina ratio (0.6), but different uranium fluorination temperatures (350°F for FF-A1 and 450°C for FF-A2) and different plutonium fluorination times (20 hr for FF-A1 and 10 hr for FF-A2). For Run FF-A1, retentions in the final bed of 0.5% of the plutonium charged and 0.04% of the uranium charged were reported in ANL-7438. These results were considered satisfactory for a practical process. Retention of plutonium in the final bed from Run FF-A2 was unsatisfactorily high: 3% of the plutonium charged. Thus the conditions used in this run are not acceptable.

Data have been obtained that allow comparison of uranium and plutonium volatilization in the uranium fluorination step of the two runs. The ratios of uranium to plutonium in the product trap after the uranium fluorination step were 550 for Run FF-A1 and 152 for Run FF-A2. The lower temperature for Run FF-A1 thus promoted separation of uranium from plutonium.

In Run FF-A1, fluorination to recover plutonium was begun at a temperature of 300°C, and in Run FF-A2 at 450°C. The diminishing-sphere correlation appears to represent the fluorination of plutonium at each of these temperatures. Rate constants k' of $0.69 \times 10^{-3} \text{ min}^{-1}$ and $3.0 \times 10^{-3} \text{ min}^{-1}$ have been calculated for this fluorination at 300 and 450°C, respectively. The results give a preliminary estimate of the apparent activation energy of 8.1 kcal/mole.

b. Fission Product Fluoride Chemistry (R. L. Jarry)

Last Reported: ANL-7438, pp. 109-110 (March 1968).

(i) Chemistry of Ruthenium. An experimental study of the transpiration of mixtures of ruthenium fluorides and UF_6 (a stand-in for PuF_6), using fluorine as a carrier gas and LiF as sorbent, has been completed with the performance of Experiment 7. In Experiment 7, the transpiration of ruthenium fluoride at low temperatures was measured to obtain data for a proposed process step in which plutonium would be separated from ruthenium by sublimation of PuF_6 from a cold trap at 0°C. The sorption capacities of LiF and NaF for ruthenium fluoride were also measured in the experiment. A mixture of ruthenium fluorides (tagged with ^{106}Ru to allow monitoring of ruthenium movement) and UF_6 was prepared by fluorinating UF_4 and ruthenium; the mixture was transported in the fluorine stream to a cold trap held at -78°C. Uranium and ruthenium species were transpired in a stream of fluorine as the cold-trap temperature was raised, in turn, to 0, 50, 100, and 150°C.

The gas stream from the cold trap flowed through a LiF trap at 300-400°C, a NaF trap at 100°C, and an activated alumina trap at 100°C.

Experimental conditions for Experiment 7 differed from those used in previous experiments (see Progress Reports for January, February, and March 1968; ANL-7419, p. 121, ANL-7427, pp. 120-121; ANL-7438, pp. 109-110) as follows: (1) the tagged ruthenium that was fluorinated was 75% ruthenium metal and 25% RuO₂, which is thought to approximate the ruthenium in a spent fuel element; (2) a charge with a ¹⁰⁶Ru activity of ~10⁶ counts/(min)(g Ru), rather than ~5 × 10⁴ counts/(min)(g Ru), was employed to allow the measurement of transpiration of very small quantities of ruthenium at -78, 0, and 50°C; (3) the activated alumina trap was added in series with the NaF trap to allow detection of ¹⁰⁶Ru activity swept through the two absorption traps. In Experiment 7, 2.5 g of UF₄ was used in the charge instead of 5 g used in Experiment 6 (in which the cold trap plugged).

Experiment 7 results indicate that the maximum conceivable quantity of ruthenium transpired out of the cold trap at -78, 0, and 50°C was 0.06 mg, which corresponds to a minimum decontamination factor of 1.6 × 10⁴. The bulk of the ruthenium was transpired at 100°C and above. On the basis of vapor pressure data for ruthenium fluoride species, it is concluded that any ruthenium transpired at ≤50°C was RuF₅.

The ruthenium capacity of the LiF at 350°C was 21 mg Ru/g LiF, and the capacity of the NaF at 100°C was 22 mg Ru/g NaF. Some ruthenium passed through the LiF before its capacity was reached, whereas sorption on the NaF exhibited no breakthrough until the capacity of the NaF was reached.

c. Engineering Scale Development for UO₂-PuO₂ Fuel (N. M. Levitz)

Last Reported: ANL-7445, pp. 118-119 (April 1968).

Conceptual design studies on fluoride volatility processing plants for fast breeder reactor fuels are in progress. A tentative process flowsheet has been selected for a central plant with a capacity of 1 metric ton of actinides per day (the average daily discharge rate from a 15,000-MWe network). The reference core (20% PuO₂-UO₂) and axial blanket (2% PuO₂-UO₂) fuel pins for this study have a 0.25-in.-dia, 0.015-in.-thick stainless steel cladding, and gas bonding. The radial blanket pins, of similar material (2% PuO₂-UO₂), have 0.35- and 0.51-in. diameters.

In the mechanical head-end step, the fuel element is washed to remove adhering sodium and disassembled. Pins logged with sodium are identified by an eddy-current method and put aside for separate processing;

nonlogged fuel pins are chopped into short (1/2- to 1-in.) pieces. The fuel is separated as powder from the stainless steel hulls by vibration, ball milling, or other suitable means.

d. Small-scale Studies with Irradiated Fuels (A. A. Chilenskas)

Last Reported: ANL-7427, pp. 122-123 (Feb 1968).

A series of five experiments (BRF-1 to -5) to test the inter-halogen flowsheet with irradiated UO_2 (Yankee fuel) has been completed in the senior cave facility. (Reporting of this work was delayed for patent clearance.) The primary objectives of these tests were: (1) to determine the extent of plutonium and uranium removal from the fluid bed, (2) to determine the fission product (FP) distribution for each process step, (3) to determine the FP contamination level in the uranium and plutonium products, and (4) to test several simple schemes for plutonium and uranium decontamination. Preliminary results have been reported previously.* This report summarizes the results from all five runs.

In each run, the charge was 100 g UO_2 (irradiated to 33,200 MWdt and cooled 1 to $1\frac{1}{2}$ yr) and 350 g T-61 refractory alumina powder. In the first step, the irradiated UO_2 (previously dekad) was added to a bed of refractory alumina in the fluid-bed reactor. The UO_2 was converted to U_3O_8 at 450°C in the fluid bed by reaction with 20 v/o oxygen in nitrogen. Next, in the uranium volatilization step, the uranium was separated as volatile UF_6 from the plutonium and most of the fission products by fluorinating with 10 v/o BrF_5 at 300 or 360°C . In the next step, plutonium was volatilized from the fluid bed by treatment with 10-90 v/o fluorine at $300\text{-}550^\circ\text{C}$. In Runs BRF-3 to -5, a plutonium-purification step followed. After the fluid-bed material was dumped at the end of a run, residues in the equipment components were analyzed to determine their actinide and FP contents.

The major equipment component was a 1.5-in.-dia fluid-bed reactor, which had a sintered nickel filter (to remove elutriated fines) in a chamber above the reactor. In each step, the off-gas from the reactor passed through a different series of vessels prior to discharge to the cave exhaust. The off-gas from the oxidation step passed through two cleanup traps containing activated charcoal. The process off-gas from the BrF_5 step, which contained UF_6 , Br_2 , BrF_5 , and volatile FP fluorides in nitrogen diluent, passed first through a trap containing NaF at 400°C (to remove some fission products) and then through a series of three traps containing, in turn, activated alumina (for removal of UF_6 and some FP), soda lime (for removal of Br_2 and some FP), and activated alumina (for removal of water released in the preceding trap). The off-gas from the fluorine step passed through

*Progress Reports for September 1966, November 1966, February 1967, March 1967, April 1967; ANL-7255, p. 60; ANL-7279, pp. 70-71; ANL-7308, pp. 75-76; ANL-7317, p. 87; ANL-7329, p. 74

a precooler (to collect high-boiling FP fluorides) and then through the product cold trap (where PuF_6 is collected along with some undesired FP), then through a trap containing 200 g NaF (to remove trace quantities of PuF_6), four parallel traps containing activated alumina (to remove fluorine), and a trap containing NaF at 400°C (to remove trace amounts of volatile FP). In Run BRF-3, the PuF_6 that had been collected in the cold trap was sublimed at 0°C (to separate it from FP fluorides of lower volatility) and transferred in a stream of nitrogen gas to a bed of NaF pellets at 350°C where the plutonium was collected. In Runs BRF-4 and -5, the plutonium collected in the cold trap was sublimed and transferred in a stream of nitrogen to a bed of refractory alumina at 300°C , where the PuF_6 was thermally decomposed to PuF_4 .

The results of the five experiments show:

1. Computer-calculated FP concentrations for irradiated UO_2 from the Yankee reactor were in excellent agreement with analyzed values.
2. The principal activities that volatilized during the oxidation step were krypton ($\leq 27\%$)* and ruthenium (≤ 3.5).**
3. About 13% of the gross beta-gamma activity was volatilized with the uranium during the BrF_5 step. The principal gamma activity volatilized was found to be ruthenium ($44-71\%$); other contaminants were molybdenum ($\leq 76\%$) and antimony ($< 2.7\%$). Values for other possible volatiles, such as tellurium, technetium, and neptunium, were not obtained. During the BrF_5 step, about 67% of the krypton was released to the process off-gas. Greater than 99.5% of the uranium was volatilized from the reactor along with an average of less than 0.5% of the plutonium.
4. The use of NaF pellets at 400°C as a fission product trap to effect uranium purification during the BrF_5 step was unsuccessful; only about 50% of the ruthenium that volatilized was collected. In addition, about 80% of the uranium was sorbed by this bed, contrary to the behavior of UF_6 in a F_2 stream from which little or no uranium is sorbed.
5. The volatilization of plutonium with fluorine resulted in the concurrent volatilization of less than 2% of the gross beta-gamma activity. The principal gamma activity transported was ruthenium ($3-14\%$), while up to 38% of the molybdenum and small amounts of zirconium ($\leq 0.21\%$), niobium ($\leq 5.8\%$), and antimony ($\leq 1.2\%$) were also volatilized. In addition, $\leq 9.6\%$ of the krypton was found in the process off-gas. Values for other possible contaminants, such as tellurium, technetium, and neptunium, were not obtained.

*Values for krypton in this subsection are percentages of the total quantity of krypton accounted for.

**In this subsection, values for elements other than krypton are each the percentage of the quantity charged to the fluid-bed reactor.

6. The average concentration of plutonium retained by the alumina reactor bed was 0.016 w/o of the bed. This value was obtained with a single use of the bed and with low charge-to-bed ratio. Extrapolation of these results to conditions of larger charge-to-bed ratio and recycle leads to an expectation that more than 98% plutonium would be removed from the reactor. Less than 0.01% of the uranium charged was retained by the reactor bed.

7. The decontamination of plutonium from fission products for certain process steps was examined. The decontamination factor for removal of gross gamma during plutonium volatilization from the reactor bed was 120. When sublimation of PuF_6 at 0°C followed by collection on NaF pellets at 350°C was added to the volatilization separation, a decontamination factor for gross gamma of 1400 was obtained. When sublimation at 0°C followed by thermal decomposition on alumina at 300°C was employed in addition to the primary volatilization separation, a decontamination factor for gross gamma of 3200 was achieved. In each case, the predominant gamma-active contaminant was ruthenium. [Recent experiments with ruthenium tracers indicate that much higher decontamination factors ($>10^4$) can be achieved by the sublimation method. The reasons for the lower decontamination factors in these hot-cell experiments is under study.]

8. The use of a sintered nickel filter of nominal $10\text{-}\mu$ porosity was effective in preventing the transport of particulate activity from the reactor. The concentration of volatile activities in the process off-gas discharged to the atmosphere was in all cases within the recommended limiting concentration as defined by AEC standards.

9. The actinide and FP material balances obtained ranged widely. However, the values obtained were satisfactory in providing a description of actinide and FP movement in the experimental equipment.

10. Equipment decontamination work showed that after the bed from the final run had been dumped, about 2.1%* of the gross gamma activity remained behind in the reactor and 16%** on the sintered metal filter and filter housing.

Additional investigations of irradiated fuels are awaiting equipment modifications of the senior cave facility. Components of a new manipulator system are being modified and tested in preparation for their installation in the cave. Five recently received Model J manipulators are being assembled in the service area of the cave for shakedown prior to

*Based upon the gross gamma input for all five runs.

**The filter and filter housing were cleaned by scouring the housing with 200 g of alumina following the fourth run; hence the value shown (16%) represents the accumulation for Run BRF-5 only.

installation. Two bridges have been modified and two new carriages fabricated for the two PaR electromechanical manipulators. Wall tubes have been rebored so that they will accommodate the new sealed master-slave manipulators.

2. Closed Cycle Processes--Research and Development--Compact Pyrochemical Processes

a. Process Chemistry of Molten Salt Systems (I. Johnson)

Last Reported: ANL-7445, pp. 119-120 (April 1968).

The phase diagram of the $\text{CaCl}_2\text{-MgF}_2$ system is being investigated as a part of a study of the pyrochemical reduction step of the salt-transport process. Both differential thermal analysis and chemical analysis are being used to delineate the phase diagram. The chemical studies are conducted by agitating a mixture of CaCl_2 and MgF_2 in a tantalum crucible at a temperature such that part of the MgF_2 is always a solid phase. The melt is stirred at 100 rpm for 3 to 6 hr to establish equilibrium between the liquid and solid MgF_2 phases, and then samples are taken through tantalum frits. The samples are subsequently analyzed for chloride and magnesium ions to determine the composition of the melt.

The chemical and differential thermal analyses have indicated that a eutectic exists at about 624°C and 12 m/o MgF_2 .

b. Engineering Development (R. D. Pierce)*

Last Reported: ANL-7445, pp. 120-122 (April 1968).

Two shakedown runs have been performed in the recently modified uranium and plutonium product retorting furnace. In the first experiment, ~360 g of 7/16-in. uranium rod were loaded into a beryllia crucible and heated to a furnace temperature of 1230°C (measured below the crucible) at a nominal argon pressure of 10 Torr. Only a portion of the charge melted in the time allowed because the crucible temperature was lower than expected, but the uranium that did melt retained its metallic luster and showed little evidence of atmospheric contamination of the furnace. The furnace will be modified to achieve higher crucible temperatures.

In the second experiment, 2.6 kg of Zn-20 w/o Mg were distilled in the retorting furnace at 900°C with a furnace pressure of 5 to 10 Torr. The distillate vapors were contained satisfactorily by the graphite furnace components using graphite-to-graphite vapor seals.

*Erratum: In ANL-7445, p. 120, the title of "Unit Operations Development" should be "Engineering Development." The last sentence of the first paragraph should be changed to read "The subassemblies contained 2.68 kg of stainless steel" instead of 6.68 kg.

An additional run will be made with a uranium-bearing alloy before a plutonium product is retorted in the furnace.

Design work is being carried out on mixer-settler units employing the solid-rotor pump described in ANL-7445. A five-stage mixer-settler has been proposed for the salt-transport step, rare earth-extraction step, and noble metal-separation step of the pyrochemical process for fast breeder reactor fuels.

Conventional mixer-settlers are usually designed so that two fluids are moved in the same pattern through each stage. Thus, the number of stages can be increased by merely adding one unit to another. In the pyrochemical process, however, six separate fluids (metals or salts) may be employed within five stages. The solid-rotor pump may be easily modified to provide mixing and/or pumping capability in each of the five stages. Mixing can be accomplished by adding mixing paddles to the bottom of the rotor. The paddles will not interfere with the pumping characteristics of the unit. In other stages where settling and phase separation are required, the pump can be used without paddles to pump a liquid-metal phase from beneath a molten salt layer.

Models of the various stages in the proposed mixer-settler unit are being mocked up in plastic, and mixing, phase disengagement, and settling are being tested with an acetylene tetrabromide-water system.

c. Pilot Plant Operations (R. D. Pierce)

Last Reported: ANL-7427, pp. 124-125 (Feb 1968).

An existing laboratory area is being modified to provide a Plutonium Salt Transport Facility. The facility will be utilized for engineering-scale (up to 1 kg plutonium) investigations of an integrated salt-transport process for fast breeder reactor fuels.

Four gloveboxes to be used with plutonium have been moved into the facility. The two largest gloveboxes are 14 ft long by $3\frac{1}{2}$ ft wide by $8\frac{1}{2}$ ft high, and will contain a recirculated, purified helium atmosphere. One box is connected by a transfer lock to a small air-atmosphere box ($4\frac{1}{2}$ by $4\frac{1}{2}$ by $4\frac{1}{2}$ ft) through which materials will be transferred in and out of the larger box. The other two boxes, one 10 ft long by $4\frac{1}{2}$ ft wide by 5 ft high and one 6 ft long by $4\frac{1}{2}$ ft wide by 4 ft high, will contain a once-through nitrogen atmosphere. The three largest boxes will be interconnected by transfer locks to provide for transfer of materials from one box to another.

The transfer locks, heat-removal equipment, and helium-purification system for the facility have been designed and partially installed.

Design work has been completed for about 50% of the equipment that will be installed in the boxes, and this equipment is on order. Four large 20-kW furnaces and seven pressed-and-sintered tungsten crucibles for process application have been ordered. The two largest crucibles (11 $\frac{1}{8}$ -in. OD by 10 $\frac{5}{8}$ -in. ID by 20 in. high) have been fabricated and are ready for shipment.

d. Materials Testing and Evaluation (R. D. Pierce)

Last Reported: ANL-7419, p. 126 (Jan 1968).

Pure rhenium and a Re-47 w/o W-18 w/o Mo alloy have been tested for corrosion resistance to zinc and Zn-5 w/o Mg metal phases covered by MgCl₂-30 m/o NaCl-20 m/o KCl salt layers. The rhenium and Re-W-Mo alloy are being tested as candidate materials for components of equipment used in pyrochemical processing. A Zn-5 w/o Mg alloy is used as the acceptor alloy in the salt-transport process.

The rhenium and Re-W-Mo alloy were exposed to the zinc and Zn-Mg alloy metal phases as coupons mounted on an agitator shaft. Two coupons were exposed at 800°C for 100 hr in each of four tests.

The pure rhenium coupons were attacked by both the zinc and Zn-5 w/o Mg alloy to a depth of ~0.025 mm. The mechanism of attack was rhenium dissolution. The Re-47 w/o W-18 w/o Mo alloy coupons, however, were not attacked by either the Zn or the Zn-Mg alloy in the 100-hr test period.

The Re-47 w/o W-18 w/o Mo alloy appears to be a promising material for use in zinc-rich systems. This alloy will be tested further when larger quantities of it become available.

3. General Chemistry and Chemical Engineering--Research and Development

a. Characterization of Carbon-bearing Species in Sodium

Last Reported: ANL-7445, p. 122 (April 1968).

(i) Analysis of Carbon in Sodium (F. A. Cafasso)

The presence of sodium cyanide in liquid sodium systems has frequently been observed, e.g., by collection in cold traps. It has become important to know whether or not the oxygen combustion method for the determination of total carbon in sodium is effective for carbon in the form of cyanide ions or radicals. The results of preliminary experiments show that the quantitiveness of recovery of carbon as CO₂, after the introduction of about 50 ppm of carbon as cyanide, is affected by the mode of

introduction. Samples prepared by pipetting aqueous NaCN onto the surface of solid sodium yielded incomplete and erratic recoveries, whereas if the surface was subsequently covered with additional sodium, recovery of carbon as CO_2 was complete. Further investigation of this analytical problem is continuing.

b. Characterization of Nitrogen-bearing Species in Sodium

(i) Solubility of Nitrogen in Liquid Sodium (F. A. Cafasso)

Last Reported: ANL-7427, p. 125 (Feb 1968).

The solubility of nitrogen in liquid sodium is being measured. The need for this information arises from interest in the possible use of nitrogen-containing blanket gases and from the fact that the solubility data may be important to understanding and control of nitridation, a corrosion phenomenon known to occur in liquid sodium systems.

The quantities of nitrogen dissolved, which are very small, are measured with the aid of nitrogen-15 as an isotopic tracer to distinguish the dissolved gas from contaminating atmospheric nitrogen. The measurements were made by saturating liquid sodium at a preselected temperature with ^{15}N -enriched nitrogen gas at a known pressure, stripping the dissolved nitrogen with helium, trapping the stripped gas, and then determining its quantity and isotopic composition by means of a mass spectrometer.

Solubilities were measured at 50° intervals between 450 and 600°C , and at 10 atm pressure. At least six measurements were made at each temperature, yielding the following results:

Temperature, $^\circ\text{C}$	Solubility $\times 10^{12}$, g N_2 per g Na per atm pressure
451	12 ± 8
502	19 ± 7
550	28 ± 8
600	49 ± 9

The solubility of nitrogen in sodium is found to be smaller than the solubility of either krypton or argon, by one and two decades, respectively.

c. Phase Diagram Study of the Ternary Oxide System U-Pu-O
(P. E. Blackburn and A. E. Martin)

Last Reported: ANL-7427, p. 126 (Feb 1968).

Preparations are continuing for a phase study at high temperatures of the U-Pu-O system, especially that portion of the system which is most relevant to fast reactor fuels. (Considerable additional data on this system at temperatures up to 800°C have been reported recently.)* The glovebox facility, which includes three furnaces having different functions and a helium-repurification and -recirculating system for the glovebox atmosphere, has been essentially completed. The furnaces have been heat tested in the glovebox. The heat exchanger located outside the glovebox has also been completed; tests showed that it provided adequate recirculating cooling water to the furnaces in the glovebox for their high-temperature operation. A safety review of the facility led to a number of recommendations, none of which involve major changes in the facility. Action has been initiated on all of the changes recommended.

The concurrent development of the plutonium metallographic facility has progressed satisfactorily. Improvements have been made which include the installation of automatic grinding and polishing equipment, and improvements in the microscope. After a safety review of these improvements, the facility will be placed back in partial operation. Full operation will be attained in several months when an additional glovebox, presently under construction, is connected to the existing facility. This glovebox will be used primarily for the chemical and electrolytic etching of samples, and will have a special extension for the macroexamination of samples.

d. Development of Some Special High Temperature Capabilities

Last Reported: ANL-7427, pp. 126-127 (Feb 1968).

(i) Congruently Vaporizing Composition of Plutonia
(P. E. Blackburn)

The effusion apparatus, previously used to determine the congruently vaporizing composition of urania as a function of temperature, is being coupled to a glovebox so that effusion studies of plutonium-bearing materials may be carried out. However, the coupling of the effusion apparatus to the glovebox has been delayed while modifications are being made to allow installation within the glovebox of a quadrupole mass spectrometer (which has been ordered). Design work for the required modifications has been partially completed.

*Markin, T. L., and Street, R. S., J. Inorg. Nucl. Chem. 29, 2265 (1967).

A new type of titanium sublimation pump cartridge has been installed within the effusion apparatus vacuum chamber. The new cartridge, with a lifetime of approximately one year, supersedes the previously used cartridges which required replacement every few weeks, and thus would be difficult to use within a glovebox. The new cartridge is presently operational.

e. Preparation of Nuclear Materials (P. A. Nelson)

Last Reported: ANL-7419, pp. 130-131 (Jan 1968).

A fluidized-bed process is being developed for converting UO_2 to UC. This process is also expected to be applicable to the preparation of (U,Pu)C, and shows promise of being more economical than the classical carbothermic reduction process.

A 2-in.-dia graphite fluidized-bed reactor is being used for converting UO_2 to UC. The reactor is capable of operating at temperatures up to 2000°C and pressures up to 10 atm.

Six shakedown runs have demonstrated that high reaction rates between agglomerated particles of UO_2 and graphite can be achieved at 1550°C in a bed near atmospheric pressure fluidized with argon or helium flowing at a velocity of 2 to 3 ft/sec. The UO_2 -graphite particles used in these runs were prepared in a twin-shell (V-shaped) blender. The graphite, UO_2 , and a polyvinyl alcohol binder (a dry powder) were agglomerated by mixing them together in the blender and adding small amounts of water to dissolve the binder. Small particles (~1 mm in diameter) were formed as the mixing progressed. The particles were subsequently dried at 50°C, and the binder was removed at 400°C prior to reacting the particles at 1550°C in the fluidized bed.

Analytical results from the shakedown runs indicate that acceptable oxygen removal can be achieved in a reasonable processing time. Oxygen contents of 4000 to 5000 ppm were obtained, and it is believed that lower values can be attained by operating at higher temperatures or for longer reaction times. Calculations show that about 150 g of UC can be produced in 4 hr in the 2-in.-dia reactor. Extrapolation to plant scale shows that a 12-in.-dia fluidized-bed reactor could produce about 32 kg of UC in 24 hr. This projected processing rate is highly acceptable and probably could be improved by optimizing operating conditions and procedures.

The carbon content of the product was 6 to 11% higher than would be expected from the carbon content of the feed particles. This indicates that the graphite walls of the fluid-bed reactor supplied carbon to the product. Hyde et al.,* noted that about 15% of the carbon in their

*Hyde, K. R., Landsman, D. A., Morris, J. B., Seddon, W. E., and Tulloch, H. J. C., The Preparation of Uranium Nitride and Carbonitride from Uranium Oxide in a Fluidized Bed, AERE-R-4650 (June 1964).

UC product was supplied from the walls of their 3/4-in.-dia graphite fluid-bed reactor. The magnitude of carbon pickup may be inversely related to the scale of the operation and, therefore, may be less prominent in larger production reactors.

Most of the reaction product sintered in the later stages of all of the shakedown runs mentioned above. Particles started to stick to the walls of the reactor near the top of the fluidized bed, and the sintering continued until most of the particles were immobilized. Similar sintering effects were noted by Fletcher et al.* They concluded that lack of sufficient motion of the particles allowed the sintering to take place, and that the effect could be overcome by increasing the gas velocity to compensate for the increase in particle density. This procedure was followed in the first six shakedown runs and found to be ineffective. A recent run was made in which 1% methane was added to the fluidizing gas every 10 min for a 1-min period, and the reactor temperature was raised to 1650°C for the last half-hour of the run. After each methane addition, any evidence of particles sticking to the reactor walls disappeared, and, after the bed was cooled to room temperature, none of the product was stuck to the reactor. Although final results of the run have not been evaluated, the addition of methane seems to be effective in overcoming the sticking problem.

*Fletcher, J. M., Hyde, K. R., and Landsman, D. A., The Use of Fluidized Beds for Producing Carbides, in Carbides in Nuclear Energy, McMillan, London, p. 550 (1964).

PUBLICATIONS

GENERAL REACTOR TECHNOLOGY

Fluidized-Bed Fluorination of $\text{UO}_2\text{-PuO}_2$ Fission-Product Fuel Pellets with Fluorine

L. J. Anastasia, P. G. Alfredson, and M. J. Steindler
Nucl. Appl. 4, 320-329 (1968)

Strengths of Some Uranium Compounds

R. J. Beals and J. H. Handwerk
Materials Technology--An Inter-American Approach, Proc. Conf.
San Antonio, May 20-24, 1968, ASME, New York, 1968, pp. 136-143

Application of the Pulse Method to a Specific Heat and Density-Independent Measurement of Thermal Conductivity: Extension of the Method to Very Small Specimens

R. A. DiNovi
J. Sci. Instr. 1, 379-382 (1968)

A Liquid Metal Heat-Transfer Experiment and Its Relation to Recent Theory

R. L. Merriam, R. P. Stein, and B. L. Richardson
Int. J. Heat Mass Transfer 11, 769 (1968)

T-Violation and Detailed Balance in Direct Reactions

P. A. Moldauer
Phys. Letters 26B(12), 713-715 (1968)

Electrical and Thermal Properties of Some Actinide Compounds

J. B. Moser, O. L. Kruger, and J. H. Handwerk
Proc. Conf. on Electrical and Magnetic Ceramics, British Ceramic Society, London, December 5-7, 1966, Vol. 10, pp. 129-139

The Heat Content and Specific Heat of Some Metallic Fast-Reactor Fuels Containing Plutonium

Howard Savage
J. Nucl. Mater. 25(3), 249-259 (1968)

Fast-Neutron Scattering from Ta, Re, and Pt

A. B. Smith, P. T. Guenther, and J. F. Whalen
Phys. Rev. 168, 1344-1355 (April 20, 1968)

Computers on Line with Experimental Facilities

A. B. Smith and J. F. Whalen
Nucl. News 11(4), 31 (1968)

Fuel Burn-up Predictions in Thermal Reactors: A Review. Recent Work in the United States of America

B. I. Spinrad
Fuel Burn-up Predictions in Thermal Reactors, Proc. IAEA Panel Held in Vienna, April 10-14, 1967, Intern. Atomic Energy Agency, Vienna, 1968, pp. 65-80

The Mathematics of Counterflow Heat Exchangers with Equal Heat Capacity Flow Rates

R. P. Stein

Chem. Eng. Prog. Symp. Series 64(82), 219-230 (1968)

Neutron Capture between 5 keV and 3 MeV

D. C. Stupegia, Marcia Schmidt, C. R. Keedy, and A. A. Madson

J. Nucl. Energy 22, 267-281 (May 1968)

IV. NUCLEAR SAFETY

A. Other Reactor Kinetics--Research and Development1. Fuel Meltdown Studies with TREATa. Meltdown Studies (C. E. Dickerman)

Last Reported: ANL-7438, p. 125 (March 1968).

(i) Irradiation of First Unencapsulated Mixed Oxide Pins in EBR-II. The group of 19 mixed-oxide fuel rods, unencapsulated, to be irradiated in EBR-II, has been reviewed. Questions have been asked concerning the irradiation performance and safety analyses. A memo is in preparation to supply answers to the irradiations reviewers. Similar questions were sent to the other Commission contractor who plans to supply an additional 16 mixed-oxide pins to fill out the irradiation subassembly.

(ii) TREAT Loop Experiments on Single-pin Failures under EBR-II-like Conditions. A 6% enriched EBR-II Mark-I-type pin, argon-bonded to its cladding instead of sodium-bonded, has been loaded into a Mark-I TREAT sodium loop. The loop test section incorporates stepped tantalum neutron absorbers to shape the sample power axially. A sample identical to this, designated as ID-RP-1, was run previously in a "flatop" transient programmed to approximate a reference constant power pulse of 168 W/g of fuel alloy averaged over the sample length. The sample was found to have melted and slumped against the cladding, but no fuel alloy was ejected into the coolant channel (there was, in fact, no significant damage to the cladding).

The goal of the new experiment, designated ID-RP-2, is to seek corroboration of the earlier results, using a more severe condition in order to provide a greater degree of conservatism for application of the results in reactor safety analyses. The reference sample power for ID-RP-2 is 256 W/g of fuel alloy averaged along the pin. This power level is equivalent to that of the central pin in EBR-II for reactor operation at 75 MWt in the reactor loading of EBR-II power Run 27A. Starting temperature for ID-RP-2 (which will also be the coolant inlet temperature during the transient) is specified for the range 420-450°C. The starting temperature of ID-RP-2 was about 375°C, set to approximate the actual EBR-II inlet temperature.

Running of ID-RP-2 has been scheduled so that the loop can be used for setup and checkout of the new neutron hodoscope system, as modified for higher counting rates and automated readout.*

* DeVolpi, A., The Use of Fast Framing Cameras Instead of Magnetic Recording Media to Accumulate Data at High Rates, presented at the 103rd SMPTE Conference, Los Angeles, May 1968.

(iii) Analytical Support. For reasons of convenience and economy, a computerized plotting routine has been produced to prepare graphs suitable for publication and slide requirements. Using FORTRAN IV-CDC-3600 coded programs, subroutine GRAPH has been devised and used routinely to generate report figures; GRAPH is a multipurpose routine capable of producing logarithmic, semilogarithmic, and linear plots. The program is used with the CALCOMP plotting package 580 or 780, or DD80) and subroutines LINAX, LOGAX, SCALOG, and SCANLIN. With the exception of the CALCOMP package, all routines are supplied with GRAPH. Included in GRAPH are provisions for multiple plots with different key symbols, flexibility in axis scaling and size, plotting-style options, and capability for up to three lines of BCD characters as titles.

2. Materials Behavior, Equation of State, and Energy Transfer

a. Materials Behavior and Energy Transfer

(i) Pressure Generation due to Violent Meltdown (R. O. Ivins)

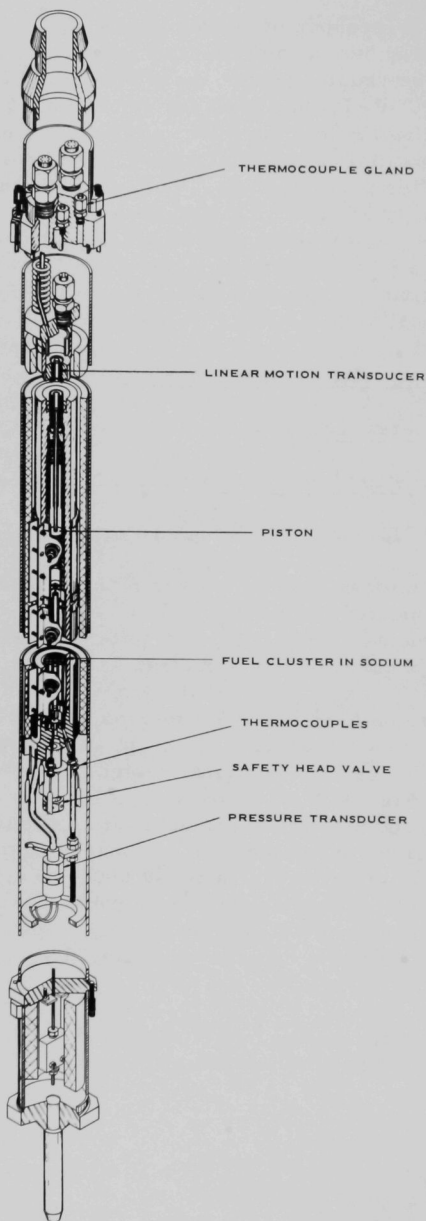
Last Reported: ANL-7427, pp. 138-141 (Feb 1968).

A series of TREAT meltdown experiments is being planned using stainless steel-clad, UO_2 -core fuel rods contained within a sodium-filled piston autoclave. These experiments should provide a better understanding of the mechanics of fuel-rod breakup during a nuclear excursion.

The piston autoclave to be used in these experiments was described in Progress Report for November 1967, ANL-7399, p. 166. However, several modifications have been made in the original design.* The revised autoclave assembly, shown in Fig. IV.A.1, consists of an inner or primary autoclave containing the fuel, sodium, and transducers (to measure temperature, pressure, and linear motion) and an outer or secondary autoclave. The primary autoclave has a design pressure rating of 6000 psi at 600°F and is equipped with a safety head valve designed to rupture at this same pressure. The secondary autoclave, with a design rating of 600 psi at 600°F, provides a double-containment system capable of holding the sodium if the safety head valve ruptures.

Two new autoclave assemblies are being fabricated and an existing one modified to the new design. Experiments are expected to begin in the near future.

*The revised design has been approved by the Committee on Reactor Safety of the Idaho Division, ANL.



3. Reactor Control and Stability

a. Reactor Stability Design Criteria (C. Hsu)

Last Reported: ANL-7403,
p. 147 (Dec 1967).

The development of analytical techniques for obtaining stability criteria for linear space-time reactor systems has been completed. The techniques investigated were: (1) Lyapunov's approach and (2) the spectrum-analysis approach. Lyapunov's method has been applied successfully to nuclear reactors to obtain necessary and sufficient conditions for the linear homogeneous models with which systematic methods for finding Lyapunov functionals can be formulated. However, to obtain the condition for general linear reactor models, finding Lyapunov functionals usually requires solving a set of partial differential equations similar to that of the original system, which is not always desirable. In this case, the method is useful only in obtaining sufficient conditions for stability criteria.

On the other hand, the spectrum-analysis approach derived from functional analysis always can be used to obtain the conditions for general linear reactor systems, but it does not explicitly associate the system stability condition to the system parameters. To compensate for this disadvantage, a parametric study is being formulated to establish the

Fig. IV.A.1

Double Autoclave Assembly for High-energy
Meltdown Experiments with Measurement of
Transient Pressure and Sodium Expulsion

relationship. Because the techniques to obtain the stability condition in most nonlinear reactor models depend on the relative stability of the linear reactor model, the spectrum-analysis method usually yields a less restrictive condition and therefore can be used when Lyapunov's approach is too restrictive.

The development of stability-analysis methods for a class of nonlinear reactor systems has been continued. The stability theorem developed (see ANL-7403) has been improved so that practical application to general reactor systems is feasible. The theorem has been applied to a simplified fast breeder reactor system. The system mathematical model used is a single-energy-group, one-delayed-group, and one-temperature model. The internal temperature feedback is assumed to be linearly proportional to the steady-state power and instantaneous reactor temperature. The final nonlinear model (it is nonlinear because the feedback is the product of the flux and temperature variations) was analyzed to obtain the relationships between the region of local stability, the steady-state power, and the magnitude of the feedback coefficient. For this reactor model, the result showed that the local region of stability is directly proportional to the largest decay constant of the system, and inversely proportional to the feedback coefficient and power. This result agrees with the physical understanding of the reactor model. Although the example is simple in form, the generalization to the more complex system is straightforward.

Two numerical examples have been studied to test the applicability of the method. The first used the distributed model with parameters similar to the EBR-II reactor system operating at full power. The local stability region was determined to be 13.6 times the operating power, which is reasonable. However, this result is valid only when the mathematical model is valid over the indicated region. The second example was taken from a point model system used to compare the various stability methods by Devought and Smets.* The recently developed stability criterion yields a larger and more applicable region of local stability. Although the result of this comparison does not prove that the derived theorem is better for all reactor stability problems, it does indicate strongly that this method can be used successfully in the stability analysis of general nonlinear space-time reactor systems. More examples will be tested and a computer algorithm will be developed for this purpose.

b. Transfer Functions (Stability) (C. Hsu)

Last Reported: ANL-7382, p. 148 (Sept 1967).

Spatially dependent transfer functions are being defined and measurements are being interpreted for various models of large fast reactors

* Devought, J., and Smets, H. B., Determination of Stability Domains in Point Reactor Dynamics, Nucl. Sci. Eng. 28(2), 226 (1967).

to determine how methods for studying system stability from transfer-function measurements of small reactors, such as EBR-II, need to be modified for the various geometries of large fast reactors.

Stability of space-time reactor systems requires that the natural eigenvalues of the system be nonpositive. A general analysis indicated that the various types of spatially dependent transfer-function measurements (e.g., point-to-point, mode-to-mode, and node-to-node) can, in theory, be used to determine the natural eigenvalues. In this analysis, each eigenvalue was obtained as a function of the coefficient of the associated space-dependent natural mode. As a result, a knowledge of the natural modes is required.

For applications to the more common case for which the natural modes are not known, an alternative procedure has been devised for the analysis of spatially dependent transfer functions. This procedure is based on Galerkin's method* for approximating space-time dependent solutions, in which the solution is assumed to be a finite combination of spatially dependent trial modes (not necessarily natural modes) with time-dependent coefficients. These coefficients are, approximately, a linear transformation of the coefficients in the natural-mode expansion, and thus contain the same eigenvalue information.

A computer program has been written that computes the eigenvalues from these time-dependent coefficients in Galerkin's method for an arbitrary system of space-time partial differential equations. Comparison of these computed eigenvalues with true eigenvalues will indicate the suitability of the procedure to experimental reactor applications.

4. Coolant Dynamics

a. Critical Flow (H. K. Fauske)

Last Reported: ANL-7445, pp. 142-143 (April 1968).

(i) Sodium Tests. The new test section has been installed in the sodium facility. Instrumentation for measuring axial pressure and temperature profiles is being checked.

(ii) Sonic Velocity. Some preliminary data on one- and two-component pressure-wave propagation have been obtained with the modified experimental facility and are being evaluated. Both compression and rarefaction pressure waves were initiated in air-water and steam-water mixtures in the void fraction range 5-35%. Amplitude attenuation was observed to be greater in the one- than in the two-component mixture. In the one-component

*Kantorovich, L. V., and Kryloff, V. I., Approximate Methods of Higher Analysis, Interscience, New York (1959).

mixture, amplitude attenuation was found to be greater with rarefaction waves than with compression waves. These preliminary indications will be pursued in greater detail with future data.

The preliminary data have suggested some modifications to the test section that will enhance the quality of future data: the distance between pressure taps can be shortened to improve the resolution of the pressure-time profiles obtained, and the chamber in which the pressure wave is initiated can be modified to eliminate undesired attenuation of the pressure pulse before it enters the active test section.

Bothersome erratic behavior of the quartz pressure transducer has been reduced by improved moisture-sealing, but improved mounting assembly may be required in future test sections.

(iii) Voiding Models. Analyses are being prepared for numerical computer studies of sodium-coolant channel-voiding models.

b. Coolant Dynamics (R. M. Singer)

Last Reported: ANL-7445, p. 143 (April 1968).

(i) Superheat. Preliminary comparison of data from the pool boiler with the sandblasted interior surface (average surface roughness = 200 $\mu\text{in.}$) with the data from the polished surface (8- $\mu\text{in.}$ roughness) indicates little difference in the incipient superheats. The pressure-temperature history seems to override the differences in the surfaces.

(ii) Transient Test Loop. An experiment is being made in a loop to simulate the conditions in a reactor core during abnormal operating conditions that include flow and power transients. Also, this loop is to be tested under FFTF conditions which include: 28-ft/sec inlet liquid velocity, 2.5×10^6 -Btu/hr-ft² heat flux, 1200°F sodium inlet temperature, and pressure ranging beyond 1 atm. The measurements to be made involve pressure pulses, voiding times, flow reversals, incipient superheats, and related phenomena resulting from flow and/or power transients. These results will be used to form a more complete theoretical heat transfer-fluid mechanics accident model.

The transient test loop has been designed, and is being fabricated and assembled. The primary heater in this loop will be of the electron-bombardment type and will be able to supply a heat flux of 5×10^6 Btu/hr-ft² (1.6 kW/cm²) over a 22.5-in. length (572 mm) of 0.25-in. tubing (6.3 mm). This heater can be used for power bursts as well as for steady heating at these high heat fluxes. Controlled flow transients (primarily flow coastdowns) will be accomplished with an electromagnetic pump.

c. Electron-bombardment-heater (EBH) Test Facility
(R. D. Carlson)

Last Reported: ANL-7427, p. 145 (Feb 1968).

A 7-pin electron-bombardment heater to simulate a reactor fuel-pin cluster has been designed. A prototype pin for this cluster has been assembled. Operations have been made at 5000 V with anode and cathode temperatures greater than 1400 and 2500°F. This prototype has been used primarily to test design features and assembly techniques, so only a slight amount of electron-bombardment heating has been achieved.

The ion pump for the EBH test chamber has been found to be defective and is being repaired.

d. Core Component Dynamics (M. W. Wambsganss)

Last Reported: ANL-7445, pp. 143-145 (April 1968).

In the investigation of the plastic deformation of cylindrical shells under impulsive loads, two computer programs have been completed for the case of an axially concentrated ring load. As discussed previously (see Progress Report for December 1967, ANL-7403, pp. 148-150), two phases may occur in the deformation history produced by ring loads. Both completed programs consider Phase-1 deformations only, i.e., hinge circles occurring at $\xi = 0$ and $\xi = \pm\xi_1(\tau)$. A more elaborate program is being written to cover loading functions such that the deformation passes into Phase 2, with hinge bands forming in place of the outer hinge circles.

The governing differential equations for Phase-1 deformations caused by a ring load are the nonlinear coupled set

$$\left. \begin{aligned} \eta_0(\tau) \frac{d\xi_1(\tau)}{d\tau} &= -2\psi(\tau) + \frac{3}{\xi_1(\tau)} - \xi_1(\tau); \\ \xi_1(\tau) \frac{d\eta_0(\tau)}{d\tau} &= 4\psi(\tau) - \frac{3}{\xi_1(\tau)} - \xi_1(\tau); \\ \frac{\partial \delta(\xi, \tau)}{\partial \tau} &= \eta_0(\tau) \left[1 - \frac{\xi}{\xi_1(\tau)} \right]; \quad 0 \leq \xi \leq \xi_1(\tau), \\ &= 0; \quad \xi > \xi_1(\tau), \end{aligned} \right\} \quad (1)$$

where η_0 is the radial velocity at $\xi = 0$, δ is the radial deflection, and ψ is the prescribed pulse shape. For a rectangular pulse:

$$\left. \begin{aligned} \psi(\tau) &= \psi_M; & \tau_0 \leq \tau \leq \tau_1; \\ &= 0; & \tau < \tau_0, \tau > \tau_1, \end{aligned} \right\} \quad (2)$$

the system of Eqs. (1) can be solved in closed form; the first computer program evaluates this solution. The second computer program solves System (1) numerically for an arbitrary pulse shape $\psi(\tau)$. In the latter program the AMD library routines DIFSUB* and DIFSYS** were used extensively. The second program was checked by running problems for rectangular pulses and comparing with exact solutions obtained from the first program.

Some preliminary conclusions may be drawn from the Phase-1 deformation problems solved thus far. A common procedure for evaluating the effects of dynamic loads is to compare the deformations produced by pulses of differing shape but having the same total impulse and peak value. However, the results obtained for a variety of pulse shapes show, at least for Phase-1 deformations, that more useful parameters for characterizing the loading are the impulse after yielding begins and some measure of the effective width of the pulse, rather than its peak value. Several "effective width" parameters were tried; the best appears to be the time centroid of the pulse shape measured from the time at which yielding begins. The impulse and mean time are defined by

$$\left. \begin{aligned} I &\equiv \int_{\tau_0}^{\tau_1} \psi(\tau) d\tau; \\ \tau_m &\equiv \frac{1}{I} \int_{\tau_0}^{\tau_1} \tau \psi(\tau) d\tau, \end{aligned} \right\} \quad (3)$$

where τ_0 is the time at which yielding begins (initial loading below the yield value produces no deformation because of the rigid plastic model used here) and τ_1 is the time at which the pulse ends.

A portion of the parameter study is shown in Figs. IV.A.2 and IV.A.3. In Fig. IV.A.2, five pulse shapes are given, each with the same

*Clark, Nancy W., DIFSUB, 3600 FORTRAN subroutine which performs one integration step for a system of first order ordinary differential equations, ANL-D250 (1966).

**Clark, Nancy W., DIFSYS, 3600 FORTRAN routine which provides input/output and control for use with ANL-D250 - DIFSUB to integrate a system of first order ordinary differential equations, ANL-D251 (1966).

impulse I . Pulses A and D have the same peak value, ψ_M , as do pulses B and E, whereas A, B, and C have the same mean time τ_m . In Fig. IV.A.3, the radial displacement of the central cross section, $\delta(0, \tau)$, is given for each pulse. Note the disparity between the curves for the same peak pulse values and the bunching of the curves for the same τ_m . Curve A is a negative exponential and so extends mathematically to infinity; truncating it at some time τ_1 would result in a lower value of τ_m , so it is to be expected that the deformation Curve A would lie above Curves B and C (the smaller the value of τ_m for a given impulse the larger the deformation). Other pulse shapes having the same I and τ_m also were tested and resulted in deformation curves very close to Curves B and C.

Parameter studies for other values of the impulse I produced similar results; in addition, the instant τ_F of time when the motion ceases was found to be a strong function of I and τ_m , but only weakly dependent on the pulse shape. The range of I over which parameter studies can be

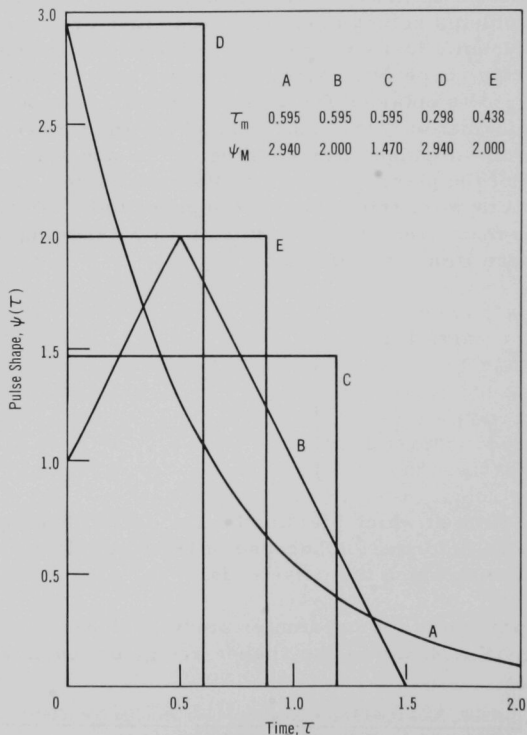


Fig. IV.A.2. Time Variation of Five Pulse Shapes, Each of Which Has the Same Impulse of $I = 1.75$

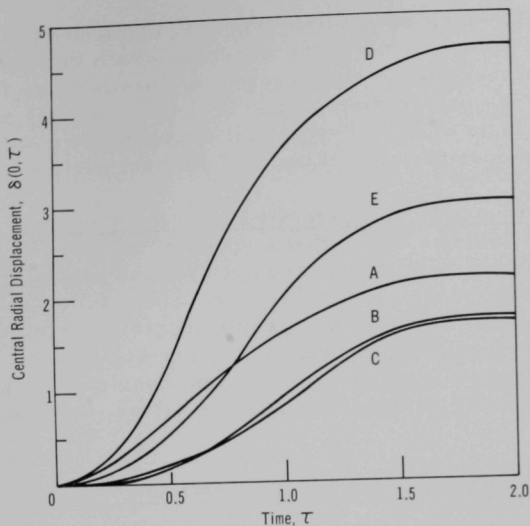


Fig. IV.A.3. Time Variation of Radial Displacement of the Central Cross Section for Each of the Five Pulses of Fig. IV.A.2

run is limited by the passage of the deformation into Phase 2. A computer program that treats both Phase-1 and Phase-2 deformation patterns for ring loads is being prepared.

If the combined Phase-1 and Phase-2 deformation calculations should lead to the same conclusion on the usefulness of I and τ_m in characterizing the effects of different pulse shapes, the result should be of value in correlating experimental measurements. The parameters I and τ_m can be determined easily from a pressure-transducer plot, and final tube-deformation shapes can be measured. The correlation parameters then will enable comparison of experiment with theory and experiments for different loading conditions with each other.

B. Operations

1. TREAT Operations (J. F. Boland)

Last Reported: ANL-7445, p. 146 (April 1968).

a. Reactor Operations. Two Zircaloy-clad UO_2 -powder fuel rods made by BNWL were irradiated in room-temperature water in transparent capsules to obtain data on failure threshold and failure mechanisms. These data will be compared with data previously obtained from similar rods which contained pelleted UO_2 fuel made by BNWL.

A 52%-enriched EBR-II-type fuel element was irradiated under steady-state conditions in a transparent capsule with thermal-flux-attenuation filters. The purpose was to obtain power-calibration data for future experiments that will use preirradiated EBR-II elements of this enrichment. Previous transient tests of EBR-II-type fuel elements have utilized fuel of lower enrichment to reduce power peaking near the fuel surface.

b. Development of Automatic Power-level-control System. Analysis of computer data has shown that a speed of 150 in./sec and an acceleration time of about 10 msec will be required for the control-rod drives for the automatic power-level-control system. Since servo valves and hydraulic actuators capable of meeting these requirements are available commercially from at least two suppliers, specifications are being prepared to obtain bid proposals on a hydraulic control-rod system consisting of two rod-drive actuators, a hydraulic power supply, servo valves, and associated control equipment.

C. Chemical Reaction--Research and Development

1. Chemical and Associated Energy Problems (Thermal)

a. Analysis of Excursion Accidents (R. O. Ivins)

Last Reported: ANL-7427, pp. 146-148 (Feb 1968).

Three additional TREAT photographic experiments were performed with Zircaloy-clad fuel rods containing UO_2 (5% enriched) pellets. These specimens were nearly identical in composition and dimensions to the vibrationally compacted UO_2 fuel rods previously tested in TREAT (experiments CEN-233T to -237T in Progress Reports for November 1967, ANL-7399, pp. 169-171, and February 1968, ANL-7427, pp. 146-147). A summary of the three recent experiments, CEN-238T, -239T, and -240T, is presented in Table IV.C.1.

The fission energy inputs of runs CEN-238T and CEN-240T (244 and 263 cal/g UO_2 , respectively) were below the input required for pressure rupture of the cladding and vigorous dispersal of fuel into the coolant. The fuel rod from run CEN-238T was intact after the transient, but exhibited a blister near the bottom end of the rod. Two thermocouples attached to this specimen indicated peak temperatures of 1806 and 1573°C approximately one second after peak power. The fuel rod from run CEN-240T failed at both ends of the rod owing to extensive metal-water reaction. A peak cladding temperature of 1647°C was recorded by the upper thermocouple on the rod.

TABLE IV.C.1. Results from In-pile (TREAT) Meltdown Experiments with Zircaloy-2-clad, UO₂-pellet-core Fuel Rods Submerged in Water

176 g UO₂ (5% enriched) as pelletized fuel
 41 g Zircaloy-2 cladding
 3000 g H₂O coolant initially at 30°C

	CEN Run Number		
	238T	239T	240T
<u>Reactor Characteristics</u>			
Integrated Power (MW-sec)	375	507	403
Peak Power (MW)	1378	2580	1420
Period (msec)	66	48	63
<u>Results</u>			
Total Fission Energy			
Input (cal/g UO ₂)	244	331	263
Fission Energy Input at			
First Indication of			
Failure (cal/g UO ₂)	-	291	-
Zircaloy-H ₂ O Reaction (%)	1.5	10.2 ^a	3.1
Final Appearance of Fuel			
Rod	Intact, slight blister	Complete fragmentation	Cladding failed at both ends of rod at end of test

^aValue may be less, owing to UO₂ + H₂O reaction.

Transient run CEN-239T involved a total fission energy input of 331 cal/g UO₂. The film record from this experiment showed a brilliant flash, indicative of cladding rupture followed by fragmentation and dispersion of the fuel into the coolant, at an energy of 291 cal/g UO₂. The extent of metal-water reaction (calculated on the basis of hydrogen produced) during this transient may actually be less than the value (10.2%) reported in Table IV.C.1, since this value has not been adjusted for any reaction between hot UO₂ and water, which also produces hydrogen.

Comparison of failures of pellet and powder (Vibra-Pac) fuel from TREAT photographic tests suggests the existence of two different modes of fuel failure for both fuel types (see Table IV.C.2). The failure energies for these modes depend, in part, on the reactor period. The modes can be defined as:

- 1) a prompt failure, which occurs during the power transient, and is manifested by rapid pressurization within the fuel specimen followed by rupture of the cladding and injection of the fuel into the coolant;
- 2) a delayed failure, which generally occurs after completion of the transient, and is due to degradation of the cladding by metal-water reaction and fuel-cladding interaction.

TABLE IV.C.2. Summary of TREAT Photographic Tests
with Zircaloy-clad UO_2 Fuels

Run Number CEN-	Fuel Type	Enrichment (w/o ^{235}U)	Reactor Period (msec)	Total Transient Energy (cal/g UO_2)	Energy at Failure (cal/g UO_2)	Mode of Failure
234T	Vibra-Pac	5	43	354	235	Prompt
233T	Vibra-Pac	5	48	335	277	Prompt
239T	Pellet	5	48	331	291	Prompt
240T	Pellet	5	63	263	263	Delayed
238T	Pellet	5	66	244	Did not fail	-
237T	Vibra-Pac	5	67	258	258	Delayed
235T	Vibra-Pac	5	71	233	Did not fail	-
229T	Vibra-Pac	10	74	357	277	Prompt
236T	Vibra-Pac	5	75	223	Did not fail	-
224T	Pellet	10	80	450	295	Prompt
225T	Pellet	10	107	330	330	Prompt
230T	Pellet	10	108	290	290	Delayed

At reactor periods less than 80 msec, the failure threshold energies* by both mechanisms were observed to occur at energies between 235 and 290 cal/g UO_2 , independent of fuel type and enrichment. At longer reactor periods, the energy required to initiate a prompt failure appears to be greater than 290 cal/g UO_2 . Further transient experiments at both long (>80 msec) and short (<80 msec) periods are planned to define more clearly failure threshold energies.

D. Effluent Control Research and Development--Gaseous Effluent Studies

1. Plutonium Volatility Safety

a. Effluent Gas Treatment (D. Vissers)

Last Reported: ANL-7427, p. 148 (Feb 1968).

Work on the removal of TeF_6 from effluent gas generated in fluorine volatility processes has been completed. A summary of the work is presented below.

Static gas-sorption studies were carried out to screen thirteen potential reagents as sorbents for TeF_6 . The most promising of these, activated alumina and B.P.L. activated charcoal, were evaluated as sorbents for TeF_6 in factorially designed sets of studies using an isotope dilution technique with $^{125\text{m}}\text{Te}$ to evaluate the TeF_6 sorption in a gas flow system. The effects of temperature (25 and 100°C), bed height (1 and 2 in.), gas velocity (20 and 40 ft min^{-1}) and tellurium hexafluoride concentration (190-500 ppm) on the removal efficiency of tellurium hexafluoride were

*The failure threshold energy is defined as the energy input to the sample at the indication of failure and not necessarily the total energy input to the sample.

evaluated; of these, bed height was found to be the most important. Activated alumina and B.P.L. activated charcoal were found to effectively remove TeF_6 (>99.99 percent) from air- TeF_6 systems (190-500 ppm TeF_6). Activated alumina also was found to be an effective sorbent for TeF_6 in the presence of low concentrations of fluorine in air.

The heat of sorption for TeF_6 on activated alumina was found to be 5 kcal mole⁻¹.

PUBLICATIONS

NUCLEAR SAFETY

Review of Nuclear Safety Experiments on Fast Reactor Core Behavior

C. E. Dickerman

Nucl. Safety 9(3), 210-217 (May-June 1968)

Transient Combined Conduction and Radiation in an Absorbing Nonemitting Medium

R. P. Heinisch, R. M. Singer, and R. Viskanta

ANL-7407 (January 1968)

Ignition Behavior of Plutonium Metal and Certain Binary Alloys

J. G. Schnizlein and D. F. Fischer

J. Electrochem. Soc. 115(5), 462-466 (1968)

PUBLICATION--General

Reactor Physics Division Annual Report, July 1, 1966 to June 30, 1967

ANL-7310 (January 1968)

ARGONNE NATIONAL LAB WEST



3 4444 00011323 3